DEPARTAMENTO DE CIÊNCIAS DA VIDA

FACULDADE DE CIENCIAS E TECNOLOGIA
UNIVERSIDADE DE COIMBRA

Tracking dendritically synthesized proteins induced by synaptic activity

Inês de Oliveira Rodrigues e Vaz da Cunha

2013

Acknowledgements

I would like to thank Inbal Isrealy for believe in me and give me the amazing opportunity of being part of her lab. I am really grateful of being part of this great group of people!

I would like to thank Yazmìn for always have some time to listen my non-sense doubts and all my fears, for her awesome Mexican humor, for the teaching and try to make me a positive person.

To Ali, thank you for all the programing and uncaging experiments, patience and friendship. You are the best!

To Anna, Ana Vaz and Zaca for the fun and crazy ideas, and for make my days in the lab less "painfully".

I would like to thank Ana Paula Elias and Cátia Feliciano, without them I would never have some results!

To Carey lab, especially Carla, thank you for all the talks and support to keep doing science and pursue my happiness.

To everyone in CCU, thank you for making this place just amazing!

I would like to Professor Ana Luísa Carvalho for her concern and support.

I would also to thank to the funding agencies, BIAL and FCT.

To all my friends, I want to thank all the time that they have for me, the support and the comfort of knowing that they will always be there, no matter what!

I would also like to thank those amazing new guys that I met in my master program. You made my life better! Thank you Bárbara for sharing the house and the life with me! Thank you Sofias for the amazing dinners! Thank you Tiago for all the jokes, dinners, deserts, cherries and long-night talks! Thank you Fiuza for trying to make me a social human being! Thank you Mário to all your sweetness, for all the understanding and happiness! Thank you Natalie and Bérangère, for the caipirinhas and craziness! To all of you thank you!

To my godmother, godfather, cousin João and Ana, I need to thank you all the time and fondness with me. Thank you for making me feel home!

To my brother, for being unique as you are! For all the things I can't translate into words! For all the thoughts we don't need to say for being shared by us.

To my father, thank you for giving me the best of you.

To my mother, for being the best friend anyone could ask for, for being my shelter, my soul, my true home, for believe in me, for being just the most spectacular person someone could yearn to know!

To all my family, from the oldest to the youngest thank you so much for being just like you! You make my life make sense. "Tenho vidas para acompanhar…"

Abstract

In 1973, the first description of an abrupt and sustained increase in the efficiency of synaptic transmission called long-term potentiation (LTP) in the hippocampus was described. LTP has since been found in all excitatory pathways in the hippocampus leading to the idea that it underlies certain forms of memory.

Synaptic plasticity refers to the ability to modify the efficacy of synaptic transmission. These changes can be short or long-term, and are activity-dependent. Long-term modifications require new protein synthesis, which may occur locally on stimulated synapses.

Using Dendra2, we have made fusions with selected plasticity proteins whose mRNAs are synaptically localized (such as CaMKII, Arc and Calmodulin). When translated, these will fluoresce green but can be converted to a red form, allowing us to distinguish between newly made and pre-existing pools. Thus, we monitor the local synthesis and subsequent trafficking of these proteins upon synaptic activity.

Synaptic plasticity refers specifically to the activity-dependent modification of the efficacy of synaptic transmission at preexisting synapses. These changes in synaptic strength can result in either potentiation (increase in synaptic efficacy) or depression (decrease on synaptic efficacy) of synaptic transmission, known as long-term potentiation (LTP) or long-term depression (LTD), respectively.

The cellular changes such as LTP and LTD are usually classified as either short-term (E-LTP/LTD), based on the posttranslational modification of preexisting proteins, or long-term (L-LTP/LTD), if they require new protein synthesis. It was shown that whereas the short-term phase of synaptic plasticity is insensitive to protein translation inhibitors, the long-term phase is sensitive to blockade by these inhibitors, showing its dependence on the synthesis of new proteins.

Local protein synthesis requires mRNA, polyribosomes and an entire complement of secretory organelles, which were recently shown to be present in some dendrites and throughout the dendritic arbor, often hundreds of microns from the cell body.

Several individual mRNAs have been found in dendrites and these transcripts code for proteins that seem to be important for synaptic plasticity and they localize in postsynaptic structures. CaMKII, Calmodulin, Arc and GluA1 are some of the candidates proteins found to be translated in these dendritically localized polyribosomes.

In this study we aim to understand whether activity can lead to the translation of proteins with dendritically localized mRNAs, and whether these are locally available to synapses following activity induced translation. For this question, we have designed and constructed probes containing native proteins fused to the photoconvertible protein Dendra2-C; a protein that is green in its native form and when exposed to UV-light it is converted to a red form. This fluorescent protein will allow us to have a time-stamp to distinguish between preexisting and newly synthesized proteins after synaptic stimulation and also to follow the role of these synaptic proteins in synaptic plasticity.

Keywords: Synaptic plasticity, local protein synthesis

Resumo

Em 1973 foi descrito pela primeira vez um aumento abrupto e continuado da eficácia na transmissão sináptica no hipocampo denominado LTP (do inglês *long-term potentiation*). O LTP foi descoberto em todas as vias excitatórias do hipocampo sugerindo o seu envolvimento em certas formas de memória.

A plasticidade sináptica refere-se à capacidade de modificar a eficácia da transmissão sináptica. Estas mudanças podem ser a curto ou longo prazo, e são dependentes de actividade. Modificações a longo prazo exigem a síntese de novas proteínas, o que pode ocorrer localmente em sinapses estimuladas. Usando Dendra2, foram criadas fusões com as proteínas associadas à plasticidade sináptica cujos mRNAs são localizados nas sinapses (como CaMKII, Arc e calmodulina). Quando traduzidsa, estas proteínas fusão vão exibir fluorescência verde, que pode ser convertido irreversivelmente para a sua forma vermelha, permitindo-nos distinguir entre proteína produzidas *de novo* e pré-existentes. Assim, somos capazes de seguir a síntese local e tráfico posterior destas proteínas após atividade sináptica.

A plasticidade sináptica refere-se especificamente à modificação da eficácia da transmissão sináptica de forma dependente da actividade em sinapses preexistentes. Estas alterações na eficácia sináptica podem resultar na potenciação (aumento da eficácia sináptica), ou na depressão (decréscimo na eficácia sináptica) da transmissão sináptica conhecido como potenciação de longo prazo (LTP), oudepressão a longo prazo (LTD), respectivamente.

As alterações celulares, tais como LTP e LTD são geralmente classificados de curto prazo (E-LTP/LTD), com base na modificação pós-tradução das proteínas pré-existentes, ou a longo prazo (L-LTP/LTD), se há necessidade de síntese de novas proteínas. Foi demonstrado que, a curto prazo a plasticidade sináptica é insensível aos inibidores de tradução da proteína, contrariamente à fase a longo prazo que é sensível ao bloqueio por esses inibidores, mostrando a sua dependência na síntese de novas proteínas.

A síntese proteíca local requer mRNAs, polirribossomas e um todo o complexo de organelos secretores, que se demonstrou recentemente estarem presente nas dendrites, frequentemente a centenas de microns do corpo da célula.

Vários mRNAs individuais têm sido encontrados nas dendrites e transcritos codificam proteínas que parecem ser importantes para a plasticidade sináptica e se localizam na região pós-sináptica. CaMKII, calmodulina, Arc e GluA1 são algumas das proteínas candidatam a serem traduzidas nestes polirribossomas localizados nas dendrites.

Neste estudo pretende-se compreender se a actividade pode levar à tradução de proteínas com mRNAs localizadas nas dendrites, e se estes estão disponíveis localmente para sinapses próximas. Para responder a esta questão, temos desenhado e construído sondas contendo proteínas nativas fundidas com a proteína fotoconvertível Dendra2-C, uma proteína que é verde, na sua forma nativa e quando exposta à luz UV é convertida para uma forma vermelha. Esta proteína fluorescente vai nos permitir distinguir entre rpoteínas preexistentes e recém-sintetizado após a estimulação sináptica e também para acompanhar o papel destas proteínas sinápticas na plasticidade sináptica.

Palavras-chave: Plasticidade sináptica, síntese proteica

Table of Contents

Abbreviations

AMPAR – (α-amino-3-hydroxy-5-metyl-4-isoxazole-propionic acid)-type glutamate receptor

ARA-C – Cytosine β-D-arabinofuranoside hydrochloride

Arc – Activity-regulated cytoskeleton-associated protein

BDNF – brain-derived neurotrophic factor

bp – base pairs

BSA – Bovine Serum Albumin

Calcium – Ca^{2+}

CaMKII – Ca^{2+}/calmodulin-dependent protein kinase II

CaMKIIα – Ca^{2+}/calmodulin-dependent protein kinase II alpha subunit

cDNA – complamentary DNA

Calmodulin – Calcium-modulated protein

CNS – Central nervous system

CREB-1 – cAMP response element binding protein-1

DG – dentate gyrus

DHPG – (*S*)-3, 5-Dihydroxyphenylglycine

E. coli – *Escherichia coli*

EC – entorhinal córtex

E-LTD – Early Long-term depression

E-LTP – Early Long-term potentiation

EPCS – Excitatory Postsynaptic Currents

ER – Endoplasmatic Reticulum

ERK – Extracellular-signal-regulated kinase

FBS – Fetal Bovine Serum

FWHM – Full-width at half maximum

g – relative centrifugal force

GABA – ɣ-aminobutyric acid

GFP – Green Fluorescent Protein

GluA1 – AMPAR subunit glutamate receptor 1

HFS – High-frequency stimulation

Kb – Kilo bases

KO – knockout

LB – Luria-Bertani

LFS – Low-frequency stimulation

L-LTD – Late phase of long-term depression

L-LTP – Late phase of long-term potentiation

LTD – long-term depression

LTP – long-term potentiation

MAP2 - microtubule-associated protein 2

MAPK – Mitogen-activated protein kinase

MCS – multiple cloning site

mGluR – Metabotropic glutamate receptor

mGluR1 – Metabotropic glutamate receptor type 1

min – minutes

MIPs – maximum intensity projections

mRNA – messenger RNA

mTOR – Mammalian target of rapamycin

NMDAR – (N-metyl-daspartate)-type glutamate receptor

ORF – open reading frame

PAFP – photoactivatable fluorescent proteins

PCR – Polymerase chain reaction

PDL – poly-D-lysine

PI3K – Phosphatidylinositide 3-kinase

PKA – Protein kinase A

PKC – Protein kinase C

PP1 – Protein phosphatase 1

PrPs – Plasticity-related protein products

PSD – postsynaptic density

PTEN – Phosphatase and tensin homolog

ROI – Region of interest

rpm – revolutions per minute

RT – Room temperature (15 – 25^{o}C)

S6K – Ribosomal S6 kinase

sec – seconds

SER – Smooth endoplasmatic reticulum

STC – Synaptic tagging and capture

TOP – 5' terminal oligopyrimidine tract

TSC1/2 – Tuberous sclerosis protein 1/2

UTR – Untranslated region

Chapter 1. Introduction

1.1. Hippocampal function, morphology and organization

The assumption that information is stored in the brain as changes in synaptic efficiency emerged about a century ago following demonstration by Cajal that the networks of neurons are not in cytoplasmic continuity [1] but communicate with each other at the specialized junctions which Sherrington called synapses. External events are represented in the brain as spatiotemporal patterns of neural activity and these patterns of activity act as agents of synaptic changes. The location of storage that leads to learning and memory must therefore be found among those synapses which support activity-dependent changes in synaptic efficacy [2]. Several cellular studies of simple behaviors have provided direct evidence supporting Ramon y Cajal's suggestion that synaptic connections between neurons are not immutable but can be modified by learning, and that those anatomical modifications serve as elementary components of memory storage [3]. In the late 1940s Hebb proposed a coincidence-detection theory in which a synapse linking two cells is strengthened if the cells are active at the same time [4].

The famous case of patient H.M., who had sustained irreparable damage to the hippocampus, highlighted the importance of the hippocampus and related brain structures in the formation of new memories [5, 6]. Compelling evidence from lesion studies in many vertebrates, including humans, shows that the hippocampus is a critical component of a neural system that is required for the initial storage of certain forms of long-term memory [7]. The hippocampus is generally considered to be an intermediate encoding structure that participates in consolidation of episodic memories [8]. Additionally, the hippocampus plays an important role in learning associations between contextual information involved in episodic memories; a role which has been demonstrated, for example, in spatial navigation tasks in mice and rats [9]. Thus the hippocampus plays a central role in the formation, consolidation, and storage of explicit memory [10].

The hippocampal circuit consists of highly organized unidirectional synaptic connections called the trisynaptic pathway: from layer II neurons of the entorhinal cortex (EC) to dentate gyrus (DG) granule cells to CA3 pyramidal cells to CA1 pyramidal cells to EC neurons [10-13]. The disruption of synaptic transmission in particular connections in the trisynaptic pathway led to impaired memory formation [14-17] and also may be involved in neurological disorders [18]. The establishment of appropriate trisynaptic connections is essential for efficient learning and memory [18]. In addition to main trisynaptic network, the hippocampus also receives cortical connections at CA1 region coming from CA3 which may play a decisive role in the computational integration of spatial information [11].

1.1.1. Pyramidal neurons

Pyramidal neurons are found throughout the mammalian forebrain, including the cerebral cortex, the amygdala and the hippocampus [1] and thus, they are associated with regions involved in advanced cognitive functions [19]. This type of neurons are structurally specialized and bi-polar neurons characterized by its triangular shaped soma, with a single thin axon that can travel far conducting signals, a large apical dendrite and several basal dendrites which receive information [20].

The unique axon of each pyramidal neuron typically projects from the base of the soma and branches profusely, making many excitatory glutamatergic synaptic contacts along its length [19].

Pyramidal neurons have short basal dendrites and bigger apical dendrites which connect to the soma. In these neurons, the dendritic tree has two distinct domains: the basal containing short dendrites near the base of the soma, and the apical domain, with bigger dendrites at the apex of the soma [19]. These are some of the main features of pyramidal neurons, although they can vary considerably between different layers, cortical regions and species (Fig.1)[21, 22].

Pyramidal neurons receive synaptic input at the soma, the axon and the dendrites. The soma and the axon receive inhibitory GABA (ɣ-aminobutyric acid)-ergic inputs, whereas most of excitatory glutamatergic synaptic inputs arrives at the dendrites from multiple sources. Generally, the distal apical tuft receives inputs from more distant cortical and thalamic locations whereas proximal dendrites receive excitatory inputs from local sources (collaterals in the same area or from an adjacent area) (Fig. 1) [19]. The different dendritic domains receive distinct synaptic inputs [23]. CA1 neurons in particular receive input to the distal tuft from the entorhinal cortex via the perforant path and from the thalamus whereas the remaining dendrites receive input from CA3 through the Schaffer collaterals [19].

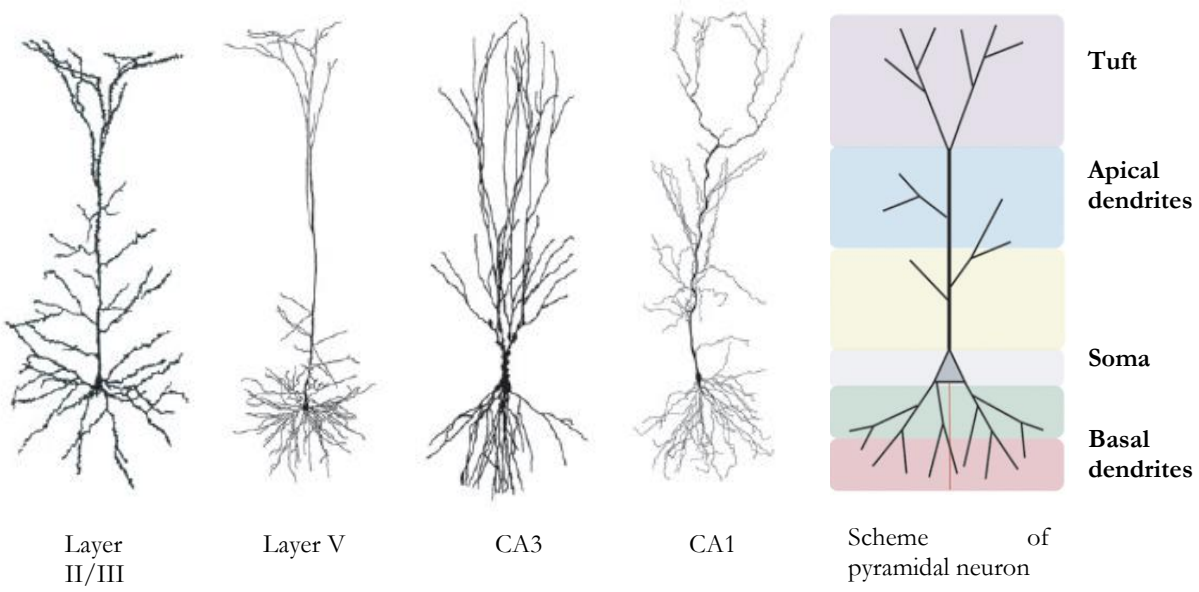

Fig. 1 – Pyramidal neuron structure and domains of synaptic input | Each type of pyramidal neuron has a basal and apical dendrites and an apical tuft, but there are considerable differences between the pyramidal neurons shown. Layer V pyramidal neurons have longer apical dendrites and fewer oblique apical dendrites than layer II/III pyramidal neurons. The basal proximal apical dendrites of layer II/III cells receive inputs from layer IV cells and also receive local-circuit excitation. The apical tuft of layer II/III cells receives inputs from other cortical areas and also receives nonspecific thalamic inputs [22-24]. The apical dendrites of hippocampal CA3 pyramidal neurons branch closer to the soma than those of CA1 pyramidal neurons, which typically have a more distinctive main apical dendrite and tuft. The basal and proximal apical dendrites of CA1 pyramidal cells receive input primarly from CA3 cells, whereas the apical tuft receives input from the entorhinal cort and thalamic nucleus reuniens [25].The apical tuft (highlighted with a light grey) of pyramidal neurons receives excitatory synaptic inputs that have different presynaptic origins to those that form synapse onto more proximal apical dendrites or basal dendrites (highlighted with a light green and pink). All cells are from rat, except for the layer II/III cell which is from the rabbit. Adapted from Spruston, 2008.

CA1 pyramidal neurons are the major output of the hippocampus [11] and activity-dependent changes such as long-term potentiation (LTP) and long-term depression (LTD) at CA1 synapses are important cellular correlates of learning and memory [24]. The strength of CA1 excitatory synapses in the hippocampus is not fixed and can change depending upon their activation pattern. The hippocampus Schaffer Collateral (SC) axons extend from CA3 pyramidal cells to the CA1 region and form excitatory synapses onto mid and proximal dendrites of CA1 pyramidal cells in the stratum radiatum [25] (Fig.2).

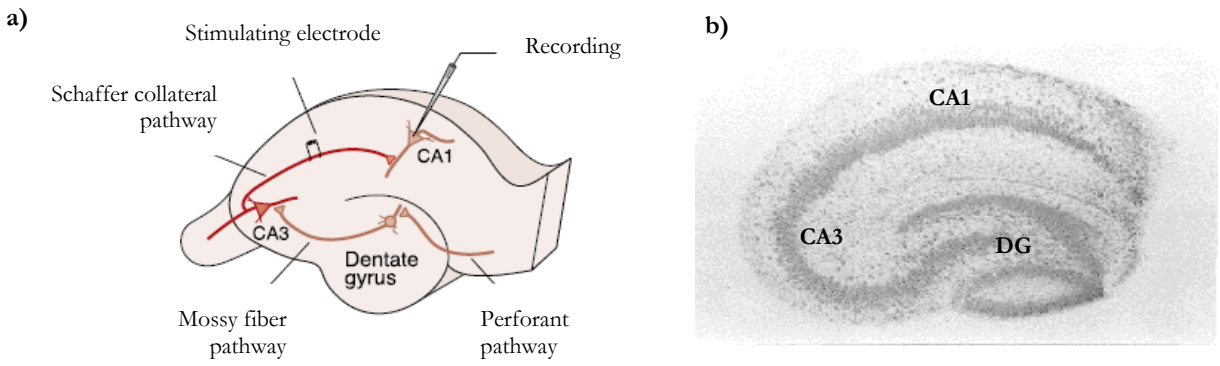

Fig. 2 – Hippocampal slice | **a)** Schematic representatio na hippocampal slice. Three major pathways, each of which gives rise to LTP. The perforant pathway from the subiculum forms excitatory connections with the granule cells of the dentate gyrus (DG). The mossy fiber pathway, formed by axons of the granule cells of the DG, connects the granule cells with the pyramidal cells in area CA3 of the hippocampus. The Schaffer collateral pathway connects the pyramidal cells of the CA3 region with the pyramidal cells in the CA1 region of the hippocampus. **b)** Organotypic slice culture of the hippocampus. Adapted from Kandel, 2001.

1.1.2. Dendrites

The intricate structure of dendrites was revealed hundred years ago by Golgi and Cajal [1]. Dendrites are arborized and electrically active neuronal structures [26] that allows them to exhibit local nonlinear membrane potential dynamics [27-29] and to transform different inputs sequences into different output patterns [30, 31]. The dendritic arbor of most neurons is remarkably stable in the mature brain [32], although there is some turnover of spines, where the majority of excitatory synapses are located [33, 34].

Dendritic protrusions, also known as dendritic spines, can undergo subtle structural rearrangements, in addition to formation and elimination, which can include changes in volume, length and width as a result of functional changes at the synapse [32]. Thus, structural plasticity might reflect changes in the size or number of protein constituents in the postsynaptic density (PSD) (whether it is perforated or not), the number and composition of synaptic glutamate receptors [32]. Accordingly, newly formed spines grow in volume as they become stable whereas most spines show a reduction in volume before disappear [35]. Moreover, given the correlation between spine head size and PSD area [36], the observation that the volume of persistent stable spines is larger than those of transient spines suggests that persistent spines have larger PSDs with higher numbers of (α-amino-3-hydroxy-5-metyl-4-isoxazole-propionic acid)-type glutamate receptors (AMPAR) and are associated with stronger synapses [32, 37].

1.1.3. Dendritic Spines

Dendritic spines are small protrusions in the dendritic shaft with diverse lengths and shapes that allow more connections in the neuropil. Its constricted neck compartmentalizes molecular signals in the spine head isolating the metabolism of each spine and allowing independent control of their function, as well as provides synapse specificity, promotes plasticity and protects the dendrite from excitotoxicity [38-40].

Pyramidal neurons are covered with thousands of dendritic spines (Fig. 3a) that constitute the postsynaptic site for most excitatory glutamatergic synapses [19]. The minimum estimate number of excitatory synaptic inputs onto a neuron is valued by the number of dendritic spines, which varies considerably in different regions and species [36, 41]. Although most of spines contain a single synapse, some contain multiple synapses (Fig. 3b) [42-44].

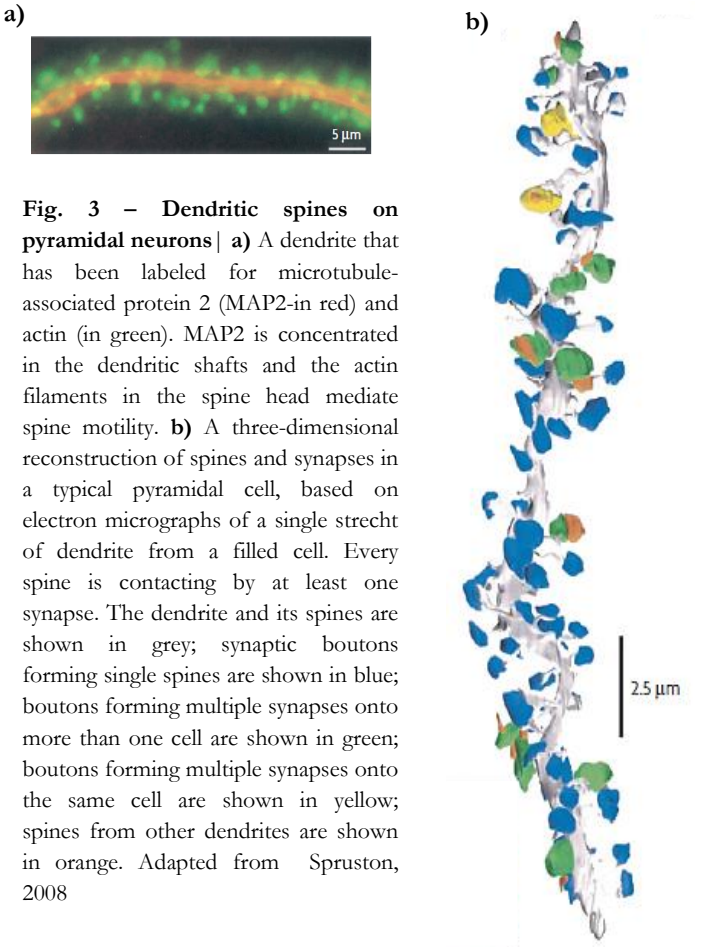

Fig. 3 – Dendritic spines on pyramidal neurons | **a)** A dendrite that has been labeled for microtubule-associated protein 2 (MAP2-in red) and actin (in green). MAP2 is concentrated in the dendritic shafts and the actin filaments in the spine head mediate spine motility. **b)** A three-dimensional reconstruction of spines and synapses in a typical pyramidal cell, based on electron micrographs of a single strecht of dendrite from a filled cell. Every spine is contacting by at least one synapse. The dendrite and its spines are shown in grey; synaptic boutons forming single spines are shown in blue; boutons forming multiple synapses onto more than one cell are shown in green; boutons forming multiple synapses onto the same cell are shown in yellow; spines from other dendrites are shown in orange. Adapted from Spruston, 2008

In the hippocampus, spines vary greatly in size and shape even along short dendritic segments (Fig. 4).

Dendritic spines can take various shapes such as filapodial, thin, stubby, branched or mushroom [45]. Filapodia are the most motile type of dendritic protrusions [46] and they are highly abundant during early

postnatal development when extensive synapse formation occurs . They turn over within hours [47], a rate that decreases with age [48-50]. However the vast majority of the filapodia undergo rapid turnover, a small percentage form a bulbous head and persists [46], suggesting that they could serve as precursors of spines that can last over days [47].

Alvarez and Sabatini, using live imaging with two-photon microscopy, have demonstrated rapid, activity-dependent spine turnover common during development which slowed as an animal matures [32]. Most of the spines have constricted necks and are either mushroom shaped with heads exceeding 0.6 μm in diameter or thin shaped with smaller heads [51]. Other spines are stubby protrusions with head widths equal to neck lengths, branched protrusions with two or more heads or single protrusions with multiple synapses along the head and neck [38].

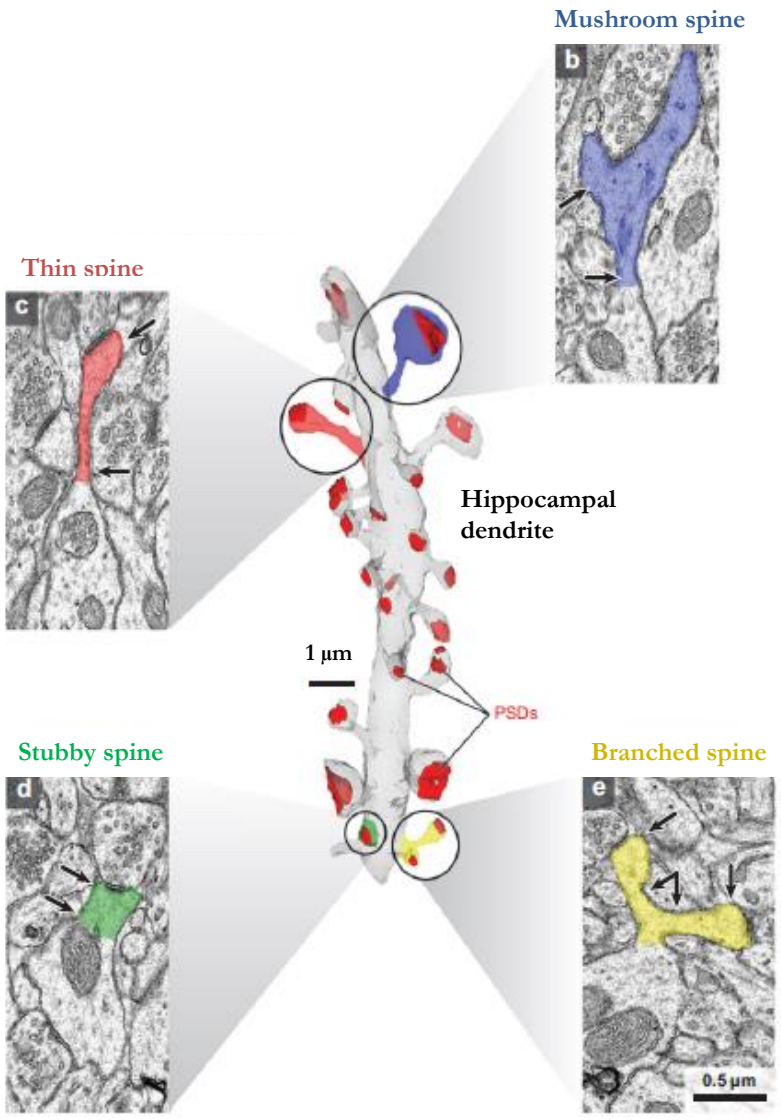

Fig. 4 – Variability in spine shape and size | A three-dimensional reconstruction of a hippocampal dendrite (grey) illustrating different spine shapes including mushroom (blue), thin (red), stubby (green) and branched (yellow). PSDs also vary in size and shape (red) | **b)** An example of a mushroom spine (blue) with a head diameter exceeding 0.6 μm and a narrow neck. **c)** An example of a thin spine (red) with a small head and narrow neck. **d)** An example of a stubby spine (green) with an equal head and neck diameter and an overall length that equals its width. **e)** An example of a branched spine (yellow) where both branches are thin spines. The arrows indicate where the head and neck diameters were measured for each spine. Adapted from Bourne and Harris, 2008

Filapodial and thin spines are considered small spines, while stubby, branched and mushroom spines are

considered to be large spines, representing protrusions with small and large heads, respectively [52]. Small spines change their form rapidly [48, 53, 54], either disappearing or growing into large spines. Intense neuronal activity that accompanies the induction of LTP can also generate or eliminate new spines [55, 56]. In contrast large spines are relatively stable *in vitro* [53] and survive more than a month [54] or even up to a year [48] in the mouse neocortex *in vivo*. Mushroom spines have larger PSDs [51], which can anchor more glutamate receptors and make these synapses functionally stronger [57-61]. The PSD is an electron-dense thickening on spine heads which is apposed to the presynaptic active zone and contains hundreds of proteins including NMDA, AMPA and metabotropic glutamate receptors, scaffolding proteins, such as PSD-95, and signaling proteins like Ca2+/Calmodulin-dependent protein kinase II (CaMKII) [62]. Spines with large PSDs will accumulate more AMPA and NMDA receptors making them more sensitive to glutamate [57]. Therefore, spine sensitivity to glutamate is highly correlated with spine structure [57], being highest at spines with largest heads and lowest in thin and filapodia spines. Mushroom spines are also more likely to contain smooth endoplasmatic reticulum (SER) [63] and polyribosomes [64], machinery that is necessary for local protein synthesis. The presence of translational machinery in mushroom spines make them able to produce new proteins that are a requirement for a long-lasting and stable spine [65-67]. These features suggest that larger spines are functionally stronger in their response to glutamate, local regulation of intracellular calcium, endosomal recycling, protein translation and degradation [38]. By contrast, small spines are more flexible, rapidly enlarging or shrinking in response to subsequent activation [68].

The structural spine plasticity seen in the hippocampus involves several physical changes such as changes in the size and composition of PSD, assembly and disassembly of actin filaments, exocytosis and endocytosis of glutamate receptors and ion channels, regulation of local protein synthesis by redistribution of polyribosomes and proteasomes, dynamic reposition of SER and mitochondria and metabolic interactions between spines [38]

The major role of dendritic spines is yet not known but several authors have suggested different hypothesis. Koch *et al* suggested that spines might increase the dendritic surface area in order to optimize the packing of a large number of synapses onto a given length of dendrite [69-71]. Alternatively, Harris and colleagues suggested that it could serve as biochemical compartments that restrict the diffusion of important molecules away from the synapse [37, 69, 72]. Spines might also have a role in regulating the electrical properties of the neuron [73].

Postsynaptic spines communicate with presynaptic terminals via adhesion molecules, possibly resulting in mutual stabilization. It was shown that spines that are attached to presynaptic terminals have been observed to be more stable than those that are not attached [74].

1.2. Synaptic Plasticity and Organization of Inputs

One of the most fascinating properties of the mammalian brain is its plasticity - the capacity of activity generated by an experience to modify neural circuit function and thereby modify subsequent thoughts, feelings and behaviors [75]. Synaptic plasticity refers specifically to the activity-dependent modification of the efficacy of synaptic transmission at preexisting synapses [75, 76]. This may result mechanistically through changes in receptors number located at synaptic sites [77], by exo- or endocytosis of the receptors in response to activity. Indeed, the rapid trafficking and turnover of AMPARs have been proposed to account for changes in synaptic strength during LTP and LTD [78, 79].

Several years ago, studies of the gill-withdrawal reflex has revealed that even elementary forms of learning in the sea snail Aplysia have distinct short- and long-term states of memory storage. Whereas one training gives rise to short-term memory lasting minutes, repeated spaced training gives rise to long-term memory lasting days to weeks [80, 81]. These behavioral stages have a parallel in the stages of the underlying synaptic plasticity - a short-term form of plasticity lasting minutes to hours and a long-term form lasting days to weeks [80]. Brief trains of high-frequency stimulation to monosynaptic excitatory pathways in the hippocampus cause an abrupt and sustained increase in the efficiency of synaptic transmission. Morevoer, stimulation with a high-frequency train of action potentials was shown to produce a prolonged strengthening of synaptic transmission in all three of the major hippocampus pathways [82]. This effect was first described in detail in 1973 in the rabbit hippocampus [82] and was called long-term potentiation (LTP).

Several properties of LTP make it an attractive cellular mechanism for information storage or memory [2]. LTP can be generated rapidly and is strengthened with repetition occurring only at synapses stimulated by afferent activity and not at adjacent synapses on the same postsynaptic cell [2]. This input specificity presumably increases the storage capacity within neural circuits [83]. LTP is cooperative because multiple inputs must be activated simultaneously to produce sufficient postsynaptic depolarization to induce potentiation. Further it is associative because a weak input that is normally insufficient to induce LTP can be paired with a strong input, leading to potentiation [84, 85]. LTP is readily elicited in *in vitro* preparations of the hippocampus by HFS and the majority of experimental work has focused on this form of LTP in hippocampal CA1 pyramidal cells, although there are many other forms of LTP [83].

LTP in the hippocampus has been shown to be the dominant form of activity-dependent synaptic plasticity in the mammalian brain [2] suggesting that it may be a key cellular mechanism for the storage of memory [86].

These activity-dependent changes in synaptic strength and neuronal excitability, LTP and LTD, can result in either potentiation (increased synaptic efficacy) or depression (decreased synaptic efficacy) of synaptic transmission, known as long-term potentiation (LTP) or long-term depression (LTD), respectively [87](Fig.

5).

LTP can be induced, for example, by high-frequency stimulation (HFS), while LTD can be elicited by low-frequency stimulation (LFS) [75].

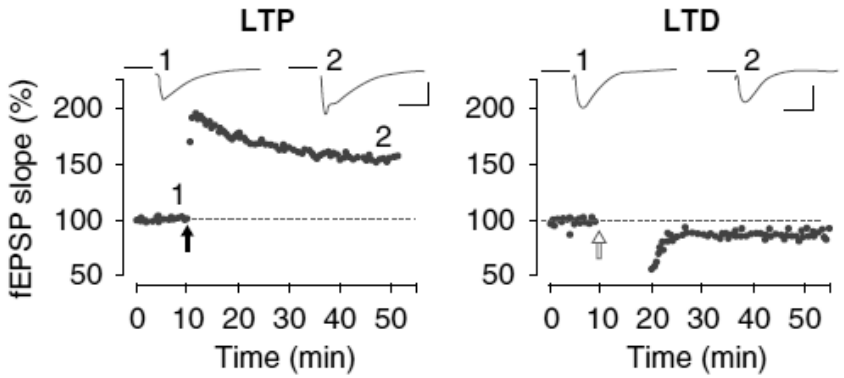

Fig. 5 – Forms of synaptic plasticity | Sample of experiments illustrating LTP and LTD in the CA1 region of the hippocampus. Synaptic strength, defined as the initial slope of the field excitatory postsynaptic potential (fEPSP, normalized to baseline) is plotted as a function of time. Left panel demonstrates LTP elicited by high-frequency tetanic stimulation (100 Hz for 1s, black arrow). Right panel illustrates LTD elicited by low-frequency stimulation (5 Hz for 3 min given twice with a 2 min interval, open arrow). Adapted from Citri and Malenka, 2008.

The ability to alter synaptic efficacy is believed to be the physiological basis for learning and by which memories can be encoded and stored [87]. Thus, LTP and LTD are thought to be essential for achieving the changes in synaptic weights that provide the cellular foundation for experience-dependent alterations in the brain [2, 87-89]. LTP and LTD may physically alter neuronal connectivity [87] and such modifications of synaptic connections are a crucial element of structural plasticity and long-term memory storage [90].

The induction of LTP requires activation of the postsynaptic (N-metyl-daspartate)-type glutamate receptor (NMDAR) during depolarization, which is normally generated by high frequency afferent activity. This activity will lead to a rise in intracellular Ca^{2+} concentration, necessary and sufficient to trigger LTP [2, 91-93]. The AMPAR channel, which is permeable primarily to Na^{+}, provides the majority of current responsible for generating synaptic responses at the resting membrane potential (-60 to -80 mV). In contrast, the NMDAR does not contribute to the postsynaptic response at resting conditions because extracellular Mg^{2+} is bound to it and blocks this ion channel. Upon sufficient postsynaptic depolarization, this blockade of the NMDAR is relieved, allowing for signaling through both types of glutamate receptors. If sufficient Ca^{2+} enters the dendritic spine to activate the signaling mechanism it will lead to LTP. This sudden increase in intracellular postsynaptic Ca^{2+} causes the activation of several protein kinases, including CaMKII, which phosphorylates AMPARs and triggers their insertion into the postsynaptic membrane, resulting in LTP. This kinase was shown to be necessary for LTP induction, as LTP is impaired in Ca^{2+}/calmodulin-dependent protein kinase II alpha subunit (CaMKIIα) knockout mutant mice [94]. NMDAR functions as a molecular coincidence

detector that allows Ca^{2+} influx only when activity occurs in conjugation with depolarization in the target dendrite [83, 95, 96]. Thus, NMDARs are the predominant source of synaptically evoked Ca^{2+} signals but contribute little to synaptic depolarization [97] and AMPARs contribute to the majority of the synaptic current/synaptic depolarization that gives rise to the synaptic potential [98] (Fig. 6).

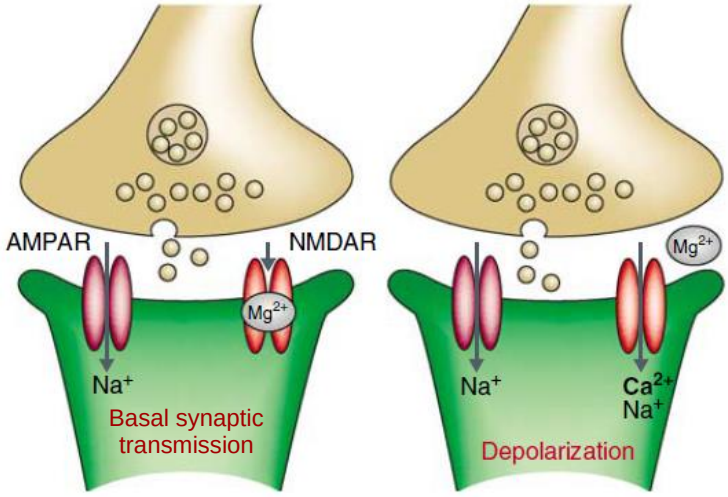

Fig. 6 – Model of synaptic transmission at excitatory synapses | During basal synaptic transmission (left panel), released glutamate binds both the AMPARs and NMDARs. Na^+ flows through AMPAR channel but not through the NMDAR channel because of the Mg^{2+} blockage. The depolarization of the postsynaptic cell (right panel) relives the Mg^{2+} block of the NMDAR channel and allows both Na^+ Ca^{2+} to flow into the dendritic spine. The resultant increase in intracellular concentration of Ca^{2+} in the dendritic spine is necessary for triggering the subsequent events that drive synaptic plasticity. Adapted from Citri and Malenka, 2008.

The conversion of the initial Ca^{2+} signal for LTP into a long-lasting signal depends on particular kinases such as CaMKII [99, 100], protein kinase C (PKC) [101] and the tyrosine kinase Fyn [102]. It was shown that inhibition of these enzymes can block LTP [2] and that CaMKII and PKC are activated in an NMDAR-dependent manner by tetanic stimulation that elicits LTP [103]. Thus, it was suggested that LTP occurs due to the maintenance of increased protein kinase activity. However, various knockout models affecting these key players were generated and none completely inhibited LTP; in all mutants LTP was more difficult to induce but it was not absent suggesting that several protein kinases are involved in long-lasting LTP [83].

Several studies show that LTP induction leads to an enlargement of spine heads, an effect specific to activated spines [104-107], which is followed by an accumulation of AMPA receptors at the synapse [106]. LTP induction is also very likely to promote the accumulation of the machinery necessary for protein synthesis [64] and induce the expression of molecules that stabilize the synaptic contact [108] required for the long-term stabilization of of potentiated spines [108]. De Roo *et al* found also that newly formed spines tend to appear in close proximity to activated spines, indicating that LTP induction favor a clustering of new

functional spines around previously activated ones, promoting possible spatiotemporal interactions between them [108].

LTP requires exocytosis of AMPARs [106], that is responsible for increase in response to glutamate during synaptic potentiation [109, 110], and also exocytosis of subunits of voltage-gated A-type K+ channels, which enhance synaptic excitability [111]. Exo- and endocytosis maintain an activity-dependent balance to fine-tune the physiological and structural responses of spines to synaptic plasticity [38].

In addition to LTP, hippocampal synapses can also undergo of long-lasting synaptic depression (LTD), which can be induced by prolonged low-frequency stimulation [96] and that is closely related to hippocampal LTP [112]: it is input specific, requires activation of NMDAR and a rise in intracellular postsynaptic Ca^{2+} concentration [83]. Weak depolarization by LFS leads to decreased synaptic efficacy through removal of the NMDAR Mg^{2+} block, although to a lesser degree than during LTP and to a modest increase in postsynaptic Ca^{2+} that results in the activation of protein phosphatases, such as calcineurin and protein phosphatase 1 (PP1) which dephosphorylated AMPARs and trigger endocytosis/removal from the postsynaptic membrane [94]. Thus, the balance between the activity of CaMKII and protein phosphatase 1 (PP1) is thought to influence the synaptic strength by controlling the phosphorylation state within a synapse – explaining how a rise in Ca^{2+} could lead to either LTP or LTD [83] (Fig. 7).

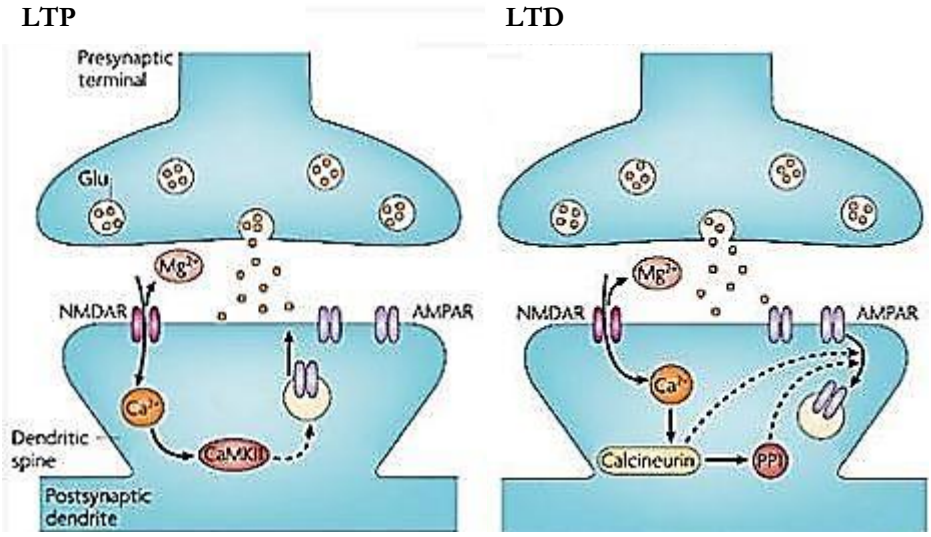

Fig. 7 – Model of NMDAR-mediated LTP and LTD | After HFS (left panel) NMDAR channel is unblocked leading to the increase in intracellular Ca2+ concentration that activates CaMKII resulting in AMPARs exocytosis, increasing synaptic efficacy. Following LFS (right panel) NMDAR channel is unblocked (in lower extent) leading to a small increase in intracellular Ca2+ concentration that activates calcineurin and PP1 resulting in AMPARs endocytosis, decreasing synaptic efficacy. Adapted from Brown University, https://wiki.brown.edu/confluence/display/BN0193S04/Neuro+193E+Home

In contrast to LTP, induction of LTD result in shrinkage [113] or retraction of dendritic spines [114]

associated with depolimerization of actin [115]. Thus, while LTD results in spine shrinkage and retraction and also decrease in spine number and size [113-115] LTP results in morphological shift from thin to mushroom spines [68], alters spine number, shape and subcellular composition in both immature [55, 56, 64, 104-106] and mature hippocampus [116-119].

Synaptic efficacy changes in the hippocampus, either through LTP or LTD, can be short-term or long-term in nature [120]. One train of stimuli produces short lasting plasticity (E-LTP/LTD), which lasts 1 to 3 hours and does not require protein synthesis. Four or more trains can induce the late phase (L-LTP/LTD), which lasts at least 24 hours and requires protein synthesis through the action of protein kinase A (PKA) in L-LTP induction [121, 122] and PP1 and PP2A activation for L-LTD induction [123] (Fig. 8). Therefore, these forms of LTP/LTD can be induced by weak and strong stimulation protocols respectively [87], that exert their action by activating different subcellular signaling pathways.

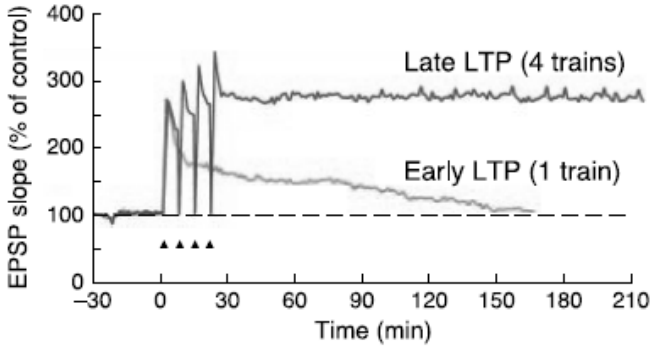

Fig. 8 – Long-term potentiation (LTP) in the hippocampus | Early and late phases of LTP in the Schaffer colateral pathway. A single train of stimuli for 1 s at 100 Hz elicited an early LTP and four trains at 10 min intervals elicited the late phase of LTP. Early LTP lasts about 1.5 hours and the late LTP lasts more than four. Adapted from Kandel, 2001.

For LTP and LTD to persist in an enduring (or late-phase) form both translation and transcription are required [84], being not necessarily coupled in time or space [124]. In either type of synaptic plasticity, changes in synaptic efficacy are restricted to activated synapses leading to specificity of synaptic plasticity [124].

1.2.1. Role of new protein synthesis in long-lasting plasticity

The cellular changes that underlie both synaptic and behavioral plasticity, such as LTP and LTD, are usually classified as either short-term (E-LTP/LTD), and are based on the posttranslational modification of preexisting proteins, or long-term (L-LTP/LTD), because they require new protein synthesis [65-67]. Several studies of synaptic plasticity have shown the short-term phase of synaptic plasticity is insensitive to protein translation inhibitors, like anisomycin, but the long-term phase is sensitive to blockade of translation by these

inhibitors, showing its dependence on the synthesis of new proteins [125-128].

The short-term forms of synaptic plasticity are thought to play a crucial role in short-term adaptations to sensory inputs, transient changes in behavioral states and short-lasting forms of memory. The majority of the forms of short-term changes are triggered by short bursts of activity that causes a transient accumulation of calcium in the presynaptic nerve terminals which causes changes in the neurotransmitter release probability [75].

The first clue to how short-term memory is switched to long-term memory came when Louis Flexner observed that the formation of long-term memory requires the synthesis of new proteins [129]. Subsequent work with *Aplysia* [130] and *Drosophila* [131] showed that with repeated training PKA moves from the synapse to the nucleus of the neuron, where it activates the transcription factor cAMP response element binding protein-1 (CREB-1). CREB-1 acts on downstream genes to activate the synthesis of protein and stimulate the growth of new synaptic connections [96].

The first evidence that metabotropic glutamate receptor type 1 (mGluR1) activation could regulate local protein synthesis came from the observation that treating synaptoneurosomes with metabotropic glutamate receptor (mGluR) agonists, such as DHPG, produced a rapid increase in RNA loading on polyribosomes [132]. Additionally, Job and Eberwine demonstrated that DHPG induces a rapid increase in dendritic expression of a GFP-based translation reporter in cultured hippocampal neurons [133]. The metabotropic glutamate receptors (mGluRs) comprise three groups, mGluR type 1 (mGluR1) being the most important in translational regulation and synaptic plasticity. This type of mGluR primes the induction of LTP in CA1 hippocampal area by prolonging the persistence of LTP induced by weak stimulation [134]. This facilitating effect of mGluR1 activation on LTP persistence requires protein but not messenger RNA (mRNA) synthesis demonstrating a role for the translation of preexisting mRNA [135]. Moreover, mGluR1 activation underlies an NMDAR-independent form of LTD in the CA1 region [136] in a protein synthesis-dependent manner, being blocked by translation inhibitors but not affected by transcription inhibitors.

DHPG induces extracellular-signal-regulated kinase (ERK)-mitogen-activated protein kinase (MAPK) phosphorylation in hippocampal slices and specific inhibitors of MEK (upstream kinase that activates MAPK) blocked mGluR-LTD [137]. Moreover, DHPG treatment of hippocampal slices and synaptoneurosomes induced activation of the phosphatidylinositide 3-kinase (PI3K) signaling pathway, including the protein kinase mammalian target of rapamycin (mTOR), and inhibitors of these molecules blocked the induction of mGluR-LTD [138]. It was shown by Tang *et al* that mTOR plays a critical role in the induction of late-phase LTP in CA1 region of hippocampus [139]. Thus, mGluR activation signals to the translation machinery via both ERK-MAPK and PI3K signaling pathways and both play a crucial role in the

establishment of mGluR-dependent synaptic plasticity (Fig. 9).

These two signal transduction pathways have emerged as key regulators of translational efficiency. Both can be activated downstream of growth factors and were also show to play important roles in enduring forms of synaptic plasticity and memory [140] and, at least in the case of ERK-MAPK pathway, evidences suggests that part of this role seems to be derived from controling translation [66].

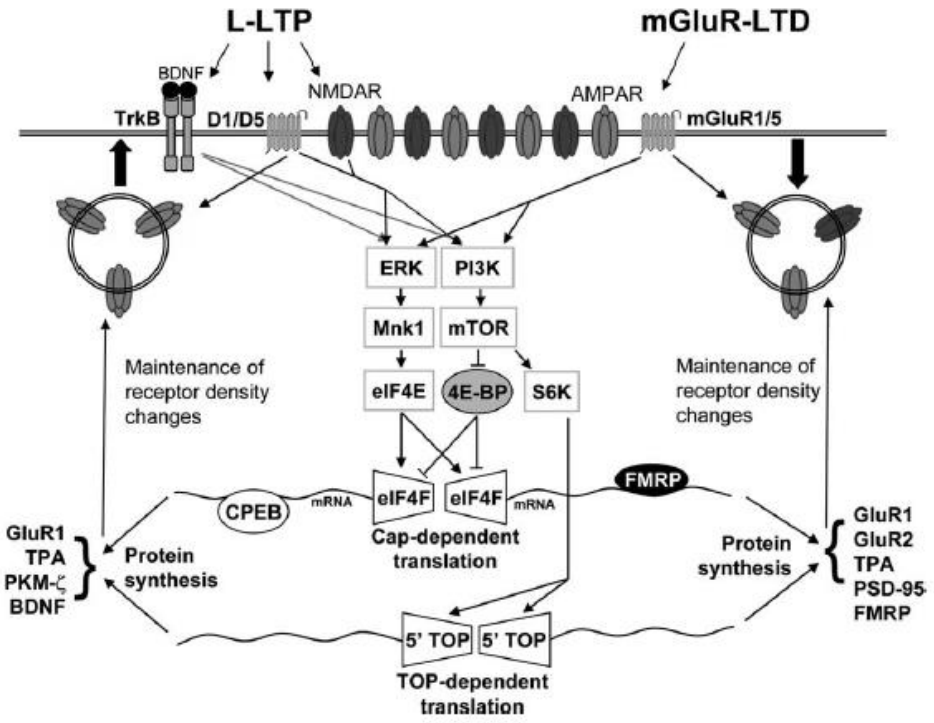

Fig. 9 – Mechanisms for protein synthesis-dependent LTP and LTD | Protein synthesis-dependent LTP (L-LTP) and mGluR-LTD activate and use similar (if not identical) pathways. To make it simple, not all protein synthesis regulatory pathways are included and second-messenger pathways upstream of ERK and PI3K are omitted. Coactivation of NMDARs and dopamine D_1/D_5 receptors initiates the insertion of glutamate receptors to the synaptic surface and stimulates both ERK and PI3K. In contrast, agonists of mGluR1/5 initiate the internalization of glutamate receptors but similarly activate the ERK and PI3K pathways. Both L-LTP and mGluR-LTD-inducing stimuli phosphorylate ERK, Mnk1 and eIF4E and stimulate eIF4F initiation complex assembly inducing cap-dependent translation initiation. By the other hand, activated PI3K phosphorylates mTOR which in turn phosphorylates and inactivates the negative regulator of cap-dependent translation initiation, 4EBP, thereby enhancing translation. Activated mTOR also phosphorylates and activates S6K (ribosomal S6 kinase) which leads to increased TOP (5' terminal oligopyrimidine tract)-dependent translation. Proteins translated in response to synaptic activity may facilitate or maintain the alterations in surface receptor number, synapse size and/or synapse number. Some of the proteins that synthesis was already demonstrated or that are required for protein synthesis-dependent plasticity are listed. Adapted from Pfeiffer *et al*, 2006.

The ERK-MAPK and mTOR signaling pathways couple synaptic activity to the translational machinery during both protein synthesis-dependent LTP and LTD [128]. The ERK pathway, that is activated downstream of NMDA, mGlu and TrkB receptors, plays important roles in synaptic plasticity and memory

[141] and its activation is required for stimulation of cap-dependent translation (Fig. 9) [66], as well as activation of mTOR. Excitatory synaptic activity drives translation by activating mGluR1s and NMDARs and this process is normally regulated by negative regulators such as Fragile x mental retardation protein (FMRP), phosphatase and tensin homolog (PTEN) and tuberous sclerosis protein ½ (TSC1/2) [128].

1.3. Local protein synthesis

Protein synthesis in neuronal cell bodies is undoubtedly important, however it could also occur in neuronal dendrites, relatively far away from the cell soma [142-144]. As neuronal compartments can extend over extremely long distances, the capability to synthesized proteins at distal regions, such as dendrites, may be advantageous in order to be able to respond more efficiently to local signals [145-147]. Indeed, emerging data indicate that local protein translation can play an important role in synaptic development and plasticity [142-144]. The synaptic potentiation induced by brain-derived neurotrophic factor (BDNF) requires local translation [65] as well as other forms of plasticity including long-term facilitation in *Aplysia* [148], long-term depression elicited by metabotropic glutamate receptor activation [149], late-phase LTP [150], dopamine-induced plasticity [151] and homeostatic plasticity induced by blockade of spontaneous neurotransmitter release [124, 143, 152].

1.3.1. Functional evidence supporting local protein synthesis

Many studies indicate that rapid dendritic protein synthesis is necessary for long-term changes in synaptic efficacy. Kang and Schuman suggested that neurotrophin-induced plasticity in hippocampal slices requires general protein synthesis within 30 min for increased synaptic efficacy over a time course of hours [65]. In a similar study, Hubber *et al* reported that general dendritic protein synthesis is required for maintenance of long-term depression within 10 min of DHPG stimulation [149]. One protein that is abundant in hippocampal dendrites and may be required for synaptic plasticity is CaMKIIα [153] and its estimated levels in hippocampal slices indicate that dendritic CaMKIIα synthesis is required within 5 min of tetanic stimulation [154] and *in vitro* synaptoneurosome preparations show increased levels of CaMKIIα within minutes of stimulation with NMDA [155]. Job and Eberwine showed that GFP mRNA can be dendritically translated and that its time constant of 7 min 14 s is consistent with previous measurements of protein synthesis-dependent synaptic plasticity [133].

Local translation could contribute to input specificity: through on-site synaptic synthesis and delivery of effector proteins or through synthesis of a synaptic marker that targets a particular synaptic site for the selective utilization of gene products made elsewhere [124]. Recently, Govindarajan and Israely showed that the efficiency of synaptic tagging and capture (STC) is inversely proportional to the distance over which proteins can be captured, being barely detectable when the distance between stimulated spines becomes as large as 70 μm or with a considerable reduced efficiency of STC when the stimulated spines are found on different dendritic branches [156] This suggests that STC is likely to be a local process operating preferentially

at the level of a dendritic branch [157]. The authors also found that stimulating 12 or more spines leads to a small proportion of the stimulated spines being potentiated in a protein synthesis-dependent manner, whereas when less than 11 spines were stimulated no potentiation was observed [156]. The results indicates that STC is spatially localized and biased toward occurring between stimulated spines phenomenon and that it is likely a phenomenon that takes place within the same dendritic branch [156].

The dysregulation of neuronal protein synthesis, resulting from altering the levels and/or identities of available proteins, could interfere with the establishment of appropriate patterns of synaptic modification. Increased availability of plasticity-related proteins would promote consolidation of synaptic changes that would otherwise be lost, compromising cognitive performance [128] and may also be compromised in certain mental retardation disorders [128].

1.3.2. Physical evidence supporting local protein synthesis

Local proteins synthesis requires mRNA, polyribosomes and an entire complement of secretory organelles [158], which were recently shown to be present in some dendrites [159, 160] and throughout the dendritic arbor, often hundreds of microns from the cell body [161]. It has been suggested that locally made proteins could function to maintain the size of large spines by the incorporation of the cell's machinery protein synthesis [52]. This is supported by the data showing that polyribosomes are preferentially translocated to large spines during synaptic plasticity [64] and that these synaptic complexes include proteins involved in plasticity and structure, such as CaMKII [162], the activity-regulated cytoskeleton-associated protein (Arc) and transmembrane proteins such as microtubule-associated protein 2 (MAP2) [163, 164]. This possible mechanism of spine stabilization is consistent with the fact that local protein synthesis is required for the induction of memory and for late LTP [165, 166] but it remains to be seen if large spines use newly made proteins.

The first evidence that dendrites have autonomous translation control came from studies of Steward and Levy in which they show dendritically localized polyribosome complexes [161], necessary to translate proteins, which are distributed preferentially near dendritic spines [64, 119] and the presence of translational machinery there suggests that protein synthesis could occur in this compartment [161]. Feig and Lipton also shown that radiolabeled amino acids are incorporated in dendrites and that their incorporation is abolished by cycloheximide, a protein synthesis blocker [167]. Several additional studies have demonstrated that the components necessary for translation are constitutively present in dendrites [159] and more recent studies have shown that some of these components undergo activity-dependent trafficking within dendrites [64].

Therefore, the localization of the translational machinery is both a necessary prerequisite for dendritic translation and a way in which protein availability can be dynamically regulated [124].

In eukaryotic cells, the localization of mRNA is an important mechanism which serves to establish or maintain cell polarity, regulate gene expression, and sequester the activity of proteins. Neurons belong to a special class of polarized cells where 10^3-10^4 synapses can be independently modified. This specificity is mediated by differences in protein composition within synapses [168] and thus, local protein translation can play an important role in synaptic development and plasticity [142-144].

Although the vast majority of neuronal mRNAs are restricted to the cell body, a number of mRNAs have been found in the dendrite as well as the soma [153]. Several individual mRNAs have been visualized in dendrites using *in situ* hybridization, such as Ca^{2+}-calmodulin-dependent protein kinase alpha subunit (CaMKIIα) [153, 169], microtubule-associated protein 2 (MAP2) [164], Shank [170] and β-actin [171]. Recently, Cajigas *et al* using next generation deep sequencing of hippocampal neuropil RNA samples revealed a dendritic-axonal set of around 2550 mRNAs [168]. Among these dendritic-axonal mRNAs CaMKIIα is the most abundant mRNA detected in the neuropil [168], consistent with its role as an organizer and regulator of synaptic function [154, 166], while *Shank1*, *Dlg4* (PSD-95), *Ddn* (Dendrin) and *MAP1a* are also relatively abundant [168], consistent with previous results [153, 164, 169, 170, 172-174]. The major advantage of deep sequencing is its ability to detect transcripts of lesser abundance such as *synGAP*, *Snap25*, *Cyfip2* and *Raptor* [168]. Also detected were mRNAs for many membrane proteins, including a large number of voltage-gated ion channels, suggesting that local translation could establish, maintain and regulate gradients these proteins which are known to exists, resulting in local control of intrinsic excitability and the dendritic integrative properties [168, 175]. Many of the proteins that populate the synapse could arise from a local, rather than somatic, source [168], supporting the hypothesis of dendritic translation.

The fact that only certain mRNAs are transported into dendrites suggests that a cis-acting signal, present only in those transcripts, mediates the targeting of these transcripts to dendrites. This signal could be contained within the sequence or structure of the mRNA itself or it could be carried within the nascent polypeptide chain [153]. For the mRNAs found in dendrites to function in local synthesis they must be transported into dendrites and dock at appropriate synaptic sites. These mechanisms are thought to involve the recognition of *cis*-acting elements in the 3' untranslated region (UTR) by specific RNA binding proteins that interact with microtubule-based transport systems [176]. The importance of mRNA trafficking to dendrites was illustrated in a study in which a mutant form of the 3'UTR of CaMKIIα was introduced (3'UTR of bovine growth hormone) and which completely abolished the dendritic localization of CaMKIIα mRNA, resulting in severely reduced dendritic levels of the protein. The mice also showed deficits in L-LTP and hippocampal-dependent long-term memory. This study raised the possibility that local CaMKIIα

translation may represent the major source of CaMKIIα protein at synaptic sites [124]. It is important to emphasize that mRNA trafficking to dendrites is not only a constitutive process, but can also be regulated by synaptic activity [177].

The presence of mRNAs and polyribosomes in proximity to synaptic sites strongly suggest that local protein synthesis in dendrites can provide a rapid supply of new gene products to activated synapses [128]. Crucial evidence for local protein synthesis was provided by experiments which showed that LTP via BDNF- and neurotrophin-3 (NT-3) can be supported isolated axonal or dendritic compartments [65]. It was also shown that establishment of L-LTP is mediated by rapid upregulation of the translation of pre-existing mRNAs [66] and that L-LTP induction in CA1 is accompanied by translocation of polyribosomes from dendritic shafts into dendritic spines [64].

Recent studies also demonstrate that the entire set of secretory organelles are present in some dendrites [159] and the endoplasmatic reticulium (ER) exists as a continuous network in dendrites, being present preferentially at potent synapses [178]. Additionally, ER-bound ribosomes provide a substrate for local mRNA translation, a process that is thought to be important also for mGluR-mediated depression [149].

Mitochondria are also abundant in the dendritic shaft and the ATP that they produce likely diffuses into spines to provide energy for signal transduction via protein kinases in the PSD, such as PKA, protein kinase C (PKC) and CaMKII, as well as for local protein synthesis by polyribosomes [38]. In contrast, mitochondria are rarely found in dendritic spines and are usually restricted to very large and complex spines such as the branched spines [179].

1.3.3. Candidates for local protein synthesis in dendrites

Several individual mRNAs have been found in dendrites using both *in situ* hybridization [153, 164, 169-171] and next generation deep sequencing of hippocampal neuropil [168]. These mRNA are coding proteins that seem to be important for synaptic plasticity and they localize in postsynaptic structures where they might have a role in structure, intracellular signaling and neurotransmitter reception. One of the most probably candidates to be translated into these dendritically localized polyribosomes is CaMKII, a cytoplasmatic protein highly enriched in the PSD [180].

1.3.3.1. Ca^{2+}/calmodulin-dependent protein kinase II (CaMKII)

Calcium/calmodulin-dependent protein kinase II (CaMKII) is a Ca^{2+}-activated enzyme that is highly abundant in the brain, constituting between 1 to 2% of the total brain protein. This kinase is enriched at synapses and it is the main protein of the postsynaptic density (PSD) (Fig. 10).

CaMKII is central to the regulation of glutamatergic synapses as concluded from studies of long-term potentiation (LPT), an activity-dependent strengthening of synapses that is thought to underlie some forms of memory and learning. At many synapses, LTP is triggered by Ca^{2+} entry into the postsynaptic cell through the NMDA receptor (Fig. 10) and several studies suggest that CaMKII detects this Ca^{2+} elevation and initiates the biochemical cascade that potentiates the synaptic transmission [95] being a major decoder of Ca^{2+} spikes is CaMKII, a key enzyme in activity-dependent synaptic plasticity [181].

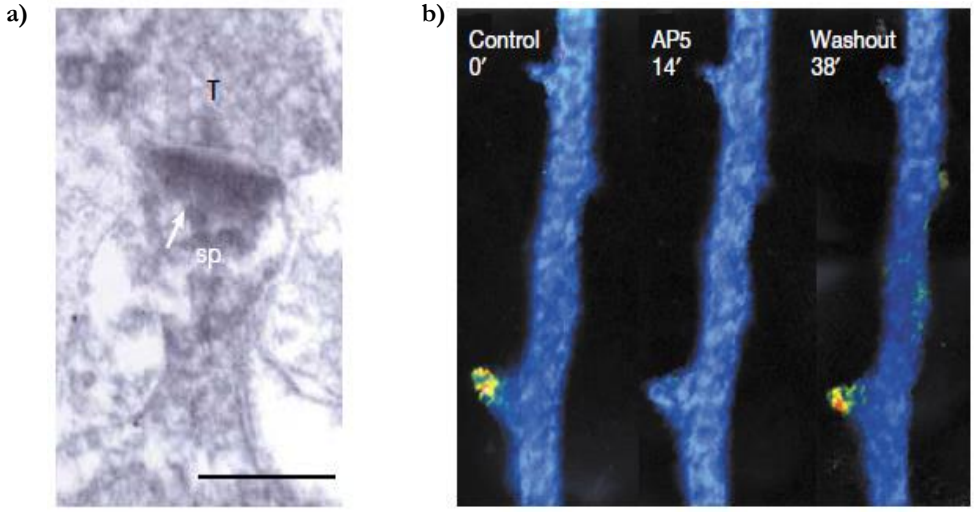

Fig. 10 – CaMKII in the postsynaptic density is ideally positioned to detect local Ca^{2+} entry through the NMDA receptor | a. Immunohistochemical localization of CaMKII shows labeling in a dendritic spine (sp), the site of glutamatergic synapses on CA1 pyramidal cells. Note the heavy labeling in the postsynaptic density (PSD; arrowhead). T, presynaptic terminal. Scale bar is 1 μm. **b.** Synaptic activation of NMDA receptor by a brief burst of synaptic activity causes the local Ca^{2+} to entry into dendritic spine. The fluorescence of calcium green, a Ca^{2+}-indicator dye, is rendered here in a pseudocolor, with red indicating the highest Ca^{2+} levels. NMDA antagonists (AP5 (D,L-2-amino-5-phosphonovaleric acid) in this case) block this entry showing the the source is the NMDA receptor. Adapted from Kovalchuk *et al*, 2000 and Lisman *et al*, 2002.

One of the most interesting features of CaMKII is that its Ca^{2+}/CaM activation can lead to its recruitment to sites where Ca^{2+} rises, such as within activated synapse [182]. Lemieux *et al* have shown that the dynamic process that localize dendritic translocation of CaMKII requires Ca^{2+} activity and microtubular interactions and this also correlates with localized synaptic plasticity [183]. These authors' work suggested that CaMKII could have a role in dendritic processing, impacting on localized synaptic remodeling. In addition to its role to regulate morphology of existing spines, CaMKII plays a role in the formation and elongation of new protrusions during LTP [184, 185]. Synaptogenesis is accompanied by confined dendritic Ca^{2+}[186], which might support the developmental process through CaMKII. Localized CaMKII could also support local translation of mRNA, including its own, required for plasticity [143]. Furthermore, some studies show that CaMKII translocates to synapses where it binds directly to the NMDA receptor [95].

CaMKII can act as a protein switch [187]; once activated by calcium/calmodulin, the enzyme can be

phosphorylated at T286 (threonine 286 at CaMKIIα subunits), an event that makes CaMKII activity persist even after calcium concentration falls to baseline level [188]. If active CaMKII subunits are introduced into CA1 neurons, the excitatory postsynaptic currents (EPCS) become larger and LTP can no longer be induced by synaptic stimulation [189, 190]. If persistent activation of CaMKII is prevented, LTP induction is prevented and mice show profound memory impairments [191, 192] and in many mutants mice that show enhanced learning, CaMKII activation is increased [193]. All together, these results indicate that activated CaMKII is sufficient to trigger LTP and that its activation is necessary for LTP induction and certain forms of learning,

There is growing knowledge of how the dendritic synthesis of proteins, including CaMKII, is affected by synaptic activity. In the hippocampus, CaMKIIα mRNA is distributed in dendrites and cell bodies, whereas βCaMKII mRNA is only present in cell bodies [169, 194]. Targeting of CaMKIIα mRNA requires several cis-acting elements in 3'untranslated region (UTR) of mRNA, one of which depends on synaptic activity for dendritic targeting [153, 162]. Neuronal depolarization recruits CaMKIIα mRNA into granules that are targeted to dendritic processes [195]. It was also shown by Bagni and colleagues that stimulation of synaptosomes with KCl or glutamate/glycine increased the association of CaMKIIα mRNA with polysomes suggesting enhanced translation initiation [196]. Aakalu and colleagues have shown that exposure to BDNF stimulates local protein synthesis of CaMKIIα mRNA in isolated dendrites, and this local synthesis is necessary to induce changes in synapse efficacy [147].

Mayford *et al* shown that the 3'UTR of CaMKIIα localizes its mRNA to dendrites [153] being independent from the protein translated. This localization process is similar to regulation of mRNA localization in other systems [197]. Mayford and colleagues also found that this newly transcribed mRNA species that were transported into dendrites would be expressed only at those translationally active synapses that received the stimulus [153] accordingly to one of the main features of synapses: specificity. Induction of LTP in hippocampal slices increase the level of CaMKIIα indicating that rapid translation of CaMKII mRNA also occurs in dendrites [154, 198]. Aakalu *et al* also shown that the 5'UTR and 3'UTR of CaMKIIα transcript are sufficient to direct its dendritic localization and translation using a reporter protein, GFP in this particular case [147].

There are other molecules that seem to be involved in long-term synaptic plasticity and could be interesting candidates to study translation into dendritically localized polyribosomes such as intracellular signaling molecules, neurotransmitter receptors subunits and structural or cell adhesion molecules. Besides CaMKII that acts as an intracellular signaling partner there is also Calcium-modulated protein (commonly known as calmodulin) and Arc as potential candidates for the study of local translation activity-dependent. Moreover, AMPAR subunit glutamate receptor 1 (GluA1) and N-cadherin can also be candidates for these study acting

as neurotransmitter receptors subunits and structural/cell adhesion molecules, respectively.

1.3.3.2. Calcium-modulated protein (Calmodulin)

Calmodulin is a calcium-binding messenger protein expressed in all eukaryotic cells that acts as a multifunctional intermediate messenger protein that transduces calcium signals by binding calcium ions and then modifying its interactions with various protein targets [199, 200].

The actual calcium sensor for CaMKII activation is not the enzyme itself but the small diffusible molecule calmodulin [181], its high intracellular concentration (~100 μM) and high on-rate constant for calcium binding account for much of what it is called the "fast calcium buffer" [201, 202]. From a signaling point of view these condition make sense: a substantial fraction of the calcium that enters the spine becomes bound to calmodulin, making it an excellent detector for calcium and an efficient activator of CaMKII subunits [203].

1.3.3.3. Activity-regulated cytoskeleton-associated protein (Arc)

Arc is a plasticity protein that is a member of the immediate early gene and its mRNA is known to localize to activate synaptic sites in an NMDA-receptor dependent manner [204], where the newly translated proteins seem to play a critical role for learning and memory-related molecular processes [205].

The neuronal Arc is among the most promising candidates for memory regulatory genes, because it is dynamically regulated and its induction highly correlates with augmented neuronal activity that is required for cognitive processes such as spatial learning and memory consolidation [206, 207]. Consistent with such an activity-dependent Arc upregulation, the knockdown or knockout (KO) of Arc in rodents causes impairments in the persistence of long-term memory [208]. It was also shown by biochemical and electron microscopy studies that the presence of Arc protein in the postsynaptic density (PSD) activates neurons [209, 210]. In the PSD, Arc interacts with the endocytic proteins endophillin and dynamin and enhances the removal of AMPAR from the postsynaptic membrane [209]. This function of Arc, together with its activity-dependent expression is implicated in several forms of protein translation-dependent synaptic long-term depression (LTD) [211, 212] and homeostatic plasticity [209, 213].

1.3.3.4. AMPAR subunit glutamate receptor 1 (GluA1)

AMPA receptors are composed of four types of subunits designated as GluA1, GluA2, GluA3 and GluA4 which combine to form tetramers [214]. AMPAR subunits differ most in their C-terminal sequences, which determines their interaction with scaffolding proteins [215].

Phosphorylation of AMPARs can regulate channel localization, conductance and open probability. GluA1

has four known phosphorylation sites, being one of this sites phosphorylated by PKC and necessary for long-term potentiation [216]. By the other side, CaMKII also phosphorylates GluA1 which helps it to be delivered to the synapse [217]. Recently, Lee *et al* showed that GluA1 is phosphorylated by CaMKII for at least one hour after LTP induction and that GluA1 is dephosphorylated by depotentiation protocols [218]. Further work also showed that procedures that produce depotentiation reduce CaMKII phosphorylation at Thr286. So, persistent CaMKII activity is required for maintaining GluA1 phosphorylation [95].

Structural changes in spines appear to precede, by minutes, the accumulation of AMPA receptors on their surface [106]. Other studies shown the requirement of exocytosis and synaptic insertion of AMPA-type glutamate receptor subunit 1 (GluA1)-containing AMPA receptors for the increase in synaptic strength during LTP [219-221]. Kopec *et al* shown that the insertion of the cytoplasmic tail of the GluA1 receptor into the synapses does not drive spine enlargement but is necessary an sufficient to permit a stable increase in spine size during LTP-induced stimuli [222]. Thus, this single receptor subunit can provide a link between these two subcellular processes.

1.4. Interaction between different kinds of plasticity

1.4.1. Synaptic Tagging and Capture (STC)

The phenomenon of synaptic tagging and capture (STC) suggests that synaptic stimulation creates an immobile "tag" at active synapses that "captures" essential protein products [223]. This means that synapses where any form of long-term potentiation (LTP) is induced, either dependent (L-LTP) or independent (E-LTP) of protein synthesis, become tagged in a protein synthesis-independent manner [223] and that the induction of L-LTP, capable of inducing protein synthesis, in one synaptic pathway can effectively convert E-LTP, not capable of producing new proteins, into L-LTP in a second independent synaptic pathway. This suggests that proteins synthesized in response to stimulation of one group of synapses are available to other stimulated synapses within the same neuron [156].

STC is also observed with LTD and cross-capture has been reported between LTP and LTD. It means that induction of L-LTP in one synaptic pathway can convert E-LTD into L-LTD in another pathway and vice versa [224], suggesting that induction of L-LTP and L-LTD may stimulate synthesis of overlapping sets of proteins capable of enabling either process [128]. Thus, the induction of long-lasting synaptic plasticity forms leads to protein synthesis and all tagged synapses can use the resulting plasticity-related protein products (PrPs) to express long-lasting forms of synaptic plasticity [84, 223]. In sum, when plasticity that leads to new protein synthesis is induced at one synapse, the resulting proteins can facilitate plasticity at nearby sites [223].

Another important component of STC is that both the synaptic tagging and the rate-limiting PrPs have limited lifetimes [84, 223] decayed within 90 minutes and approximately 120 minutes, respectively [156].

1.4.2. Cooperation between different forms of synaptic plasticity

Govindarajan and colleagues also found that L-LTP induced at one spine facilitates tag formation and consequent L-LTP expression at a neighboring spine where only subthreshold stimulation was given subsequent to the original L-LTP stimulation [156]. It suggested that PrPs could altering the excitability near the stimulated spines [89], facilitating the induction of long-term forms of synaptic plasticity. It means that proteins previously synthesized in response to a strong stimulus can be used by a neighboring spine that received a small stimulus, but strong enough to tag this synapse for following long-term change. So, these prompted the idea that there is cooperation between neighboring spines that share newly synthesized proteins.

1.4.3. Competition between different forms of synaptic plasticity

Synaptic capture implies that the local availability of essential proteins is sufficient to promote the consolidation of LTP and LTD. However, if the supply of essential proteins is limiting competition can also be observed among groups of tagged synapses for consolidation of the accompanying synaptic changes [225].

This idea suggests that if the PrPs pool is limited there will be competition among synapses for proteins that would further restrict the engram to such a dendritic compartment because spines close to the site of translation would use up limiting PrPs and reduce their concentration at more distant spines [157]. Fonseca *et al* have shown that different inputs can compete for PrPs when the protein pool was made limited by the application of a translation inhibitor [225]. Govindarajan and colleagues also demonstrate that when PrPs pool is limited it will lead to competition among stimulated synapses for the expression of long-term forms of synaptic plasticity, specifically L-LTP [156]. This competition is specific to stimulated spines. Thus, it was suggest that the amount of proteins that can be produced within a dendritic compartment at certain time is limited such that two stimulated spines close together in space and time may compete for the available proteins and for the expression of long-term forms of synaptic plasticity.

The competition between stimulated synapses occurs only for protein-dependent forms of plasticity and not for independent forms [156]. Therefore, there is no competition for early-phase synaptic plasticity between stimulated spines.

1.4.4. Implications for Synaptic Organization: Spine Clustering

The long-lasting LTP induction will preferentially occur within distinct dendritic branches and not throughout the dendritic arbor, resulting in a preferential spatial clustering within dendritic branches of synapses that would participate in a long-term memory engram. This cluster would be enhanced by the competitive nature of L-LTP induction and STC, since the proteins will be capture near the location of the L-LTP induction, resulting in less protein availability to synapses farther away [156]. These results suggest that hippocampal CA1 cells store long-term memory engrams at synapses that tend to be clustered within dendritic branches as opposed to dispersed throughout the dendritic arbor [157], which would facilitate the formation of memories and increase the ability for memories to be recalled [157, 226].

1.5. Photoconvertible proteins

Green fluorescent protein (GFP) and its homologs from jellyfishes, anthozoans and copepods represent a unique protein family capable of self-catalyzed formation of a chromogenic group within the protein globule. The GFP (from *Aequorea victoria*) allows the direct genetic encoding of a strong fluophore and thus is widely use molecular and cellular biology [227].These GFP-like proteins become fluorescent or colored after protein translation, requiring no external enzymes or cofactors except molecular oxygen. Most of the works related with GFP-like proteins utilize fluorescent protein markers allowing *in vivo* visualization of diverse cellular processes [228].

Photobleaching of a fluorescent protein fused to a protein of interest is a widely used technique for studies of protein mobility by tracking photobleached and non-photobleached protein exchange rate [229]. Moreover optical marking methods have become common and they are based on photo-induced alteration of spectrum of certain fluorescent proteins [230, 231]. Nevertheless there are some limitations to these methods, such as dimness and instability of the photoconverted product and the unavailability of simple, efficient or specific illumination for marking. To overcome this, Ando and colleagues developed the first photoconvertable protein, named Kaede, which the green chromophore can be converted to a red one and its red fluorescence is comparable to the green and more stable [232].

Over the last few years, a number of photoactivatable fluorescent proteins (PAFP) have been developed [233]. Among them there are the Anthozoa-derived PAFPs Kaede [232], EosFP and the monomeric mEosFP [234], KikGR [235] and Dendra[236]. These PAFPs mature in the dark to a green fluorescent state and when subjected to irradiation of UV-light it results in the chemical transformation of green fluorophore into a red one [237](Fig.11.a).

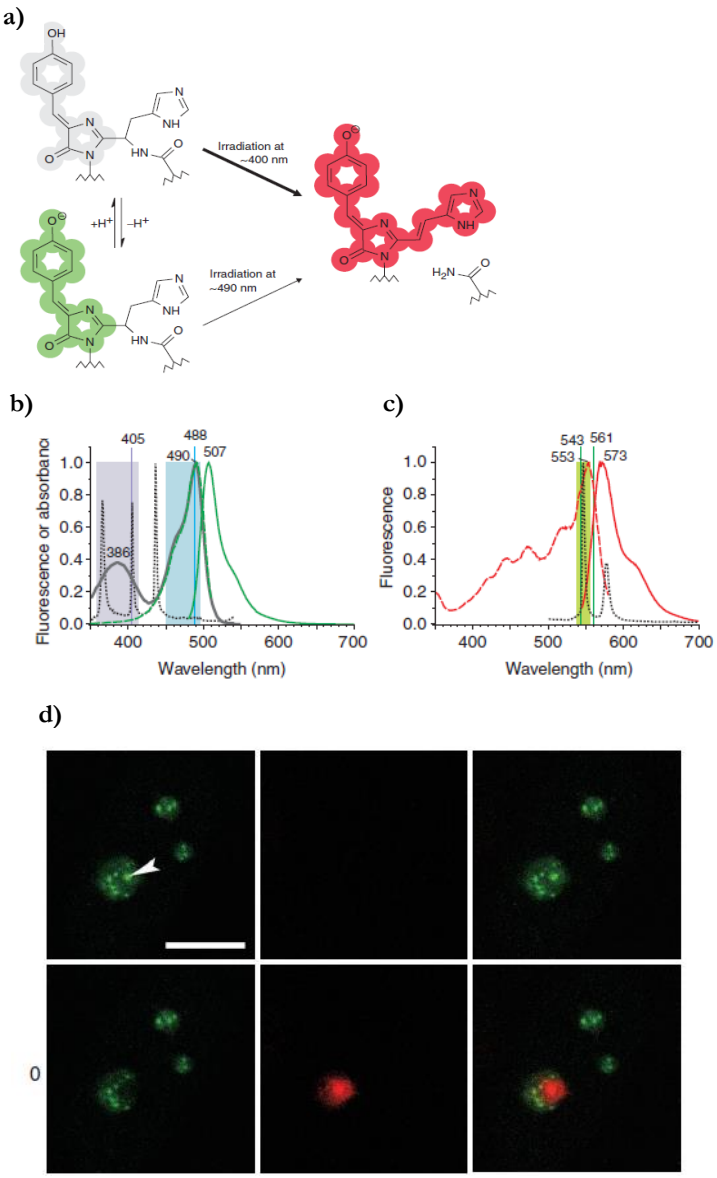

Fig. 11 – Photoconversion mechanism for Dendra2 | **a)** Before phtoconversion, the chromophore of Dendra2 exists in an equilibrium between neutral (nonfluorescent) and anionic (green fluorescent) states. Excitation of the neutral chormophore at approximetly 400 nm results in a very efficient photoconversion into the red state. The key event in the green-to-red photoconversion is the appearance of double Cα=C bond in the chromophore-forming His residue and the cleavege of the protein backbone. Green anionic chormophore of Dendra2 can also be converted into the red state by intense blue light irradiation at approximately 490 nm, albeit this conversion is less efficient. Chromophores are highlighted according to the emission colors; **b)** Spectral properties of Dendra2 green state before photoconversion; **c)** Spectral propertis of Dendra2 red state after photoconversion; Dashed lines: excitation spectra; solid lines:emission spectra; gray line in panel c: absorption spectrum for Dendra2; dotted black lines: emission spectrum of standard mercury lamp. The recommended excitation filters bandpass (violet, blue and green rectangles) and laser lines (violet, blue and green vertical lines) are shown; **d)** Image of single cell before (upper row) and after Dendra photoaconversion at the point designated by the arrow; Left column, green signal; middle column, red signal; right column, overlay; Numbers on the left indicate time after photoactivation in minutes; Bar: 10 μm. Adapted from Chudakov *et al*, 2007 and Gurskaya *et al*, 2006.

The most common area of PAFP application is the photobleaching and subsequent tracking of target objects in living systems. In addition, PAFP photoconversion can be used to observe target protein degradation at single cell level [238]. Among all the PAFPs available nowadays, with regard to the photobleaching and tracking of proteins only the monomeric PAFs – PA-GFP, PS-CFP2, mEosFP, Dendra2, Dronpa, rsFastLime and mTFP0.7 – are suited for this task [228]. The other photoactivatable proteins reported, including Kaede, KikGR, EosPF and KFPs, display a tendency to form homo-dimers and tetramers and can therefore only be reliable utilized as photolabels of organelles and cells [239].

Chudakov and colleagues generated two monomeric photoactivatable proteins, PS-CFP [240] and Dendra [236] and their derivatives PS-CFP2 and Dendra2, which display enhanced brightness of both initial and photoactivated forms and an accelerated maturation rate at 37^{o}C. Both PS-CFP2 and Dendra2 allow an easy irreversible photoconversion with high dynamic ranges and reliable visualization of both initial and photoconverted states [239].

Dendra2 is a Kaede-like [232] fluorescent protein, capable of high-contrasting photoconversion from a green to a red fluorescent form. In the dark, these proteins mature to the green fluorescent state, while irradiation with UV-light (approximately 400 nm) results in their irreversible transition into red fluorescent state (Fig.11.a,b, c and d). Kaede-like PAFPs are characterized by high contrasting ratiometric photoswitching from the green to the red fluorescent state that allows the visualization and tracking of the redistribution of both initial green and activated red forms of Dendra2 [239]. The unique feature of Dendra2 is that blue excitation light (standard GFP excitation filter) can be used for the photoconversion step instead of the potentially damaged 405-nm laser line [241].

1.6. Objectives

The main objective of this study is to gain insights as to how dendritically synthesized proteins contribute to synaptic plasticity following activity at single inputs, and thereby understand how local protein synthesis may be important for long lasting changes in neuronal connectivity. It is known that long lasting plasticity at individual spines requires the synthesis of new proteins, and that these new proteins are available over a limited span of time and space. Therefore, it is possible that activity at a spine allows it to capture newly made proteins, and that the capturing of newly made proteins contributes to the structural plasticity expressed at that spine. Furthermore, if proteins are able to move between activated spines, they may contribute towards setting the amount of plasticity expressed at that spine.

Therefore, we aim to track the localization of newly synthesized proteins by generating reporters in which candidate mRNAs are fused to a photoconvertible fluorescent probe, Dendra 2, which can be irreversibly converted from a green fluorescing to a red fluorescing state with near-UV irradiation, thereby allowing us to differentiate between *pre-existing* and *newly made* proteins. The candidate mRNAs will be selected from published data describing the localization of mRNAs in neuronal dendrites. Upon expression in neurons, these reporters will fluoresce green. Prior to synaptic stimulation, the proteins will be converted from a green to a red state, such that pre-existing tagged proteins will fluoresce red whereas newly synthesized tagged proteins will fluoresce green. This unique characteristic of Kaede-like proteins acts as a time stamp by which we can determine when proteins were generated. This irreversible change will allow us to distinguish between these two protein pools, and to optically track where newly synthesized proteins are being utilized. As dendritically localized mRNAs have been proposed to be available for use upon synaptic activity, tagging these may increase our ability to observe activity directed protein synthesis.

We will track where newly synthesized proteins localize in order to determine whether these proteins preferentially concentrate at stimulated synapses. Additionally, if proteins are found to preferentially distribute near or at stimulated spines, we will further examine whether different forms of activity are conducive to their capture at the spine.

Therefore, the first step of this work is to understand the kinetics of the photoconversion phenomena in hippocampal pyramidal neurons using Dendra2-C (Evrogen). This will be accomplished through 2-photon microscopy and a custom designed filter that allows blue light to broadly stimulate transfected neurons. We will compare the kinetics of Dendra photoconversion to that of Dendra fusions to selected proteins of interest. Specifically, we have selected several candidate proteins to probe with this approach, based on the dendritic localization of the mRNA, and based on an understanding of the candidate protein's role in synaptic or structural plasticity. These include proteins located in the post synaptic density such as intracellular signaling molecules, neurotransmitter receptors subunits and structural proteins. To begin with, we will

generate fusions to and track: CaMKIIα, Calmodulin, Arc and GluA1.

As the limited availability of newly made proteins has been implicated in playing a role in competition for plasticity between synapses, we are interested in determining whether newly made proteins can interchange (or move) between activated synapses. We want to know whether competition or cooperation between specific pools of proteins exists after activity, and if newly made proteins are specifically involved in this process. Such a role has implications for mental retardation disorders in which normal levels of protein translation are altered.

Chapter 2. Material and methods

2.1. Biological material

2.1.1. Bacterial material: *Escherichia coli* strain DH5α

The *Escherichia coli* (*E. coli*) strain DH5α (Invitrogen) was used for vector perpetuation and cloning procedures.

2.1.2. Animal material

All animal experiments were carried out in accordance with European Union regulations on animal care and use, and with the approval of the Portuguese Veterinary Authority (DGV).

The mice sacrifice for the experiments were from C57BL/6 strain. The animals used were P0-1 pups for dissociated neuronal hippocampal primary cultures, P7-9 for organotypic culture and also adults around P90 for hippocampal tissue extraction to get total RNA.

2.2. Constructs

2.2.1. pDrive Cloning Vector

pDrive Cloning Vector (QIAGEN) was supplied with *QIAGEN®PCR Cloning Kit* and it was used for the cloning of PCR fragments (Appendix I).

2.2.2. pDendra2-C Vector

pDendra2-C (Evrogen) is a mammalian expression vector encoding green-red fluorescent protein Dendra2 (Appendix II) that we will use as probe to follow native protein synthesized on dendrites. This vector was used for the generation of fusions to the Dendra2C and expression of Dendra2 alone in eukaryotic (mammalian) cells.

2.3. Molecular Biology methods

2.3.1. Bacterial Transformation (*E. coli*) by heat shock

After de-freeze, an amount between 1 to 10 ng (between 1 to 10 µL) of circular DNA was added to 50 µL of competent *E. coli* DH5α cells (Invitrogen) in an Eppendorf tube and mixed gently. The cells were incubated 30 min on ice, heat-shocked at 42ºC for 30 seconds and returned on ice for 2 min. Then, 950 µL of Luria-Bertani broth (LB broth) at room temperature (RT) was added to the tube and the cells incubated at 37ºC for 1 hour with vigorous shaking (225 rpm). After incubation, centrifuge at 13000 rmp for 30 seconds, remove the supernatant and resuspend the pellet in 100 µL of LB. This volume of transformation mix was then spread onto LB-agar plates (Sigma Aldrich) containing the appropriate selection antibiotic. The plates were incubated overnight at 37ºC.

2.3.2. RNA extraction from hippocampal tissue

The hippocampal tissues used to extract total RNA were removed from P90 mouse that were anesthetized with isoflurane and sacrifice by cervical dislocation or guillotine. All tissues were frozen in dry ice and kept at -80ºC.

2.3.2.1. Purification of total RNA using RNeasy Mini Kit (QIAGEN)

The *RNeasy® Mini Kit* (QIAGEN) and protocol were used for purification of total RNA from hippocampal tissue according to the manufacturer's instructions. This method was employed when highly concentrated and pure RNA samples were required.

2.3.2.2. Extraction from total RNA using TRIZOL method

To extract large amounts of total RNA from hippocampal tissue the TRIZOL method was employed. The hippocampal tissue was collected into Eppendorf tube and frozen into dry ice. The tissue was then grinded in 100 µL of *TRI* reagent (BIO-RAD), added an additional 200 µL of *TRI* reagent (BIO-RAD) and vortex for 15 sec. We added 100 µL of chloroform, shake vigorously for 15 sec and store on ice for 15 min. The mixture

was centrifuged at 16 000 *g*s (Eppendorf Centrigfuge 5415 R) for 15 min at 4ºC, the aqueous phase transferred into a fresh new Eppendorf tube. To precipitate the RNA it was mixed with 125 µL of isopropanol, stored on ice for 10 min and centrifuged for 10 min at 4ºC. The supernatant was removed, discard and the pellet washed with 125 µL of 70% ethanol. To remove the ethanol the pellet was air-dried for 15 min and resuspended into 12 µL of DEPC-treated water.

2.3.2.3. Estimation of RNA concentration

The RNA concentration was estimated by spectrophotometry using *NanoDrop 2000 Spectrophotometer* (Thermo Scientific) and assuming that one unit of absorbance at 260 nm corresponds to 44 µg/mL of DNA. The ratio between the absorbance values at 260 and 280 nm gives an estimate of RNA purity with respect to contaminants such as proteins.

The RNA samples were stored at -80ºC.

2.3.3. Reverse Transcription reaction: cDNA synthesis

The *QuantiTect® Reverse Transcription Kit* (QIAGEN) and protocol were used to obtain complementary DNA (cDNA) from mice RNA according to manufacturer's instructions. The amount of reagents and enzymes used were doubled to assure that all RNA was converted into cDNA. This method was employed to enabling fast and sensitive cDNA synthesis and genomic DNA (gDNA) removal.

2.3.4. Isolation of plasmid DNA

For plasmid DNA isolation, the bacteria were incubated overnight (until 15 hours) in LB broth (Sigma Aldrich) with adequate antibiotic at 37ºC.

2.3.4.1. Large-scale (maxi) and Medium-scale (midi) isolation of purified plasmid DNA

The *HiSpeed® Plasmid Purification Kit* (QIAGEN) and protocol were used for large-scale and medium-scale isolation of plasmid DNA according to the manufacturer's instructions. This method was employed when large and medium amount of highly pure DNA samples were required.

2.3.4.2. Small-scale (mini) isolation of purified plasmid DNA

The *QIAprep® Spin Miniprep Kit* (QIAGEN) and protocol were used for small-scale isolation of plasmid DNA according to the manufacturer's instructions. This method was employed when small amount of highly pure DNA were required

2.3.4.3. Estimation of DNA concentration

The DNA concentration was estimated by spectrophotometry using *NanoDrop 2000 Spectrophotometer* (Thermo Scientific) and assuming that one unit of absorbance at 260 nm corresponds to 50 μg/mL of DNA. The quality of the sample was established using the A_{260}/A_{280} (for RNA contamination and polysaccharides) and A_{260}/A_{230} (for protein contamination and phenolic compounds) ratios. Pure samples were expected to have 1.8 – 2.0 for both ratios.

The DNA samples were stored at -20°C.

2.3.5. Agarose Gel Electrophoresis

DNA samples were resolved by electrophoretic separation when loaded onto a horizontal agarose gel submerged in 1x TAE buffer [40 mM Tris, 20 mM acetic acid, 1 mM EDTA] or TBE buffer [90 mM Tris, 90 mM boric acid, 2 mM EDTA] after addition of *6x Orange DNA loading Dye* (Fermentas) (1x final concentration) to the DNA samples. *Quick-Load 1 kb Ladder*, *100 bp Ladder* and *50 bp Ladder* (New England Biolabs) were used as the molecular weight marker and applied on the gel without addition of loading buffer.

For PCR products and plasmids digest, about 10 mm thick gels were prepared using 2 – 0.8% (w/v) agarose, depending on the size of the DNA fragments. Gels were run at 70 V between 30 to 90 min.

Two methods were used to visualize the DNA on the gel: 5% (v/v) GreenSafe Premium (NZYtech)was added to the agarose gel prior to electrophoresis or agarose gels were post-stained for approximately 30 min in *GelRed* solution (15%(v/v) *GelRed* (VWR) in 1x TAE buffer or 0.5x TBE buffer). The DNA fragments were visualized on a UV Trans Illuminator (Gel Doc™XR+ (*BIO-RAD*)) and photographed.

2.3.6. Polymerase chain reaction (PCR) methods for DNA fragment amplification

The PCR on plasmid DNA was used to amplify inserts for cloning purposes or to confirm the presence and orientation of plasmid inserts. The PCR on cDNA was used to amplify inserts for cloning purposes. *C1000™ Thermal Cycler* (BIO RAD) was used in the PCR amplification procedures.

The primer designed followed the parameters suggested by Griffin and Griffin [242] and were synthesized by *Sigma* (Table I for primer sequences). Specific *primers* were generally 20-30 nucleotides long with restriction sites for endonucleases in 5' ends. The annealing temperature was calculated based on the Wallace rule [243]. In order to maximize annealing strength primers were designed to end (3'end) with G or C.

2.3.6.1. Amplification of DNA fragments from plasmid templates

The PCR reaction was carried out according to Saiki and colleagues [244]. The total reaction mixtures of 50 µL were set up using water, 1.25 units of *TaKaRa Ex Taq™* (TaKaRa Bio Inc.) or *DreamTaq™ DNA Polymerase* (Thermo Scientific), 10x (1x final c.c.) *Ex Taq™ Buffer* (Mg^{2+} free) (TaKaRa Bio Inc.) or 10x (c.c. final) *DreamTaq™ Buffer* (20 mM $MgCl_2$) (Thermo Scientific), 2 to 4 mM of $MgCl_2$, 0.2 µM of dNTP mixture (Fermentas), 0.5 µM of each primer forward and reverse and 100 ng of plasmid DNA. The PCR was carried out with an initial 95°C denaturation for 1.5 min, followed by 35 cycles of 95°C for 30 sec, 50°C – 70°C annealing for 30 sec and 72°C extension for 1 kb/min (depending on the size of the amplification product); and one extension cycle at 72°C for 5 – 10 min. The samples were stored at 4°C or at -20°C.

2.3.6.2. Amplification of DNA fragments from plasmid templates using *Pfu* DNA Polymerase

For fragment amplification using *Pfu* (*Pyrococcus furiosus*) DNA polymerase with proofreading activity, total reaction mixtures of 50 µL were set up using water, 1.25 units of *NZYProof DNA polymerase* (nzytech), 10x (1x final c.c.) *NZYProof DNA polymerase buffer* (nzytech)[200mM Tris-HCl, pH 8.8, 100 mM $(NH_4)_2SO_4$, 100 mM KCl, 20 mM $MgSO_4$, 1 nuclease.free mg/mL BSA, 1% (v/v) Triton X-100], 2 mM of $MgCl_2$, 0.2 µM of dNTP mixture (Thermo Scientific), 0.5 µM of each primer forward and reverse and 100 ng of plasmid DNA. The PCR was carried out with an initial 95°C denaturation for 2 min, followed by 35 cycles of 95°C for 30 sec, 50°C – 70°C annealing for 30 sec and 72°C extension for 1 kb/min (depending on the size of the

amplification product); and one extension cycle at 72°C for 10 min. The samples were stored at 4°C or at -20°C.

2.3.6.3. Amplification of DNA fragments from plasmid templates using *AccuPrime PFX* DNA Polymerase

For fragment amplification using AccuPrime™*Pfx* DNA polymerase with proofreading activity, total reaction mixtures of 50 µL were set up using water, 5 units of AccuPrime™*Pfx* DNA polymerase (Invitrogen), 10x (1x final c.c.) AccuPrime™*Pfx* Reaction mix (Invitrogen), 0.3 µM of each primer forward and reverse and 150 ng of plasmid DNA. The PCR was carried out with an initial 98°C denaturation for 3 min, followed by 35 cycles of 98°C for 1 min, 55°C annealing for 1 min and 68°C extension for 1 kb/min (depending on the size of the amplification product); and one extension cycle at 68°C for 10 min. The samples were stored at 4°C or at -20°C.

2.3.6.4. Amplification of DNA fragments from cDNA templates

The PCR reaction was carried out according to Saiki and colleagues [244]. The total reaction mixtures of 50 µL were set up using water, 1.25 units of *TaKaRa Ex Taq™* (TaKaRa Bio Inc.) or *DreamTaq™ DNA Polymerase* (Thermo Scientific), 10x (1x final c.c.) *Ex Taq™ Buffer* (Mg^{2+} free) (TaKaRa Bio Inc.) or 10x (1x final c.c.) *DreamTaq™ Buffer* (20 mM $MgCl_2$) (Thermo Scientific), 2 to 4 mM of $MgCl_2$, 0.2 µM of dNTP mixture (Fermentas), 0.5 µM of each primer forward and reverse and 500 ng of cDNA. The PCR was carried out with an initial 95°C denaturation for 1.5 min, followed by 35 cycles of 95°C for 30 sec, 50°C – 70°C annealing for 30 sec and 72°C extension for 1 kb/min (depending on the size of the amplification product); and one extension cycle at 72°C for 5 – 10 min. The samples were stored at 4°C or at -20°C.

2.3.6.5. Amplification of DNA fragments from cDNA templates using *Pfu* DNA Polymerase

For fragment amplification using *Pfu* (*Pyrococcus furiosus*) DNA polymerase with proofreading activity, total reaction mixtures of 50 µL were set up using water, 2.5 units of *PfuUltraTM HF DNA polymerase* (Agilent Technologies), 10x (1x final c.c.) *PfuUltraTM HF reaction buffer* (Agilent Technologies), 3 mM of $MgCl_2$, 0.2 µM of dNTP mixture (Thermo Scientific), 0.5 µM of each primer forward and reverse and 100 ng of cDNA. The PCR was carried out with an initial 95°C denaturation for 2 min, followed by 35 cycles of 95°C for 30

sec, 50ºC – 70ºC annealing for 30 sec and 72ºC extension for 1 kb/min (depending on the size of the amplification product); and one extension cycle at 72ºC for 10 min. The samples were stored at 4ºC or at -20ºC.

2.3.6.6. Amplification of DNA fragments from cDNA templates using KOD hot start DNA polymerase

KOD (*Thermococcus kodakaraensis*) Hot Start DNA polymerase with proofreading activity was used for amplification of difficult DNA sequences. The total reaction mixtures of 50 µL were set up using water, 25 µL of KOD Hot Start Master Mix (Novagen®), 0.3 µM of each primer forward and reverse and 4 µg of cDNA. The PCR was carried out with an initial 95ºC denaturation for 2 min, followed by 35 cycles of 95ºC for 20 sec, 50ºC – 70ºC annealing for 10 sec and 70ºC extension for 1 kb/min (depending on the size of the amplification product). The samples were stored at 4ºC or at -20ºC.

2.3.6.7. Amplification of DNA fragments from PCR products: nested PCR

For difficult fragment amplification using *Pfu* DNA polymerase with proofreading activity, total reaction mixtures of 50 µL were set up using water, 2.5 units of *PfuUltraTM HF DNA polymerase* (Agilent Technologies), 10x (1x final c.c.) *PfuUltraTM HF reaction buffer* (Agilent Technologies), 3 mM of $MgCl_2$, 0.2 µM of dNTP mixture (Thermo Scientific), 0.5 µM of each primer forward and reverse and 1 µL of PCR product. The PCR was carried out with an initial 95ºC denaturation for 2 min, followed by 35 cycles of 95ºC for 30 sec, 50ºC – 70ºC annealing for 30 sec and 72ºC extension for 1 kb/min (depending on the size of the amplification product); and one extension cycle at 72ºC for 10 min. The samples were stored at 4ºC or at -20ºC.

2.3.6.8. Colony PCR amplification

The colony PCR amplification was used to confirm the presence and orientation of plasmid inserts transformed in *E. coli*. A small amount of bacterial colony was used as DNA template for the PCR reaction. The total reaction mixtures of 50 µL were set up in water, 1.25 units of *NZYTaq DNA polymerase* (nzytech) or *DreamTaq™ DNA Polymerase* (Thermo Scientific), and 10 x (1 x final c.c.) *NZYTaq DNA polymerase buffer* (nzytech) [670 mM Tris-HCl, pH 8.8, 160 mM $(NH_4)_2SO_4$, 0.1% (v/v) Tween 20] or 10x (1 x final c.c.) *DreamTaq™ Buffer* (20 mM $MgCl_2$) (Thermo Scientific), 2 mM of $MgCl_2$, 0.2 µM of dNTP mixture (Thermo

Scientific) and 0.5 μM of each primer forward and reverse. The PCR was carried out with an initial 100°C denaturation for 2 min, 95°C denaturation step for 1.5 min followed by 35 cycles of 95°C for 30 sec, 50°C – 70°C annealing for 30 sec and 72°C extension for 1 kb/min (depending on the size of the amplification product); and one extension cycle at 72°C for 5 – 10 min. The samples were stored at 4°C or at -20°C.

2.3.7. Site-directed Mutagenesis of pDendra2-C Vector

The directed mutagenesis of pDendra2-C Vector was done to replace the *start codon* (ATG) of Dendra protein for another codon, in this case one that codifies glycine (GGG), to insert a *stop* codon in the end of the *open reading frame* of Dendra2 and also to put *in frame* the endonuclease restriction sites of *Afe*I and *Age*I, used to clone the 5'UTR and ORF of native proteins by removing 7 nucleotids. The *QuikChange II Site-Directed Mutagenesis kit* (Agilent Technologies) and protocol were used for these purpose according to the manufacturer's instructions.

The primers designed followed the parameters suggested on the instruction manual of the *QuikChange II Site-Directed Mutagenesis kit* (Agilent Technologies) and were synthesized by *Sigma* (Table I for primer sequences).

2.3.7.1. PCR for Site-directed mutagenesis

C1000™ Thermal Cycler (BIO RAD) was used in the PCR for site-directed mutagenesis.

For site-directed mutagenesis total reaction mixtures of 50 μL were set up using water, 2.5 units of *PfuUltra* HF DNA polymerase (Agilent Technologies), 10x (1 c. c. final) of reaction buffer (Agilent Technologies), 1 μL of provided dNTPs mix, 0.2 μM of each primer forward and reverse and 50 ng of dsDNA, in this case pDendra2-C Vector.

The PCR for single amino acid changes (replacement of ATG for GGG codon) was carried out with an initial denaturation step of 95°C for 30 sec, followed by 16 cycles of 95°C for 30 sec, 55°C for 1 min and 68°C for 5 min. For multiple amino acid deletions (deletion of 7 nucleotides) or insertion (insertion of *stop* codon) the PCR was carried out with an initial denaturation step of 95°C for 30 sec, followed by 18 cycles of 95°C for 30 sec, 55°C for 1 min and 68°C for 5 min.

2.3.7.2. Digestion of methylated DNA

The samples were then put into ice for 2 min to cool the reaction to 37°C and added 10 units of *Dpn*I to

each amplification reaction. After gently mixing, each reaction was incubated at 37ºC for 1 hour to digest the parental, nonmutated and methylated supercoiled dsDNA.

The bacterial transformation was done as explained on section 2.3.1. and 1 to 4 µL of the *Dpn*I-treated DNA was used.

Table I – Oligonucleotide sequences

Oligo	5' or 3' primer	Oligonucleotide sequence	Comments
3'UTRa CaMKIIα Forward	5'	AGATCGTCCACTTCCACAGATC	Amplify first 2116 bp of 3'UTR of CaMKIIα from cDNA for cloning in pDrive Cloning Vector
3'UTRa CaMKIIα Reverse	3'	GGTTCTGGGGCAGGACAAGGGCCC	Amplify first 2116 bp of 3'UTR of CaMKIIα from cDNA for cloning in pDrive Cloning Vector; *Apa*I site underline
3'UTRa2 CaMKIIα Forward	5'	GATCCTCGAGAAGGACCAGGCCAG	Amplify first 2116 bp of 3'UTR of CaMKIIα from pDNA inserting *Xho*I site (underline) for cloning in pDendra2-C Vector
3'UTRb CaMKIIα Forward	5'	CAAGAATGGGCCCTTGTCCTGC	Amplify last 1298 bp of 3'UTR of CaMKIIα from cDNA/pDNA for cloning in pDrive Cloning Vector or pDendra2-C Vector; *Apa*I site underline
3'UTRb CaMKIIα Reverse	3'	GACTCCGCGGTTCCAATCCATAGGA	Amplify last 1298 bp of 3'UTR of CaMKIIα from pDNA inserting *Sac*II site (underline) for cloning in pDendra2-C Vector
3'UTRb2 CaMKIIα Reverse	3'	CGCGGATCCTTCCAATCCATAGGACCAGGAC	Amplify last 1298 bp of 3'UTR of CaMKIIα from pDNA inserting *Bam*HI site (underline) for cloning in pDendra2-C Vector
5'UTR GluA1 Forward	5'	GTAAGCGCTGAAGAATCAAAGGGAGGG	Amplify 5'UTR and ORF of GluA1 inserting *Age*I site (underline) for cloning in pDendra2-C Vector
5'UTR GluA1 Reverse	3'	GTAAGCGCTGTACAATCCTGTGGCTCC	Amplify 5'UTR and ORF of GluA1 inserting *Afe*I site (underline) for cloning in pDendra2-C Vector; Red: mutated STOP codon

3'UTR GluA1 Forward	5'	GTACTCGAGCTGGAGCAGACAGGAAAC	Amplify 3'UTR of GluA1 inserting *Xho*I site (underline) for cloning in pDendra2-C Vector
3'UTR GluA1 Reverse	3'	GTACCGCGGAATGGGTCCACAGTGATTTAATTC	Amplify 3'UTR of GluA1 inserting *Sac*II site (underline) for cloning in pDendra2-C Vector
5'UTRCalmodulin Forward	5'	GTAAGCGCTGGGAGTCTCGTGTCCGTGGTG	Amplify 5'UTR and ORF of Calmodulin for cloning in pDendra2-C Vector; Underline is AfeI site
5'UTRCalmodulin Reverse	3'	GTAACCGGTCCATTTTGCAGTCATCATCTG	Amplify 5'UTR and ORF of Calmodulin; Underline is AgeI site for cloning in pDendra2-C Vector; Red: changed stop codon
3'UTRCalmodulin Forward	5'	GTACTCGAGAGACCTACTTTCAACTACTTTTCC	Amplify 3'UTR of Calmodulin inserting *Xho*I site (underline) for cloning in pDendra2-C Vector
3'UTRCalmodulin Reverse	3'	GTACCGCGGAAGGCTGCAGAAATGTTTATTG	Amplify 3'UTR of Calmodulin inserting *Sac*II site (underline) for cloning in pDendra2-C Vector
5'UTR Arc Forward	5'	CTAACCGGTGCGAGTTCTCCCGCAGCCGCA	Amplify 5'UTR and ORF of Arc inserting *Age*I site (underline) for cloning in pDendra2-C Vector
5'UTR Arc Reverse	3'	CTGACCGGTCTATTCAGGCTGGGTCCTGTC	Amplify 5'UTR and ORF of Arc inserting *Age*I site (underline) for cloning in pDendra2-C Vector ; Red: mutated STOP codon
3'UTR Arc Forward	5'	CCGCTCGAGAGGGGCCAGCCCAGGGTCCCC	Amplify 3'UTR of Arc inserting *Xho*I site (underline) for cloning in pDendra2-C Vector
3'UTR Arc Reverse	3'	CCGCTCGAGAAGTTTCATAGTTTTATTAAC	Amplify 3'UTR of Arc inserting *Xho*I site (underline) for cloning in pDendra2-C Vector
Mut Dendra2C Forward	5'	GCGCTACCGGTCGCCACCGGGAACACCCCGGGAATTAAC	Mutagenesis of ATG from Dendra2-C ORF; Blue: mutated codon
Mut Dendra2C Reverse	3'	GTTAATTCCCGGGGTGTTCCCGGTGGCGACCGGTAGCGC	Mutagenesis of ATG from Dendra2-C ORF; Blue: mutated codon
Mut EL Forward	5'	GCTAGCGCTACCGGTGGGAACACCCCGGG	Mutagenesis to eliminate 7 nucleotides before ORF of Dendra2 to put *in frame* the restriction sites of *Afe*I and *Age*I sites (underline)

Mut EL Reverse	3’	CCCGGGGTGTTCCCACCGGTAGCGCTAGC	Mutagenesis to eliminate 7 nucleotides before ORF of Dendra2 to put *in frame* the restriction sites of *Afe*I and *Age*I sites (underline)
Mut STOP	5’	GCCCAGCCAGGTGTAAGGTCCGGCGACAGCG	Mutagenesis to insert *stop* codon after ORF od Dendra2; Purple: nucleotides inserted
Mut STOP	3’	CGCTGTCGCCGGACCTTACACCTGGCTGGGC	Mutagenesis to insert *stop* codon after ORF od Dendra2; Purple: nucleotides inserted
M13 Forward	5'	AACAGCTATGACCATG	Check orientation of PCR product inserted in pDrive Cloning Vector
M13 Reverse	3'	GTTTTCCCAGTCACGAC	Check orientation of PCR product inserted in pDrive Cloning Vector
cD2C Forward	5'	GCTGGTTTAGTGAACCGTC	Check orientation of PCR product inserted in 5’ side of pDendra2-C Vector
cD2C Reverse	3'	CTACAAATGTGGTATGGCTG	Check orientation of PCR product inserted in 3’ side (MCS) of pDendra2-C Vector

2.3.8. DNA purification

The DNA purification methods were used to purify PCR products as well as to clean digested plasmids and fragments.

2.3.8.1. Purification of PCR products using QIAquick PCR Purification Kit (QIAGEN)

The *QIAquick PCR Purification Kit* (QIAGEN) and protocol were used for purification of PCR products according to the manufacturer’s instructions. This method was employed when pure DNA samples were required.

2.3.8.2. DNA purification from agarose gels

2.3.8.2.1. QIAEX II Gel Extraction Kit (QIAGEN)

The *QIAEX II Gel Extraction Kit* (QIAGEN) and protocol were used for purification of DNA fragments from agarose gels according to the manufacturer's instructions. This method was employed when pure DNA samples were required.

2.3.8.2.2. QIAquick Gel Extraction Kit (QIAGEN)

The *QIAquick Gel Extraction Kit* (QIAGEN) and protocol were used for purification of DNA fragments from agarose gels according to the manufacturer's instructions. This method was employed when pure DNA samples were required.

2.3.9. Restriction digestion with endonucleases

2.3.9.1. Plasmid DNA

To linearize plasmids for cloning procedures an amount of 2 μg of plasmid DNA was digested at 37ºC or 25ºC during 2 hours, in a total volume of 100 μL, containing 20 units of restriction enzyme and 10 x (1 x final c.c.) restriction buffer. The enzymes were heat inactivated at 65ºC for 20 min and the mixture purified as described on section 2.3.8.1.

To separate fragments from plasmid DNA (pDrive Cloning Vector) for following cloning in different vector (pDendra2-C) an amount of 2 μg of plasmid DNA was digested at 37ºC during 2 hours, in a total volume of 100 μL, containing 20 units of restriction enzyme and 10 x (1 x final c.c.) restriction buffer. The enzymes were heat inactivated at 65ºC for 20 min and the mixture purified as described on section 2.3.8.2.2.

2.3.9.2. PCR product

To digest PCR products for cloning procedures, 2 μg of amplified PCR product was digested at 37ºC during 2 hours, in a total in a total volume of 100 μL, containing 20 units of restriction enzyme and 10 x (1 x final c.c.) restriction buffer. The enzymes were heat inactivated at 65ºC for 20 min and the mixture purified as described on section 2.3.8.1.

2.3.10. Ligation reaction: T4 DNA ligase

To set up the ligation reactions, a molar ratio of purified insert:purified vector of 3:1 was used for cohesive (sticky) end ligation reactions and 5:1 for blunt end ligation reactions, preferentially. The total reaction mixtures of 20 μL were set up using 10 x (1 x final c.c.) T4 DNA ligase buffer [50 mM Tri-HCl, 10 mM $MgCl_2$, 10 mM DTT, 1 mM ATP, pH 7.5], the appropriate volume of insert and vector, 20 units of T4 DNA ligase (New England Biolabs), and water. After mixing carefully with pipette, the reactions were incubated at room temperature for 2 hours (for cohesive ends) or at 16ºC overnight (for blunt ends). The reaction mixture was then transformed in *E. coli* DH5α competent cells, as described on section 2.3.1., and plated in appropriate medium. A colony-PCR was then conducted, as described on section 2.3.6.8., to confirm the presence and orientation of plasmid inserts.

2.3.11. Cloning procedures

2.3.11.1. Cloning into the commercial pDrive Cloning Vector using QIAGEN PCR Cloning Kit

The *QIAGEN®PCR Cloning Kit* (QIAGEN) and protocol were used to insert PCR products in the supplied pDrive Cloning Vector (Appendix I) in a very fast, easy and highly efficient way. This kit takes advantage of the single A overhang at each end of PCR products generated by *Taq* and other non-proofreading DNA polymerases.

Once we used a proofreading DNA polymerase to generate the PCR products we did an additional reaction to add the single A overhang at each end of PCR products. The total reaction mixtures of 40 μL were set up in water, 5 units of *DreamTaq* DNA polymerase (Thermo Scientific), 10 x (0.5 x final c.c.) *DreamTaq™ Buffer* (20 mM $MgCl_2$) (Thermo Scientific), 5 μM dNTPs, 16 μL of PCR reaction and were incubated at 72ºC during 30 min.

This strategy was used to clone the 5'UTR and open reading frame (ORF) of GluA1, the 5'UTR of CaMKIαI and the first 2116 bp of 3'UTR of CaMKIIα into the pDrive Cloning Vector.

2.3.11.1.1. Cloning of 5'UTR and ORF of GluA1 into pDrive Cloning Vector

5'UTR and ORF of GluA1 was amplified (see section 2.3.6.2.) using the primers listed in Table I with annealing temperature of 57.8ºC. Samples were loaded in a 0.8% agarose gel (see section 2.3.5.) and amplified fragment purified from agarose gel as explained on section 2.3.8.2.1. This purified PCR product was then

inserted in pDrive Cloning Vector as explained on section 2.3.11.1.1.

2.3.11.1.2. Cloning of 5'UTR of CaMKIIα into pDrive Cloning Vector

5'UTR of CaMKIIα was amplified (see section 2.3.6.5.) using the primers listed in Table I with annealing temperature of 55ºC. Samples were loaded in a 1.8% agarose gel (see section 2.3.5.) and amplified fragment purified from agarose gel as explained on section 2.3.8.2.1. This purified PCR product was then inserted in pDrive Cloning Vector as explained on section 2.3.11.1.2.

2.3.11.1.3. Cloning of first 2116 bp of 3'UTR of CaMKIIα into pDrive Cloning Vector

The first 2116 bp of 3'UTR of CaMKIIα was amplified (see section 2.3.6.5.) using the primers listed in Table I with annealing temperature of 62.6ºC. Samples were loaded in a 0.8% agarose gel (see section 2.3.5.) and amplified fragment purified from agarose gel as explained on section 2.3.8.2.1. This purified PCR product was then inserted in pDrive Cloning Vector as explained on section 2.3.11.1.3.

2.3.11.2. Cloning into the pDendra2-C Vector

To construct a probe with a native protein (5'UTR, ORF and 3'UTR) fused with a fluorescent protein we used the pSTOP Mut EL Dendra2-C Vector (Appendix II) while for the construct with only the UTRs of CaMKIIα the pSTOP Dendra2-C Vector was used. 5'UTR, ORF, first 2116 bp of 3'UTR and last 1298 bp of 3'UTR of CaMKIIα, 5'UTR, ORF and 3'UTR of Calmodulin, 5'UTR, ORF and 3'UTR of Arc, 5'UTR, ORF and 3'UTR of GluA1 and 5'UTR, ORF and 3'UTR of N-cadherin, were cloned by amplification, restriction digestion and ligation into the pDendra2-C Vector.

2.3.11.2.1. pDendra2-C Vector digestion

2 to 10 µg of site-directed mutated Dendra2-C Vector was linearized at 37ºC or 25ºC for 2 to 6 hours, in the reaction mixtures described in section 2.3.9.1. The enzymes were heat inactivated at 65ºC for 20 min. The digestion reaction was loaded in a 0.8% agarose gel (see section 2.3.5.)to confirm that it was digested and thereafter purified as explained in section 2.3.8.1.

2.3.11.2.2. Cloning of first 2116 bp of 3'UTR of CaMKIIα into STOP EL Mut Dendra2-C and STOP Dendra2-C Vector

First 2116 bp of 3'UTR of CaMKIIα was already cloned into pDrive Cloning Vector and it was used as template for the following PCR. The first 2116 bp of 3'UTR of CaMKIIα was amplified (see section 2.3.6.2.) using the primers listed in Table I with annealing temperature of 65ºC. Samples were loaded in a 0.8% agarose gel (see section 2.3.5.) and amplified fragment purified from agarose gel as explained on section 2.3.8.1.

6 µg of first 2116 bp of 3'UTR of CaMKIIα was digested (see section 2.3.9.1.) using *Apa*I (2 hours at 25ºC) and *Xho*I (2 hours at 37ºC) as endonucleases restriction enzymes. The enzymes were heat inactivated at 65ºC for 20 min. The digestion reaction was loaded in a 0.8% agarose gel (see section 2.3.5.) to confirm that it was digested and thereafter purified from agarose gel as explained in section 2.3.8.1.

The ligation reaction was carried out as described in section 2.3.10. To 100 ng of pSTOP Dendra2-C Vector or 100 ng of pSTOP EL Mut Dendra2-C Vector (4.7 Kb), 300 ng of first 2116 bp of CaMKIIα (2.1 Kb) were used. Reactions were incubated for 2 hours at room temperature and then transformed in *E. coli* DH5α competent cells (using half of total volume of ligation reaction) (see section 2.3.1.) and plated in solid LB plus kanamycin (50 µg/mL). Positive colonies were screened using colony PCR (section 2.3.6.8.). The primers used in the colony PCR were the 3'UTRa2 CaMKIIα forward and the cD2C reverse (Table I). The PCR samples were resolved by electrophoretic separation (see section 2.3.5.), bands visualized on a UV Trans Illuminator (Gel Doc™XR+ (*BIO-RAD*)) and photographed. The plasmids of positive clones (vector with the insert in the right direction) were isolated (see section 2.3.4.2.) and digested again (see section 2.3.9.1.) to confirm the presence of inserted fragment and size of STOP Dendra2-C and STOP EL Mut Dendra2-C Vector. The plasmids of positive clones were isolated (see section 2.3.4.2.) and sent for sequencing (STABvida sequencing services).

2.3.11.2.3. Cloning of last 1298 bp of 3'UTR of CaMKIIα into STOP EL Mut Dendra2-C and STOP Dendra2-C Vector

Last 1298 bp of CaMKIIα was amplified (see section 2.3.6.6.followe by 2.3.6.7.) using the primers listed in Table I with annealing temperature of 50ºC. Samples were loaded in a 0.8% agarose gel (see section 2.3.5.) and amplified fragment purified from agarose gel as explained on section 2.3.8.1.

6 µg of last 1298 bp of CaMKIIα was digested (see section 2.3.9.2.) using *Apa*I and *Bam*HI as endonucleases restriction enzymes for 2 hours at 37ºC. The enzymes were heat inactivated at 65ºC for 20

min. The digestion reaction was purified as explained in section 2.3.8.1.

The ligation reaction was carried out as described in section 2.3.10. To 100 ng of STOP Dendra2-C Vector or 100 ng of STOP EL Mut Dendra2-C Vector (4.7 Kb), 300 ng of last 1298 bp of CaMKIIα (1.2 Kb) were used. Reactions were incubated at at room temperature during 2 hours and then transformed in *E. coli* DH5α competent cells (using half of total volume of ligation reaction) (see section 2.3.1.) and plated in solid LB plus kanamycin (50 µg/mL). Positive colonies were screened using colony PCR (section 2.3.6.8.). The primers used in the colony PCR were the 3'UTRb CaMKIIα forward and the cD2C reverse (Table I). The PCR samples were resolved by electrophoretic separation (see section 2.3.5.), bands visualized on a UV Trans Illuminator (Gel Doc™XR+ (*BIO-RAD*)) and photographed. The plasmids of positive clones (vector with the insert in the right direction) were isolated (see section 2.3.4.2.) and digested again (see section 2.3.9.1.) to confirm the presence of inserted fragment and size of STOP Dendra2-C and STOP EL Mut Dendra2-C Vector.. The plasmids of positive clones were isolated (see section 2.3.4.2.) and sent for sequencing (STABvida sequencing services).

2.3.11.2.4. Cloning of 3'UTR of CaMKIIα into STOP EL Mut Dendra2-C Vector

Once the first 2116 bp and the last 1298 bp of 3'UTR of CaMKIIα were cloned into STOP EL Mut Dendra2-C Vector 4-6 µg of both plasmids were digested (see section 2.3.9.1.). The STOP EL Mut Dendra2-C-2116 bp Vector was digested with *Apa*I and *Bam*HI to linearize the plasmid and the STOP EL Mut Dendra2-C-1298 bp Vector was digested with *Apa*I and *Bam*HI endonucleases to remove the fragment of interest. The enzymes were heat inactivated at 65ºC for 20 min. The digestion reaction was loaded in a 0.8% agarose gel (see section 2.3.5.) to confirm that it was digested. Thereafter the STOP EL Mut Dendra2-C-2116 bp Vector was purified as explained in section 2.3.8.1. and the fragment 1298 bp was purified from agarose gel as explained in section 2.3.8.1.

The ligation reaction was carried out as described in section 2.3.10. To 85 ng of STOP EL Mut Dendra2-C-2116 bp Vector (6.8 Kb), 250 ng of 1298 bp of 3'UTR of CaMKIIα (1298 bp) were used. Reactions were incubated at room temperature during 2 hours and then transformed in *E. coli* DH5α competent cells (using half of total volume of ligation reaction) (see section 2.3.1.) and plated in solid LB plus kanamycin (50 µg/mL). Positive colonies were screened using colony PCR (section 2.3.6.8.). The primers used in the colony PCR were the 3'UTRa2 CaMKIIα forward and the cD2C reverse (Table I). The PCR samples were resolved by electrophoretic separation (see section 2.3.5.), bands visualized on a UV Trans Illuminator (Gel Doc™XR+ (*BIO-RAD*)) and photographed. The plasmids of positive clones (vector with the insert in the right direction) were isolated (see section 2.3.4.2.) and digested again (see section 2.3.9.1.) to confirm the presence of inserted fragment and size of STOP Dendra2-C and STOP EL Mut Dendra2-C Vector. The

plasmids of positive clones were isolated (see section 2.3.4.2.) and sent for sequencing (STABvida sequencing services).

2.3.11.2.5. Cloning of 3'UTR of CaMKIIα into STOP Dendra2-C Vector

Once the first 2116 bp and the last 1298 bp of 3'UTR of CaMKIIα were cloned into pSTOP Dendra2-C Vector 4-6 µg of both plasmids were digested (see section 2.3.9.1.). The pSTOP Dendra2-C-2116 bp Vector was digested with *Apa*I and *Bam*HI to linearize the plasmid and the pSTOP Dendra2-C-1298 bp Vector was digested with *Apa*I and *Bam*HI endonucleases to remove the fragment of interest. The enzymes were heat inactivated at 65ºC for 20 min. The digestion reaction was loaded in a 0.8% agarose gel (see section 2.3.5.) to confirm that it was digested. Thereafter the pSTOP Dendra2-C-2116 bp Vector was purified as explained in section 2.3.8.1. and the fragment 1298 bp was purified from agarose gel as explained in section 2.3.8.2.

The ligation reaction was carried out as described in section 2.3.10. To 90 ng of pSTOP Dendra2-C-2116 bp Vector (6.8 Kb), 270 ng of 1298 bp of 3'UTR of CaMKIIα (1298 bp) were used. Reactions were incubated at room temperature during 2 hours and then transformed in *E. coli* DH5α competent cells (using half of total volume of ligation reaction) (see section 2.3.1.) and plated in solid LB plus kanamycin (50 µg/mL). Positive colonies were screened using colony PCR (section 2.3.6.8.). The primers used in the colony PCR were the 3'UTRb CaMKIIα forward and the cD2C reverse (Table I). The PCR samples were resolved by electrophoretic separation (see section 2.3.5.), bands visualized on a UV Trans Illuminator (Gel Doc™XR+ (*BIO-RAD*)) and photographed. The plasmids of positive clones (vector with the insert in the right direction) were isolated (see section 2.3.4.2.) and digested again (see section 2.3.9.1.) to confirm the presence of inserted fragment and size of STOP Dendra2-C Vector. The plasmids of positive clones were isolated (see section 2.3.4.1.) and sent for sequencing (STABvida sequencing services).

2.3.11.2.6. Cloning of 5'UTR and ORF of Calmodulin into STOP EL Mut Dendra2-C Vector

5'UTR and ORF of Calmodulin was amplified (see section 2.3.6.2.) using the primers listed in Table I with annealing temperature of 65ºC. Samples were loaded in a 0.8% agarose gel (see section 2.3.5.) and amplified fragment purified as explained on section 2.3.8.1.

2 µg of 5'UTR and ORF of Calmodulin was digested (see section 2.3.9.1.) using *Afe*I and *Age*I as endonucleases restriction enzymes for 2 hours at 37ºC. The enzymes were heat inactivated at 65ºC for 20 min. The digestion reaction was purified as explained in section 2.3.8.1.

The ligation reaction was carried out as described in section 2.3.10. To 100 ng of STOP EL Mut Dendra2-C

Vector (4.7 Kb), 500 ng of 5'UTR and ORF of Calmodulin (600 bp) were used. Reactions were incubated at 16ºC overnight and then transformed in *E. coli* DH5α competent cells (using half of total volume of ligation reaction) (see section 2.3.1.) and plated in solid LB plus kanamycin (50 μg/mL). Positive colonies were screened using colony PCR (section 2.3.6.8.). The primers used in the colony PCR were the cD2C forward and the 5'UTR Calmodulin reverse (Table I). The PCR samples were resolved by electrophoretic separation (see section 2.3.5.), bands visualized on a UV Trans Illuminator (Gel Doc™XR+ (*BIO-RAD*)) and photographed. The plasmids of positive clones (vector with the insert in the right direction) were isolated (see section 2.3.4.2.) and digested again (see section 2.3.9.1.) to confirm the presence of inserted fragment and size of STOP EL Mut Dendra2-C Vector. The plasmids of positive clones were isolated (see section 2.3.4.2.) and sent for sequencing (STABvida sequencing services).

2.3.11.2.7. Cloning of 3'UTR of Calmodulin into 5'UTR+ORF Calmodulin-STOP EL Mut Dendra2-C Vector

3'UTR of Calmodulin was amplified (see section 2.3.6.3.) using the primers listed in Table I with annealing temperature of 55ºC. Samples were loaded in a 0.8% agarose gel (see section 2.3.5.) and amplified fragment purified as explained on section 2.3.8.2. 0.5 μg of 3'UTR of Calmodulin was digested (see section 2.3.9.1.) using *Xho*I and *Sac*II as endonucleases restriction enzymes for 2 hours at 37ºC and the were enzymes heat inactivated for 20 min at 65ºC. The digestion reaction was purified as explained in section 2.3.8.1.

2 μg 5'UTR+ORF Calmodulin STOP EL Mut Dendra2-C Vector plasmid was digested with *Xho*I and *Sac*II (see section 2.3.9.1.) also for 2 hours at 37ºC to be linearized. The enzymes were heat inactivated at 65ºC for 20 min. The digestion reaction was loaded in a 0.8% agarose gel (see section 2.3.5.) to confirm that it was digested and thereafter the p5'UTR+ORF Calmodulin STOP EL Mut Dendra2-C Vector was purified as explained in section 2.3.8.1.

The ligation reaction was carried out as described in section 2.3.10. To 53 ng of 5'UTR+ORF Calmodulin STOP EL Mut Dendra2-C Vector (5.3 Kb), 160 ng of 3'UTR of Calmodulin (3378 bp) were used. Reactions were incubated at room temperature during 2 hours and then transformed in *E. coli* DH5α competent cells (using half of total volume of ligation reaction) (see section 2.3.1.) and plated in solid LB plus kanamycin (50 μg/mL). Positive colonies were screened using colony PCR (section 2.3.6.8.). The primers used in the colony PCR were the 3'UTR Calmodulin forward and the cD2C reverse (Table I). The PCR samples were resolved by electrophoretic separation (see section 2.3.5.), bands visualized on a UV Trans Illuminator (Gel Doc™XR+ (*BIO-RAD*)) and photographed. The plasmids of positive clones (vector with the insert in the right direction) were isolated (see section 2.3.4.2.) and digested again (see section 2.3.9.1.) to confirm the presence of inserted fragment and size of 5'UTR+ORF Calmodulin-STOP EL Mut Dendra2-C Vector. The

plasmids of positive clones were isolated (see section 2.3.4.1.) and sent for sequencing (STABvida sequencing services).

2.3.11.2.8. Cloning of 5'UTR and ORF of Arc into STOP EL Mut Dendra2-C Vector

5'UTR and ORF of Arc was amplified (see section 2.3.6.2.) using the primers listed in Table I with annealing temperature of 68ºC. Samples were loaded in a 0.8% agarose gel (see section 2.3.5.) and amplified fragment purified as explained on section 2.3.8.1.

4 µg of 5'UTR of Calmodulin was digested (see section 2.3.9.1.) using *Nhe*I as endonucleases restriction enzymes for 2 hours at 37ºC. The enzymes were heat inactivated at 65ºC for 20 min. The digestion reaction was purified as explained in section 2.3.8.1.

The ligation reaction was carried out as described in section 2.3.10. To 100 ng of STOP Mut EL Dendra2-C Vector (4.7 Kb), 300 ng of 5'UTR of Calmodulin (1.4 Kb) were used. Reactions were incubated for 2 hours at room temperature and then transformed in *E. coli* DH5α competent cells (using half of total volume of ligation reaction) (see section 2.3.1.) and plated in solid LB plus kanamycin (50 µg/mL). Positive colonies were screened using colony PCR (section 2.3.6.8.). The primers used in the colony PCR were the cD2C forward and the 5'UTR Arc reverse (Table I). The PCR samples were resolved by electrophoretic separation (see section 2.3.5.), bands visualized on a UV Trans Illuminator (Gel Doc™XR+ (*BIO-RAD*)) and photographed. The plasmids of positive clones (vector with the insert in the right direction) were isolated (see section 2.3.4.2.) and digested again (see section 2.3.9.1.) to confirm the presence of inserted fragment and size of STOP EL Mut Dendra2-C Vector. The plasmids of positive clones were isolated (see section 2.3.4.2.) and sent for sequencing (STABvida sequencing services).

2.3.11.2.9. Cloning of 3'UTR of Arc into 5'UTR+ORF Arc-STOP EL Mut Dendra2-C Vector

3'UTR of Arc was amplified (see section 2.3.6.2.) using the primers listed in Table I with annealing temperature of 61ºC. Samples were loaded in a 0.8% agarose gel (see section 2.3.5.) and amplified fragment purified as explained on section 2.3.8.1.

2 µg of 3'UTR of Arc was digested (see section 2.3.9.1.) using *Xho*I as endonucleases restriction enzymes for 2 hours at 37ºC. The enzymes were heat inactivated at 65ºC for 20 min. The digestion reaction was purified as explained in section 2.3.8.1.

The ligation reaction was carried out as described in section 2.3.10. To 100 ng of 5'UTR+ORF Arc -STOP Mut EL Dendra2-C Vector (6.1 Kb), 300 ng of 3'UTR of Arc (1.7 Kb) were used. Reactions were incubated

for 2 hours at room temperature and then transformed in *E. coli* DH5α competent cells (using half of total volume of ligation reaction) (see section 2.3.1.) and plated in solid LB plus kanamycin (50 µg/mL). Positive colonies were screened using colony PCR (section 2.3.6.8.). The primers used in the colony PCR were the 3'UTR Arc forward and the cD2C reverse (Table I). The PCR samples were resolved by electrophoretic separation (see section 2.3.5.), bands visualized on a UV Trans Illuminator (Gel Doc™XR+ (*BIO-RAD*)) and photographed. The plasmids of positive clones (vector with the insert in the right direction) were isolated (see section 2.3.4.2.) and digested again (see section 2.3.9.1.) to confirm the presence of inserted fragment and size of 5'UTR+ORF Arc-STOP EL Mut Dendra2-C Vector. The plasmids of positive clones were isolated (see section 2.3.4.1.) and sent for sequencing (STABvida sequencing services).

2.3.11.2.10. Cloning of 5'UTR and ORF of GluA1 into STOP EL Mut Dendra2-C Vector

5'UTR and ORF of GluA1 was already cloned into pDrive Cloning Vector so 4 µg of pDrive Cloning Vector-5'UTR of GluA1 was digested (see section 2.3.9.1.) using *Afe*I as endonucleases restriction enzymes for 2 hours at 37°C. The enzymes were heat inactivated at 65°C for 20 min. The digestion reaction was loaded in a 0.8% agarose gel (see section 2.3.5.) to confirm that it was digested and thereafter purified from agarose gel as explained in section 2.3.8.2.2.

The ligation reaction was carried out as described in section 2.3.10. To 100 ng of STOP EL Mut Dendra2-C Vector (4.7 Kb), 500 ng of 5'UTR and ORF of GluA1 (2.8 Kb) were used. Reactions were incubated at 16°C overnight and then transformed in *E. coli* DH5α competent cells (using half of total volume of ligation reaction) (see section 2.3.1.) and plated in solid LB plus kanamycin (50 µg/mL). Positive colonies were screened using colony PCR (section 2.3.6.8.). The primers used in the colony PCR were the cD2C forward and the 5'UTR GluA1 reverse (Table I). The PCR samples were resolved by electrophoretic separation (see section 2.3.5.) and bands visualized on a UV Trans Illuminator (Gel Doc™XR+ (*BIO-RAD*)) and photographed. The plasmids of positive clones (vector with the insert in the right direction) were isolated (see section 2.3.4.2.) and digested again (see section 2.3.9.1.) to confirm the presence of inserted fragment and size of STOP EL Mut Dendra2-C Vector. The plasmids of positive clones were isolated (see section 2.3.4.2.) and sent for sequencing (STABvida sequencing services).

2.3.11.2.11. Cloning of 3'UTR of GluA1 into 5'UTR+ORF GluA1-STOP EL Mut Dendra2-C Vector

3'UTR of GluA1 was amplified (see section 2.3.6.2.) using the primers listed in Table I with annealing temperature of 60°C. Samples were loaded in a 0.8% agarose gel (see section 2.3.5.) and amplified fragment

purified as explained on section 2.3.8.1.

2 μg of 3'UTR of GluA1 was digested (see section 2.3.9.1.) using *Xho*I and *Sac*II as endonucleases restriction enzymes for 2 hours at 37ºC. The enzymes were heat inactivated at 65ºC for 20 min. The digestion reaction was purified as explained in section 2.3.8.1.

4 μg 5'UTR+ORF GluA1-STOP EL Mut Dendra2-C Vector plasmid was digested with *Xho*I and *Sac*II (see section 2.3.9.1.) also for 2 hours at 37ºC to be linearized. The enzymes were heat inactivated at 65ºC for 20 min. The digestion reaction was loaded in a 0.8% agarose gel (see section 2.3.5.) to confirm that it was digested and thereafter the 5'UTR+ORF GluA1-STOP EL Mut Dendra2-C Vector was purified as explained in section 2.3.8.1.

The ligation reaction was carried out as described in section 2.3.10. To 100 ng of 5'UTR+ORF GluA1-STOP Mut EL Dendra2-C Vector- (7.5 Kb), 300 ng of 3'UTR of GluA1 (2.8 Kb) were used. Reactions were incubated for 2 hours at room temperature and then transformed in *E. coli* DH5α competent cells (using half of total volume of ligation reaction) (see section 2.3.1.) and plated in solid LB plus kanamycin (50 μg/mL). Positive colonies were screened using colony PCR (section 2.3.6.8.). The primers used in the colony PCR were the 3'UTR GluA1 forward and the cD2C reverse (Table I). The PCR samples were resolved by electrophoretic separation (see section 2.3.5.), bands visualized on a UV Trans Illuminator (Gel Doc™XR+ (*BIO-RAD*)) and photographed. The plasmids of positive clones (vector with the insert in the right direction) were isolated (see section 2.3.4.2.) and digested again (see section 2.3.9.1.) to confirm the presence of inserted fragment and size of 5'UTR+ORF GluA1-STOP EL Mut Dendra2-C Vector. The plasmids of positive clones were isolated (see section 2.3.4.1.) and sent for sequencing (STABvida sequencing services).

2.4. Cell Culture and Transfection

2.4.1. Dissociated hippocampal primary culture

2.4.1.1. Glass coverslip preparation

To prepare the glass coverslips for primary hippocampal neuron culture, the coverslips were drop onto 100 mL 95% ethanol and shacked for several days, changing the ethanol each day. After at least four days, the coverslips were let to dry inside the 6-well or 12-well plate during some hours and then poured some drops of 0.1 mg/mL poly-D-lysine (PDL) on top of the coverslips. The coverslips were incubated overnight at room temperature with PDL.

In the following day the coverslips were washed at least 6 times with sterile milli-Q water and let dry for 2 hours. 1 μg/mL laminin was then poured into the coverslips and let to incubate at 37ºC for at least 3 hours. Then the coverslips were washed 6 times with PBS, 2 times with Hanks Plus [10 mM HEPES, 33.3 mM D-

glucose, 1x Penicillin/Streptomycin, in HBSS] filtered solution, wrapped in aluminum paper and store at 4ºC for at maximum 1 month.

2.4.1.2. Dissection, digestion and collection of hippocampal neurons

To do primary hippocampal neuron culture P0-1 C57BL/6 mice were used. The mice were sacrifice and the hippocampus removed using a dissection microscope. Then, the hippocampus were chopped into pieces and put in 15 mL tube with Dissection medium (DM) with Ca^{2+} [Hanks Plus, 0.3% BSA, 12 mM $MgSO_4$, 2mM $CaCl_2$].

After that the cells were centrifuged for 1 min at 1000 rpm, washed in 10 mL of Hanks Plus, centrifuged again, the supernatant aspirated and incubated with pre-warmed filtered DS1 solution [35 mg trypsin, 1 mg DNase, 2.5 mL Digestion solution [4.2 mM $NaHCO_3$, 25 mM HEPES, 137 mM NaCl, 5 mM KCl, 7 mM Na_2HPO_4, in sterile ddH_2O]] for 6 min at 37ºC, periodically agitating. Then the cells were centrifuged, the supernatant aspirated and the cells mixed with pre-warmed filtered DM+TI [20 mg Trypsin inhibitor, 3 mL DM without Ca^{2+}] and incubated for 2 min at 37ºC. After incubation, the cells were centrifuged again, the supernatant removed and the cells washed with 10 mL ice-cold DM without Ca^{2+} [Hanks Plus, 0.3% BSA, 12 mM $MgSO_4$]. The cells were centrifuged again, the supernatant removed and the cells mixed with DM+DNase [0.5 mg DNase, 2 mL ice-cold DM without Ca^{2+}]. Using fire-polished pipettes of three different diameters the cells were triturated until no piece of hippocampus was seen. The cells were counted [mix 20 µL of trypan-blue with 5 µL of cell suspension], plated in a chosen volume of plating medium [1x B27 supplement, 1x glutamax, 1x Penicillin/Streptomycin, 5% Fetal Bovine Serum heat-inactivated, in neurobasal medium A] and kept at 37ºC. The cells were followed to analyze its state and control the glial proliferation.

During the first week the media was not changed. On the DIV 7 the medium was changed to culture media [1x B27 supplement, 1x glutamax, 1x Penicillin/Streptomycin, in neurobasal A] with 1x ARA-C [2.43 mg cytosine β-D-arabinofuranoside hydrochloride in 10 mL sterile ddH_2O].

2.4.2. Lipofectamine transfection

The dissociated hippocampal primary cultures were transfected with Lipofectamine 2000 (Invitrogen). For transfection of cells in one well of 12-well plate to 50 µL of neurobasal medium A (no serum) was added 1.5 µL of Lipofectamine 2000 and let it sit for 5 min. Meanwhile, to 50 µL of neurobasal medium A was added 1 µg construct DNA. Both solutions were then combined and let sit for 20 min at room temperature. The culture medium in the wells should be removed but kept for later use. Later, 500 µL of neurobasal medium A was added to each well and the mixture added drop-by-drop and incubated at 37ºC for 6 hours. Then, 500 µL

of old medium and 500 µL of new culture medium (culture medium with 1x ARA-C) was added to the plate. For this procedure the cells used were 1-week old.

2.4.3. Organotypic Hippocampal Cultures

Cultured hippocampal slices were prepared from postnatal day 7-10 C57BL/6J mice [245]. Briefly, 350 µm thick slices were made with a chopper in ice-cold ACSF containing 2.5 mM KCl, 26 mM $NaHCO_3$, 1.15 mM NaH_2PO_4, 11 mM D-glucose, 24 mM sucrose, 1 mM $CaCl_2$ and 5 mM $MgCl_2$, and cultured on membranes (Millipore). The slices were maintained in an interface configuration with the organotypic culture media [1x MEM (Invitrogen), 20% horse serum (Invitrogen), GlutaMAX 1 mM (Invitrogen), 27 mM D-glucose, 30 mM HEPES, 6 mM $NaHCO_3$, 1M $CaCl_2$, 1M $MgSO_4$, 1.2% ascorbic acid, 1 µg/ml insulin]. The pH was adjusted to 7.3, and osmolarity adjusted to 300-310 mOsm.

2.4.4. Gene gun transfection

Hippocampal neurons from organotypic slice cultures were transfected using a Helios gene gun (Bio-Rad) after 6-7 days *in vitro* (DIV). Gold beads (10 mg, 1.6 µm diameter, Bio-Rad) were coated with 100 µg of constructs purified as explained on section 2.3.4.1. made for us according to the manufacturer's protocol and delivered biolistically into the slices at 180 psi. Expression is visible 48 hours later using the Zeiss Lumar V12 and the experiments were performed 2–4 days post-transfection.

2.5. Two-photon imaging

Two-photon imaging was performed using a galvanometer-based scanning system (Prairie Technologies) on a BX61WI Olympus microscope, using a Ti:sapphire laser (910 nm for imaging Dendra-2C; Coherent) controlled by PrairieView software. Slices were perfused with oxygenated ACSF [127 mM NaCl, 2.5 mM KCl, 25 mM $NaHCO_3$, 1.25 mM NaH_2PO_4, 25 mM D-glucose, 2 mM $CaCl_2$ y 1 mM $MgCl_2$ (equilibrated with O_2 95%/CO_2 5%)] at room temperature at a rate of 1.5 mL/min. Secondary or tertiary dendrites of pyramidal neurons were imaged using a water immersion objective (60x, 1.0 NA, Olympus LUMPlan FLN) with a digital zoom of 8x or 10x. Images stacks (0.3 µm per section) were collected at 5, 10, 20 min before photoconversion protocol and after protocol the images stacks were collected at 1, 5, 10, 20 and 30 min at a resolution of 1024 x 1024 pixels. At the end of the procedure a stack of the whole cell was collected (1 µm

per section) with a digital zoom of 1x at a resolution of 1024 x 1024 pixels.

2.6. Photoconversion protocol

For this purpose the hippocampal neurons from organotypic slice cultures were transfected with STOP Dendra2-C plasmid and 5'UTR+ORF Calmodulin-STOP EL Mut Dendra2-C-3'UTR Calmodulin plasmids (altered and construct by us, respectively) as explained in section 2.4.4. By previous experience we knew that UV-light (405 nm) is the more efficient than blue-light to convert green fluorescent state into red. To achieve that we exposed the cells to 15 sec of UV-light with ~2 mW power light and image during 30 min (5, 10, 20 and 30 min) to follow the basal changes in translation and degradation of these proteins.

2.7. Translation Stimulation protocol

2.7.1. DHPG

For global stimulation with DHPG (mGluR agonist), 50 μM of DHPG was added to ACSF and circulated at 1.5 mL/min for 5 min. After stimulation protocol the circulation was change again to ACSF and neuron image for 30 min to follow changes in translation promote by this protocol.

2.7.2. Uncaging LTP

For single spine stimulation the protocol used by Govindarajan *et al* was used [156]. 2.5 mM MNI-caged-L-glutamente and 50 μM Forskolin was added to ACSF and circulated at 1.5 mL/min for 2 min. Spine well separated from neighbors was choose to be stimulated using 30 mW laser power at back focal aperture. Thirty 4 ms long pulses at 0.5 Hz were used for stimulation. After stimulation protocol the circulation was change again to ACSF and neuron image for 30 min to follow changes in translation promote by this protocol.

2.8. Analysis of fluorescent intensity and volume changes

The analysis of fluorescent intensity was done using custom software written in Matlab. First, maximum intensity projections (MIPs) for each time point have been calculated from z-stacks and MIPs in different

time points were registered with a cross correlation method. Total fluorescence either at a dendrite or spine was calculated by summing all the values at the region of interest (ROI). After fluorescence intensity analysis we normalized the data to the baseline image and calculated the ratio of green fluorescence state and the ratio of red fluorescence state.

The analysis of volume change was done using full-width at half maximum (FWHM) method to estimate the spine diameter [156] at each time point and assuming that spines are spherical.

Chapter 3. Results and Discussion

3.1. Site-directed Mutagenesis of pDendra2-C vector

The aim of our study is to track dendritically synthesized proteins after synaptic activity in order to determine what is their contribution to neuronal plasticity at the level of single spines. As dendritically localized mRNA have been proposed to be available for use upon synaptic activity, we wanted to know where newly made proteins are used relative to active dendritic inputs. To accomplish this goal, we have generated fluorescently tagged reporters that will allow us to track where newly made proteins are utilized. We made fusion proteins to a photoconvertible fluorescent probe, monomeric Dendra2, which can be irreversible, converted from a green fluorescing to a red fluorescing form with near-UV irradiation [236]. Upon expression in neurons, these reporters will localize to dendrites and fluoresce green. Prior to synaptic stimulation, the proteins will be irradiated with near-UV-light to convert them from a green to a red state, such that pre-existing tagged proteins will fluoresce red whereas newly synthesized proteins will fluoresce green. This irreversible change will allow us to distinguish between the old and the new protein pools, and to optically track where newly synthesized proteins are being utilized. We have designed several constructs using native proteins thought to be important for synaptic plasticity whose mRNAs are dendritically localized. We cloned either the entire mRNA transcript (5'UTR+ORF+3'UTR) of these candidates or the untranslated regions of the native proteins alone into the pDendra2-C vector, and modified this vector as described in following sections. This will allow us to decipher where such proteins are utilized in respect to stimulated synapses.

3.1.1. Site-directed mutagenesis of pDendra2-C vector to eliminate the start codon

To ensure that the endogenous proteins are synthesized as fusions to Dendra2 (as one protein), we decided to remove the *start* codon of Dendra2. We designed primers for site-directed mutagenesis in which we changed the ATG that encodes the first amino acid (methionine) of Dendra2 to another amino acid, in this case glycine (GGG), which is a very small amino acid and, like methionine, is also a hydrophobic amino acid (Fig. 12).

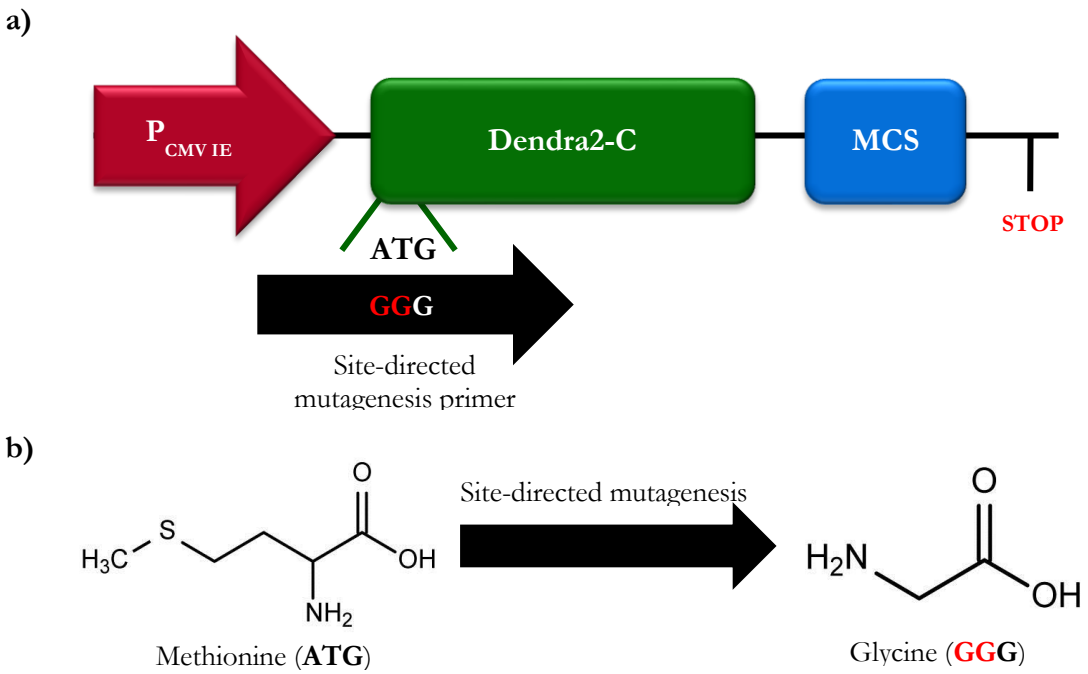

Fig.12 – Site-directed mutagenesis scheme | **a)** Schematic site-directed mutagenesis reaction with the mutagenesis primer used to change the *start* codon to a glycine codon; in red are the nucleotides added to achieve the mutation **b)** Site-directed mutagenesis in terms of amino acid structural change. The nucleotides that were changed appear in red and lead to the modification of the amino acid as shown.

So, using the Dendra2-C vector as a template together with the primers for site-directed mutagenesis we conducted a mutant strand synthesis reaction to change a *start* codon (ATG) to one that encodes glycine (GGG), and digested the methylated original template in order to eliminate all the non-mutated plasmid DNA (using the kit from *QuikChange II Site-Directed Mutagenesis kit* from Agilent Technologies). Then *E. coli* DH5α competent cells were transformed and the positive colonies were selected in medium supplemented with Kanamycin (50 µg/mL). Positive plasmid were isolated and sent for sequencing to confirm that the mutagenesis result was as expected. This pDendra2-C Vector without the *start* codon was called pMut Dendra2-C vector and used for subsequent cloning steps.

3.1.2. Site-directed mutagenesis of pMut Dendra2-C vector to correct the reading frame for the endonuclease restriction sites of *Afe*I and *Age*I

To ensure that native proteins were cloned *in frame* with Dendra2 protein we decided to eliminate seven nucleotides present in pMut Dendra2-C vector between *Afe*I and *Age*I restriction sites and the Dendra2 *open reading frame*. For that we designed primers for site-directed mutagenesis where we eliminated these nucleotides (Fig.13).

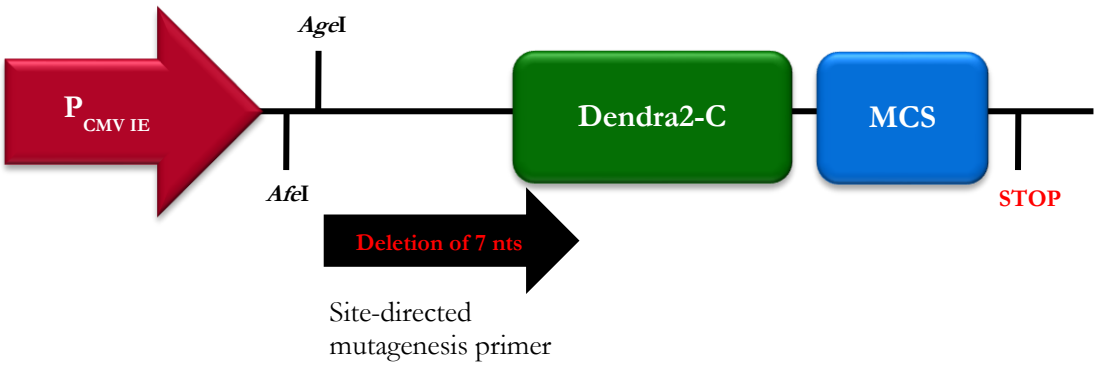

Fig.13 – Schematic site-directed for eliminating 7 nucleotides between *Afe*I and *Age*I restriction sites and the Dendra2 coding region | This ensured that *Afe*I and *Age*I restriction sites were *in frame* with the ORF of Dendra2.

So, using pMut Dendra2-C vector as a template together with the primers for site-directed mutagenesis we created a first strand synthesis reaction to eliminate these 7 in the Dendra2 plasmid. We followed this by digestion of the methylated template as before in order to eliminate all the non-mutated pDNA. Then *E. coli* DH5α competent cells were transformed and the positive colonies with the construct were grown in medium supplemented with Kanamycin (50 µg/mL). Plasmid of one colony was isolated and sent for sequencing. The site-directed mutagenesis worked leading to a pDendra2-C vector without these 7 nucleotides and with the *Afe*I and *Age*I restriction sites i*n frame* with the ORF of Dendra2.The correct *n frame* version of pMut Dendra2-C vector, called from now on pEL Mut Dendra2-C vector, was then used for the next site-directed mutagenesis reactions.

3.1.3. Site-directed mutagenesis of pDendra2-C vector and pEL Mut Dendra2-C vector to insert a stop codon at the end of the Dendra2 open reading frame

Finally, in order to ensure that Dendra2 protein translation ends properly we added a *stop* codon at the end of the ORF of Dendra2 protein. Again, we designed site-directed mutagenesis primers in which we inserted this codon (Fig.14).

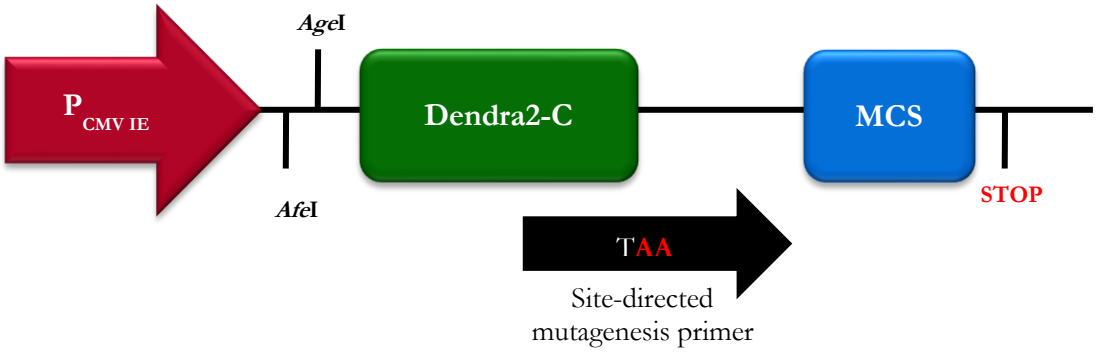

Fig.14 – Schematic site-directed mutagenesis reaction to insert a *stop* codon at the end of Dendra2 ORF | The red nucleotides were added to insert the stop codon.

We conducted two parallel reactions. Using either pDendra2-C vector or pEL Mut Dendra2-C vector as a template, we carried out site-directed mutagenesis to introduce a *stop* codon at the end of Dendra2 ORF, followed by digestion of methylated template that eliminated all the non-mutated pDNA. Then, *E. coli* DH5α competent cells were transformed and the positive colonies were grown in medium supplemented with Kanamycin (50 μg/mL). One plasmid colony was isolated and sent for sequencing for each of the reactions. The site-directed mutagenesis worked leading to a pMut EL Dendra2-C vector and a pDendra2-C vector containing a *stop* codon at the end of the open reading frame of Dendra2.

The pSTOP Dendra2-C vector (Fig.15.a) was then used for cloning of 5'UTR and 3'UTR of CaMKIIα while the pSTOP EL Mut Dendra2-C vector (Fig.15.b) was used for cloning all of the remaining 5'UTRs, ORFs and 3'UTRs.

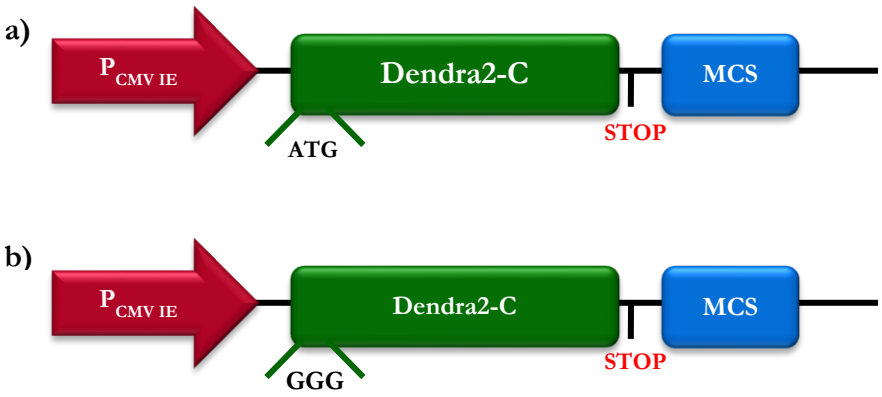

Fig.15 – Vector designed used for cloning native transcripts | **a)** STOPDendra2-C vector scheme. This vector was used only for the cloning of the 5' and 3'UTRs of CaMKIIα. The only site-directed mutagenesis done was to insert the *stop* codon at the end of the Dendra2 ORF. **b)** pSTOP EL Mut Dendra2-C vector scheme. This vector was used for cloning all of the 5'UTRs, ORFs and 3'UTR fragments of the native proteins of interest. The *start* codon was replaced with a glycine, and 7 nucleotides were removed between *Afe*I and *Age*I restriction sites and the Dendra2 ORF ensuring that *Afe*I and *Age*I restriction sites ahead of the Dendra2 ORF in order to ensure that *Afe*I and *Age*I restriction sites are *in frame* with the Dendra2 ORF for creating Dendra2 fusion proteins. Also, a stop codon was inserted at the end of the Dendra2 ORF.

Using the vectors shown in figure 15 it was possible to generate several translational reporters for native proteins thought to be important for synaptic plasticity. The tagged plasticity related proteins will be synthesized as fusions to Dendra2 in order to probe their role in long lasting functional and structural changes which occur in dendritic spines following activity.

3.2. Cloning of 3'UTR of CaMKIIα cDNA into pDendra2-C

Both Mayford and colleagues as well as Mori *et al.* demonstrated that the 3'UTR of CaMKIIα is sufficient to target its mRNA to dendrites [153, 162]. Therefore, we designed two constructs that would allow us to add either a 5'UTR and ORF or the 5'UTR alone of CaMKIIα into Dendra2. This first version was designed to allow us to faithfully visualize the dynamic localization of CaMKIIα protein after synaptic plasticity, while the second construct was designed to report only the dendritic targeting and translation of Dendra2 at the dendrite, similarly to the report by Aakalu *et al* [147]. This design serves to create a control for and potential confounds resulting from the overexpression of the native protein. Two parallel cloning strategies were designed: one in which the UTRs and ORF of CaMKIIα were cloned together, and another in which just the untranslated region of CaMKIIα was cloned.

It was shown by Mayford and colleagues that the 3'UTR of CaMKIIα is required for the targeting of these transcripts to dendrites [153] and that the 3' untranslated region is also responsible for the regulation of multiple aspects of mRNA processing such as nuclear export, cytoplasmic localization, translational efficiency and mRNA stability [246]. Based on these data, we decided to include the 3'UTR of all of the other candidate proteins in their respective tagged constructs, with the idea that these 3' UTRs may also contribute to the dendritic localization of these proteins and to the regulation of their translation locally following synaptic activity.

First, we decide to clone the 3'UTR of CaMKIIα into the STOP EL Mut Dendra2-C vector. This step was the first to be done because one of the endonucleases used to cut this region and insert it into the vector also cuts the open reading frame of CaMKIIα. Therefore, we cloned the 3'UTR first both in this vector and in the STOP Dendra2-C vector.

To obtain this construct a strategy was designed to clone the 3'UTR of CaMKIIα into the STOP EL Mut Dendra2-C vector or into the STOP Dendra2-C vector (Fig.16). The cloning of the 3'UTR of CaMKIIα was difficult to carry out probably due to secondary structures that these DNA sequence may form, and therefore, we designed a two step approach in which we first cloned an initial 2116 bp segment, and then cloned the last 1298 bp. Therefore, we designed two constructs for each plasmid, one with the first 2116 bp of 3'UTR of CaMKIIα (Fig.16) and the other with the last 1298 bp of 3'UTR (Fig.16). We then joined both fragments in order to obtain the complete 3'UTR. The two transcripts were cloned in the multiple cloning sites in the Dendra2-C vector.

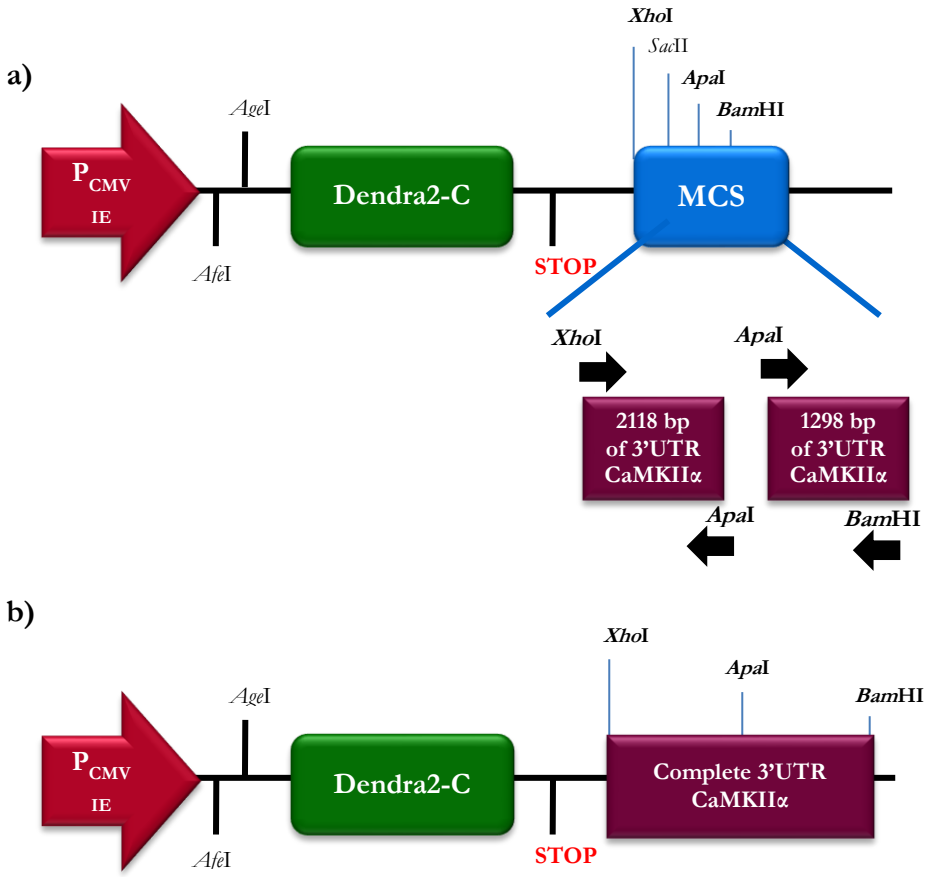

Fig.16 – Strategy for cloning the 3'UTR of CaMKIIα into Dendra2. | **a)** Both the STOP EL Mut Dendra2-C vector and STOP Dendra2-C vector contain the $P_{CMV\ IE}$ promoter, the Dendra2-C protein, the stop codon in Dendra2-C and a multiple cloning site (MCS); Specific primers were designed to introduce the recognition sites of the endonucleases *Xho*I and *Apa*I in the 2118 bp amplification product and the recognition sites of the endonucleases *Apa*I and *Bam*HI in the 1298 bp amplification product; **b)** Final construct containing the full 3'UTR CaMKIIα region in Dendra2 vector.

The primers were designed to introduce endonuclease recognition sites in the amplification products. In the primers to amplify the first 2116 bp of the 3'UTR of CaMKIIα, the endonuclease recognition site for *Xho*I (5') was added, and the reverse primer contained a site for the endogenous *Apa*I recognition site (3'). In the primers to amplify the last 1298 bp of 3'UTR of CaMKIIα region, the forward primer was designed to include an endogenous *Apa*I recognition site (5') and the endonuclease *Bam*HI (3') recognition site was introduced in the reverse primer. These endonuclease recognition sites are located in the multiple cloning site of pDendra2-C vector.

To test for primer specificity, the 2116 bp of 3'UTR CaMKIIα was amplified by PCR using three different primer annealing temperatures (65ºC, 60ºC and 55ºC). As seen in figure 17, a single band was observed corresponding to the expected 2116 bp fragment of the 3'UTR of CaMKIIα in lane 1 and 2. The primer annealing temperature of 65ºC was chosen for the 2116 bp CaMKIIα PCR reaction, in order to avoid cloning

of any non-specific fragments.

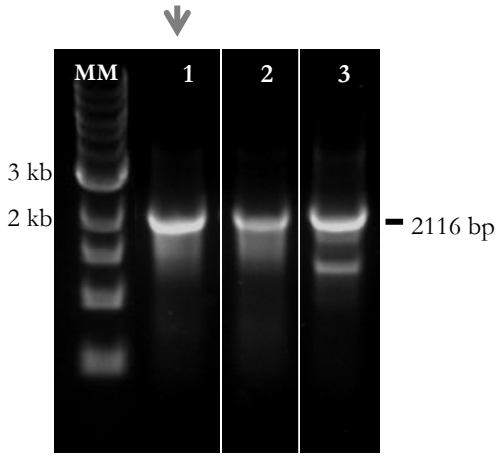

Fig. 17 – PCR product of CaMKIIα 3' UTR – part 1| A 1 Kb ladder was run in the MM lane of the 0.8% agarose gel.
Lane 1 – 3: The 2116 bp 3'UTR of CaMKIIα amplified product can be seen with various annealing temperatures (65°C, 60°C and 55°C, respectively); The arrow indicates the selected annealing temperature.

To test for primer specificity, the 1298 bp of 3'UTR CaMKIIα was amplified using the primers 3'UTRb CaMKIIα forward and 3'UTRb CaMKIIα reverse by PCR using the lowest annealing temperature possible (50°C) due to the low efficiency of this reaction. It was followed by a *nested* PCR with the primers 3'UTRb CaMKIIα forward and 3'UTRb2 CaMKIIα reverse) containing both *Apa*I and *Bam*HI endonuclease sites. The 1298 bp of 3'UTR CaMKIIα was very difficult to clone that could be explained by the fact that this region has several nucleotide repetitions that may form strong secondary structures. We tried several strategies for cloning this 3'UTR CaMKIIα region being the *nested* PCR the only one efficient: first we amplified this fragment using KOD (*Thermococccus kodakaraensis*) Hot Start DNA polymerase followed by a PCR using as template the PCR product from KOD reaction. As seen in figure 18, a single band was observed corresponding to the expected size of the second 3'UTR CaMKIIα amplified product (1298 bp) in lane 1 of both gels.

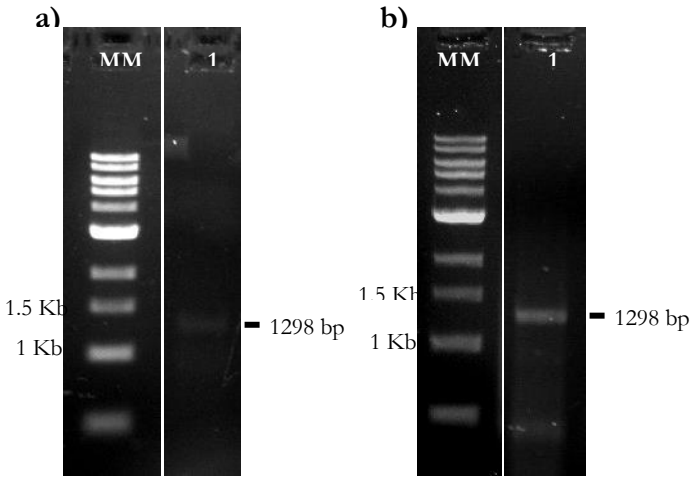

Fig. 18 – PCR product of CaMKIIα 3' UTR – part 2| **a)** PCR reaction using the primers 3'UTRb CaMKIIα forward and 3'UTRb CaMKIIα reverse and KOD proofreading enzyme; A 1 Kb ladder was run in the MM lane of the 0.8% agarose gel; Lane 1: 1298 bp of 3'UTR of CaMKIIα amplified product using as annealing temperature 50°C (expected size 1298 bp). **b)** *Nested* PCR reaction using the primers 3'UTRb CaMKIIα forward and 3'UTRb2 CaMKIIα reverse and the PCR product shown in a) as template; A 1 Kb ladder was run in the MM lane of the 0.8% agarose gel; Lane 1: 1298 bp of 3'UTR of CaMKIIα amplified product using as annealing temperature 50°C (expected size 1298 bp).

Amplification of both fragments was then performed with *Pfu* polymerase to avoid the introduction of mutations in the DNA.

Following amplification, the 2116 bp 3'UTR CaMKIIα product was purified and digested with *Xho*I and *Apa*I endonucleases. The pSTOP Dendra2-C vector and pSTOP EL Mut Dendra2-C were also linearized with *Xho*I and *Apa*I (Fig. 19). The digested plasmid was run on a 0.8% agarose gel and the expected band was visible (4.7 Kb). This reaction was purified to obtain the linearized plasmid.

The same process was carried out with the 1298 bp of 3'UTR of CaMKIIα fragment. After the 1298 bp band was amplified, the PCR product and vector backbone was purified and digested with *Apa*I and *Bam*HI endonucleases.

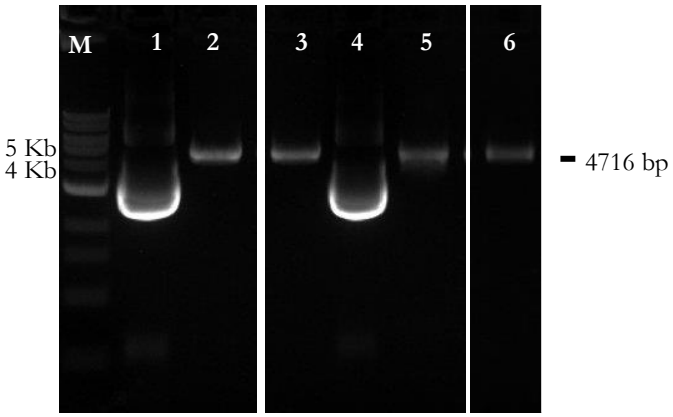

Fig. 19 – Dendra2C vector backbone, 4.7 kb | A 1 Kb ladder was run in the MM lane of the 0.8% agarose gel.
Lane 1: Uncut STOP Dendra2-C (supercoiled);
Lane 2: STOP Dendra2-C Vector digested with *Xho*I and *Apa*I (expected size 4716 bp);
Lane 3: STOP Dendra2-C Vector digested with *Apa*I and *Bam*HI (expected size 4716 bp);
Lane 4: Uncut STOP Mut EL Dendra2-C Vector (supercoiled);
Lane 5: STOP EL Mut Dendra2-C Vector digested with *Xho*I and *Apa*I (expected size 4716 bp);
Lane 6: STOP EL Mut Dendra2-C Vector digested with *Apa*I and *Bam*HI (expected size 4716 bp).

The digested fragments were ligated and transformed in *E. coli* DH5α competent cells. Colonies transformed with the construct were capable of growing in medium supplemented with Kanamycin (50 μg/mL). A colony PCR was then conducted to select positive clones with the primers designated in figure 20, for each of the respective clones. For the Dendra2-C-2116 bp 3'UTR CaMKIIα, a 2116 bp amplified product was expected for a positive clone, whereas for Dendra2-C-1298 bp 3'UTR CaMKIIα an amplified product of 1298 bp was expected. Several STOP Dendra2-C-2116 bp 3'UTR CaMKIIα positives clones were observed (Fig.21a), as well as positive clones containing the STOP EL Mut Dendra2-C-2116 bp 3'UTR CaMKIIα construct (Fig.21b).

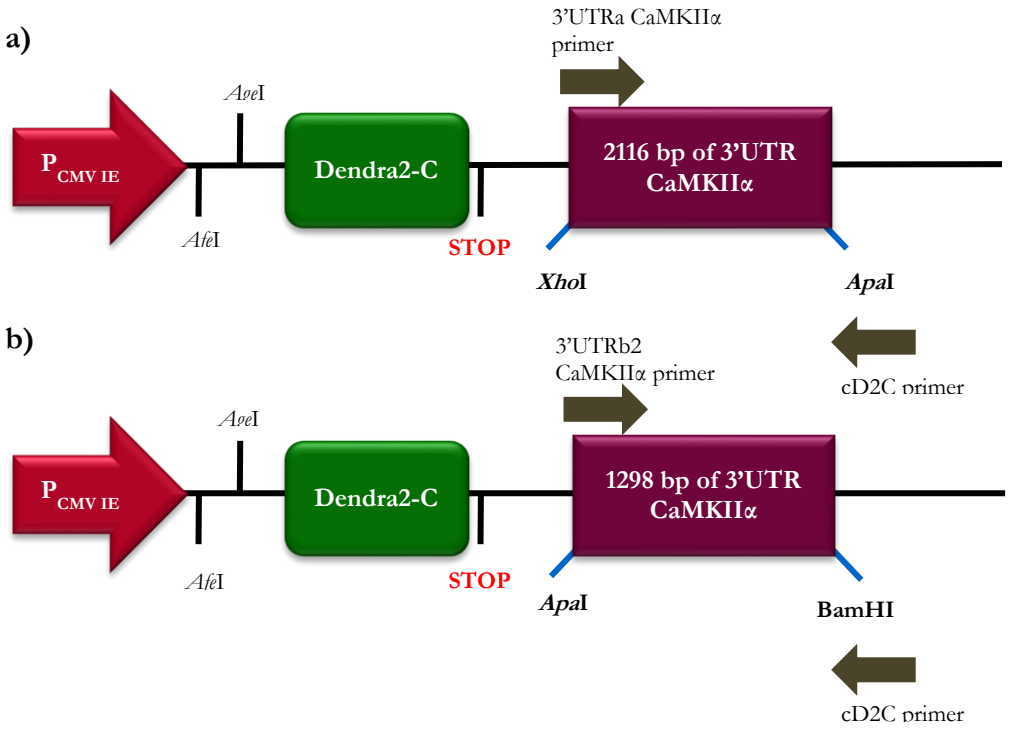

Fig.20 – Colony PCR screening for CaMKIIα 3'UTR-Dendra2 constructs| **a)** For Dendra2-C-2116 bp 3'UTR CaMKIIα screening, the 3'UTRa CaMKIIα primer forward and the cD2C reverse primer were chosen; **b)** For the Dendra2-C-2116 bp 3'UTR CaMKIIα, the 3'UTRb2 CaMKIIα primer forward primer and the cD2C reverse primer were chosen.

Positive clones 1 and 26 containing the 3'UTR of CaMKIIα with Dendra were selected (Fig 21a, lanes 1 and 26) and positive clones 9, 16 and 27 containing the frame shift corrected 3'UTR of CaMKIIα in Dendra were also selected (Fig. 21b, lanes 9, 16 and 27). These were isolated and digested again with the same restriction enzymes used in the cloning to confirm the presence of the correctly sized insert and vector backbone. As seen in figure 22, all the constructs digested showed the expected insert size (2116 bp) and plasmid size (4.7 Kb).

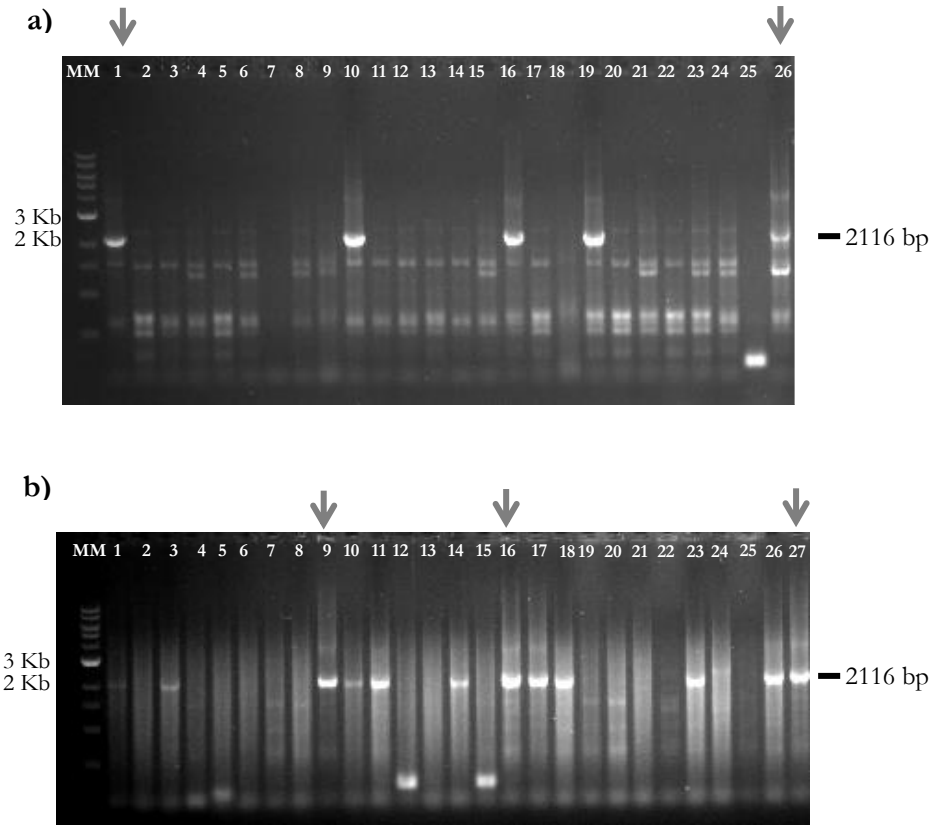

Fig.21 – 3'UTR CaMKIIα Dendra positive clones obtained by colony PCR. | A 1 Kb ladder was run in the MM lane of each 0.8% agarose gel **a)** STOP Dendra2-C 2116 bp 3'UTR CaMKIIα colonies screening (expected size for positive clone: 2116 bp); **b)** STOP EL Mut Dendra2-C 2116 bp 3'UTR CaMKIIα colonies screening (expected size for positive clone: 2116 bp); Arrows indicate the clones selected to isolate.

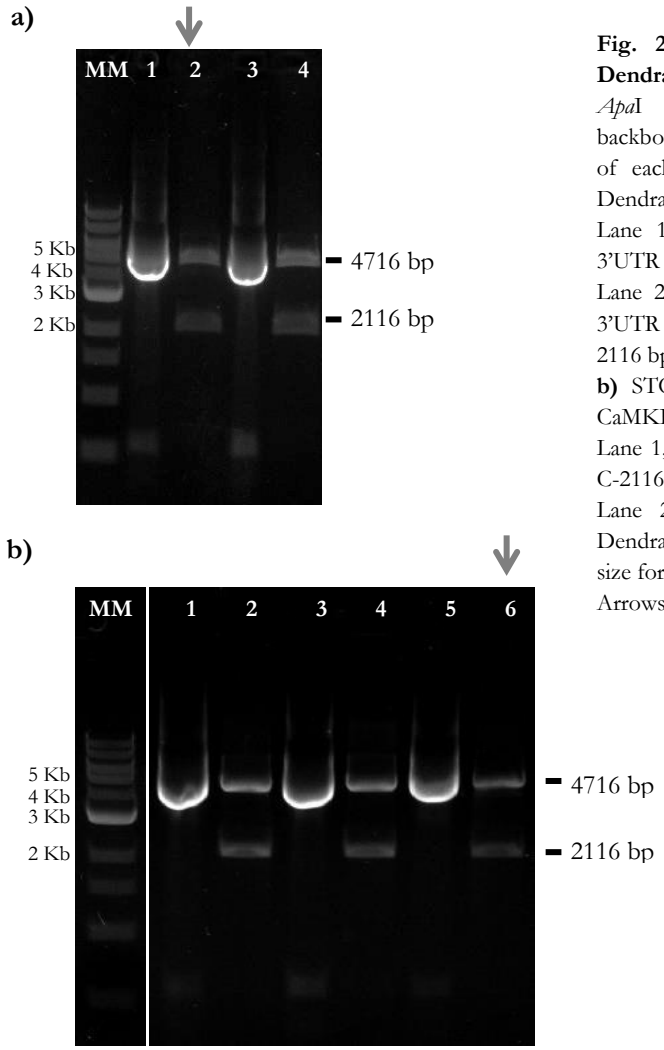

Fig. 22 – Validation of 3'UTR CaMKIIα Dendra plasmids | Digestion with *Xho*I and *Apa*I endonucleases to confirm insert and backbone. A 1 Kb ladder was run in the MM lane of each 0.8% agarose gel **a)** Digested STOP Dendra2-C 2116 bp 3'UTR CaMKIIα;
Lane 1, 3: Uncut pSTOP Dendra2-C-2116 bp 3'UTR CaMKIIα (supercoiled);
Lane 2, 4: Digested STOP Dendra2-C-2116 bp 3'UTR CaMKIIα (expected size for positive clone: 2116 bp + 4716 bp) ;
b) STOP EL Mut Dendra2-C-2116 bp 3'UTR CaMKIIα;
Lane 1, 3 and 5: Uncut STOP EL Mut Dendra2-C-2116 bp 3'UTR CaMKIIα (supercoiled);
Lane 2, 4 and 6: Digested STOP EL Mut Dendra2-C-2116 bp 3'UTR CaMKIIα (expected size for positive clone: 2116 bp + 4716 bp);
Arrows indicate the clones selected to sequencing.

Plasmid STOP Dendra2-C-2116 bp 3'UTR CaMKIIα from clone 1 (Fig.22a, lane 2) was isolated and sent for sequencing. Frame shifted plasmid STOP EL Mut Dendra2-C-2116 bp 3'UTR CaMKIIα from clone 27 (Fig.22b, lane 6) was isolated and sent for sequencing. Sequencing results from both positive clones tested indicated that the constructs contained the expected fragments in the correct orientations and without mutations.

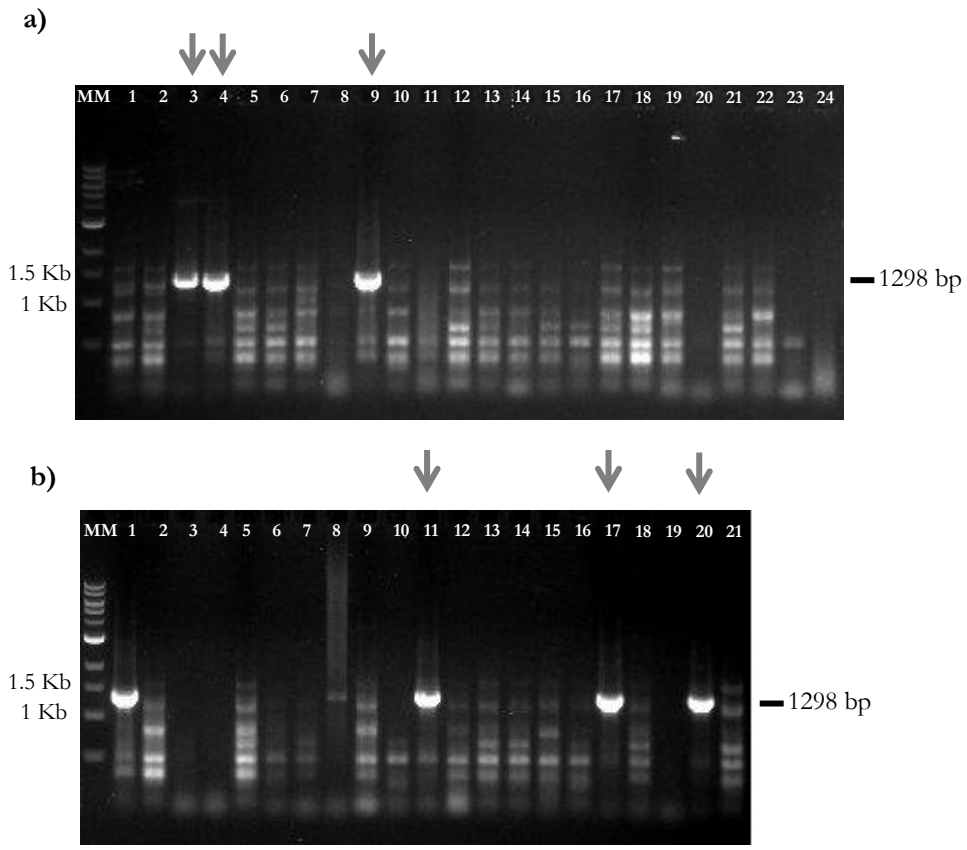

Fig.23 – Identification of 3'UTR CaMKIIα Dendra2-1298 bp positive clones with colony PCR. | A 1 Kb ladder was run in the MM lane of each 0.8% agarose gel **a)** STOP Dendra2-C-1298 bp 3'UTR CaMKIIα colonies screening (expected size for positive clone: 1298 bp); **b)** STOP EL Mut Dendra2-C-1298 bp 3'UTR CaMKIIα colonies screening (expected size for positive clone: 1298 bp); Arrows indicate the clones selected to isolate.

Positive clones were also obtained for the smaller 1298 bp fragment of the 3'UTR of CaMKIIα, in both the normal and the frame shifted Dendra vector backbones (Fig.23). Clones 3, 4 and 9 from STOP Dendra2-C-1298 bp 3'UTR CaMKIIα (Fig 23a, lanes 3, 4 and 9) and clones 11 and 17 from STOP EL Mut Dendra2-C-1298 bp 3'UTR CaMKIIα (Fig. 23b, lanes 11 and 17) were isolated and digested again with the same endonucleases to confirm the presence of the insert and the plasmid. As seen in figure 24, all of the constructs digested showed the expected insert size (1298 bp) and plasmid (4.7 Kb).

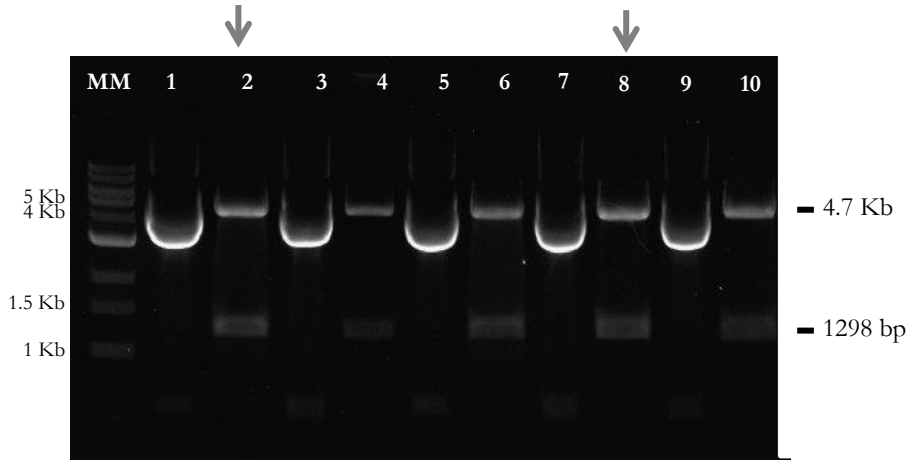

Fig. 24 – Confirmation of Dendra2 with 1298 bp 3'UTR CaMKIIα insert. Plasmids were digested with *Apa*I and *Bam*HI endonucleases to confirm insert presence | A 1 Kb ladder was run in the MM lane of each 0.8% agarose gel.
Lane 1, 3 and 5: Uncut STOP Dendra2-C-1298 bp 3'UTR CaMKIIα (supercoiled);
Lane 2, 4 and 6: Digested STOP Dendra2-C-1298 bp 3'UTR CaMKIIα (expected size for positive clone: 1298 bp + 4716 bp);
Lane 7 and 9: Uncut STOP EL Mut Dendra2-C-1298 bp 3'UTR CaMKIIα (supercoiled)
Lane 8 and 10: Digested STOP EL Mut Dendra2-C-1298 bp 3'UTR CaMKIIα (expected size for positive clone: 1298 bp + 4716 bp); Arrows indicate the clones selected to sequencing.

Plasmid STOP Dendra2-C-1298 bp 3'UTR CaMKIIα from clone 3 (Fig.24a, lane2) and plasmid STOP EL Mut Dendra2-C-1298 bp 3'UTR CaMKIIα from clone 11 (Fig.24b, lane 8) were isolated and sent for sequencing. Both constructs were properly orientated and without mutations.

After obtaining both pieces of the 3'untranslated region of CaMKII in the Dendra vector, the constructs were joined together as follows:

- STOP Dendra2-C-2116 bp 3'UTR CaMKIIα with STOP Dendra2-C-1298 bp 3'UTR CaMKIIα
- STOP EL Mut Dendra2-C-2116 bp 3'UTR CaMKIIα with STOP EL Mut Dendra2-C-1298 bp 3'UTR CaMKIIα.

We digested the two plasmids (with and without the frame shift) containing the 2116 bp size 3'UTR fragments with both *Apa*I and *Bam*HI enzymes and ran the products on an agarose gel (Fig. 25). The expected band was visible (6825 bp for STOP Dendra2-C-2116 bp 3'UTR and 6832 bp for STOP EL Mut Dendra2-C-2116 bp 3'UTR CaMKIIα Vector) and the reaction was purified to obtain the linearized plasmid. The same procedure was done for the plasmids containing the 1298 bp 3'UTR CaMKIIα fragments.

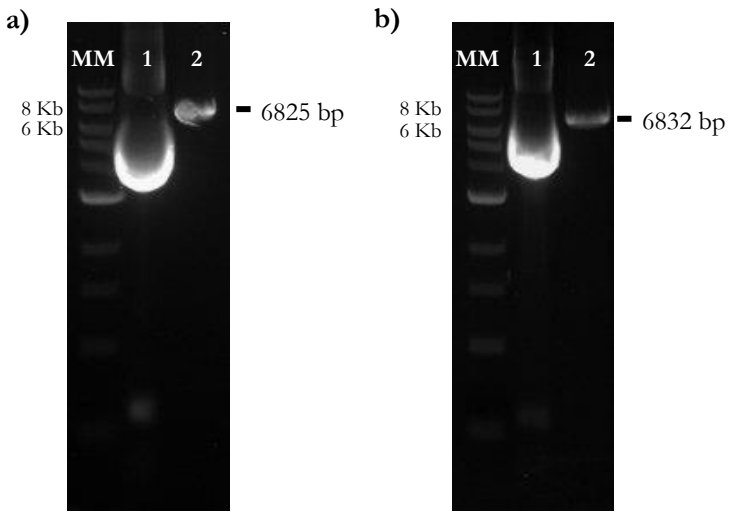

Fig.25 –3'UTR CaMKIIα Dendra2 -2116 bp plasmid digestion | A 1 Kb ladder was run in the MM lane of each 0.8% agarose gel;
a) STOP Dendra2-C-2116 bp 3'UTR CaMKIIα digestion;
Lane 1: Uncut STOP Dendra2-C-2116 bp 3'UTR CaMKIIα vector (supercoiled);
Lane 2: Digested STOP Dendra2-C-2116 bp 3'UTR CaMKIIα with *Apa*I and *Bam*HI (expected size: 6825 bp);
b) STOP EL Mut Dendra2-C-2116 bp 3'UTR CaMKIIα digestion;
Lane 1: Uncut STOP EL Mut Dendra2-C-2116 bp 3'UTR CaMKIIα vector (supercoiled);
Lane 2: Digested STOP EL Mut Dendra2-C-2116 bp 3'UTR CaMKIIα with *Apa*I and *Bam*HI (expected size: 6832 bp);

The 1298 bp 3'UTR CaMKIIα restriction fragments were ligated into STOP Dendra2-C-2116 bp 3'UTR and STOP EL Mut Dendra2-C-2116 bp 3'UTR CaMKIIα Vector and transformed in *E. coli* DH5α competent cells. Colonies transformed with the construct were capable of growing in medium supplemented with Kanamycin (50 μg/mL). The 3'UTRa CaMKIIα primer forward that amplifies from the 5'end of 3'UTR of CaMKIIα and the cD2C primer reverse that amplifies from the 3'end of Dendra2-C were used for STOP Dendra2-C-3'UTR CaMKIIα and STOP EL Mut Dendra2-C-3'UTR CaMKIIα vector colonies screening (Fig. 26). A 3373 bp amplified product was expected in the positive clones. Several STOP Dendra2-C-3'UTR CaMKIIα (Fig. 27a) and STOP EL Mut Dendra2-C-3'UTR CaMKIIα (Fig. 27b) positives clones were observed with the expected amplification product size of 3373 bp.

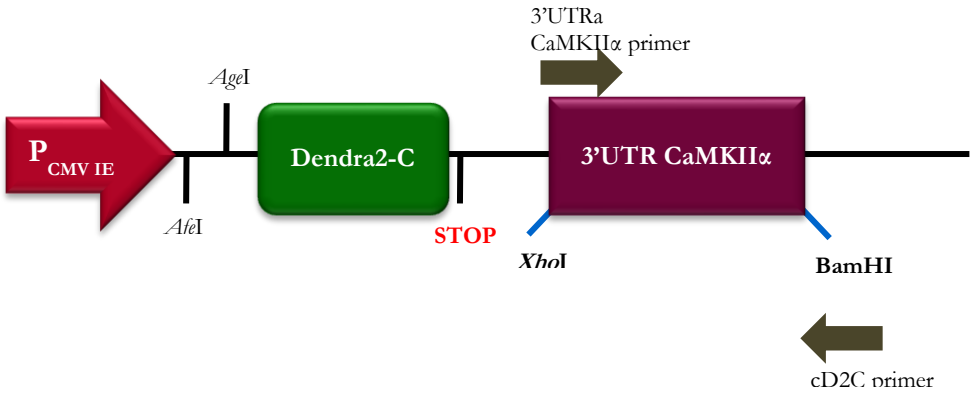

Fig.26 – Primers chosen for the screening of Dendra2-C-3'UTR CaMKIIα | For Dendra2-C-3'UTR CaMKIIα screening, the 3'UTRa CaMKIIα forward and the cD2C reverse primer were used.

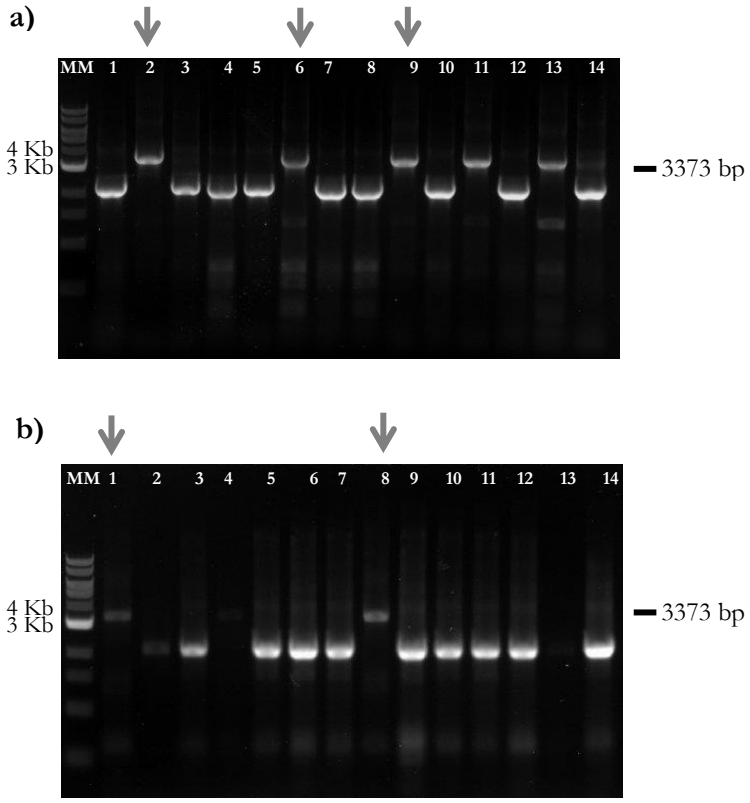

Fig.27 – Complete Dendra2-C-3'UTR CaMKIIα clones by colony PCR | A 1 Kb ladder was run in the MM lane of each 0.8% agarose gel **a)** STOP Dendra2-C-3'UTR CaMKIIα colonies screening (expected size for positive clone: 3373 bp); **b)** STOP EL Mut Dendra2-C-3'UTR CaMKIIα colonies screening (expected size for positive clone: 3373 bp); Arrows indicate the clones selected to isolate.

Plasmids from clone 2, 6 and 9 STOP Dendra2-C-3'UTR CaMKIIα (Fig. 27a, lanes 2, 6 and 9) were isolated and digested again with the same endonucleases to confirm the presence of insert and that the

plasmid was not altered during the cloning process. The same procedure was done with plasmids from clone 1 and 8 STOP EL Mut Dendra2-C-3'UTR CaMKIIα (Fig. 27b, lanes 1 and 8).

As seen in figure 28, all the constructs digested shown the expected insert size (3373 bp) and plasmid size (4.7 Kb). The plasmid from clone 6 (Fig.28a, lane 4) of STOP Dendra2-C-3'UTR CaMKIIα construct was isolated and sent for sequencing and the plasmid from clone 8 (Fig, 28b, lane 4) of STOP EL Mut Dendra2-C-3'UTR CaMKIIα was also isolated and sent for sequencing. Both constructs were properly orientated and without mutations.

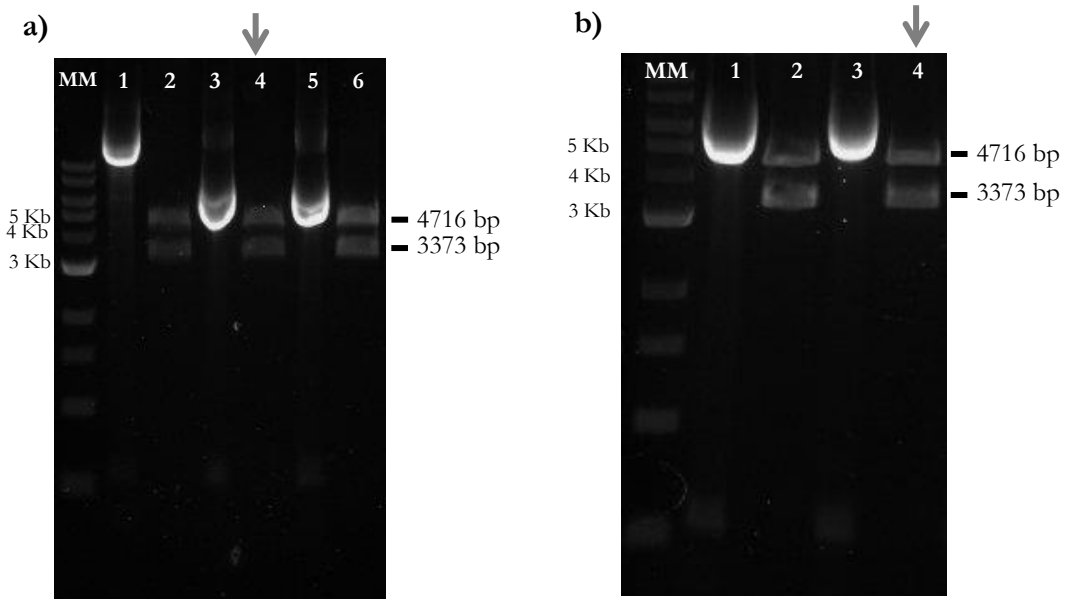

Fig.28 – Dendra2 3'UTR CaMKIIα construct confirmation | A 1 Kb ladder was run in the MM lane of each 0.8% agarose gel;
a) STOP Dendra2-C-3'UTR CaMKIIα digestion;
Lane 1, 3 and 5: Uncut STOP Dendra2-C-3'UTR CaMKIIα Vector (supercoiled);
Lane 2, 4 and 6: Digested STOP Dendra2-C-3'UTR CaMKIIα with *Xho*I and *Bam*HI (expected size: 4716 bp + 3373 bp);
b) STOP EL Mut Dendra2-C-3'UTR CaMKIIα digestion;
Lane 1, 3 and 5: Uncut STOP EL Mut Dendra2-C-3'UTR CaMKIIα Vector (supercoiled);
Lane 2, 4 and 6: Digested STOP EL Mut Dendra2-C-3'UTR CaMKIIα with *Xho*I and *Bam*HI (expected size: 4716 bp + 3373 bp); Arrows indicate the clones selected to sequencing.

These constructs will be introduced into CA1 pyramidal neurons in hippocampal organotypic slices by biolistics and tested for their ability to be dendritically localized and photoconverted. Additionally, these constructs will be used as backbones for cloning the 5'UTR or the 5'UTR-ORF of CaMKIIα, respectively, which can give us more information about the regulation and diffusion of this protein after synaptic activity [147].

3.3. Cloning of Calmodulin cDNA into pDendra2-C

To obtain a construct with the Calmodulin UTRs and open reading frame fused with Dendra2 we designed a strategy where we first cloned the 5'UTR-ORF into the restriction sites *Afe*I (5') and *Age*I (3') of the frame shifted Dendra vector previously described (pSTOP EL Mut Dendra2-C vector) (Fig. 29), followed by the cloning of the 3'UTR into the *Xho*I (5') and *Sac*II (3') restriction sites. The primers were designed to introduce the recognition sequences of *Afe*I (5') and *Age*I (3') in the PCR product of the 5'UTR-ORF, while the recognition sequences of *Xho*I (5') and *Sac*II (3') were introduced into the 3'UTR product. The primers for the Calmodulin 5'UTR-ORF product also accounted for the correct frame when cloned into the Dendra2 construct such that the fusion protein is properly generated.

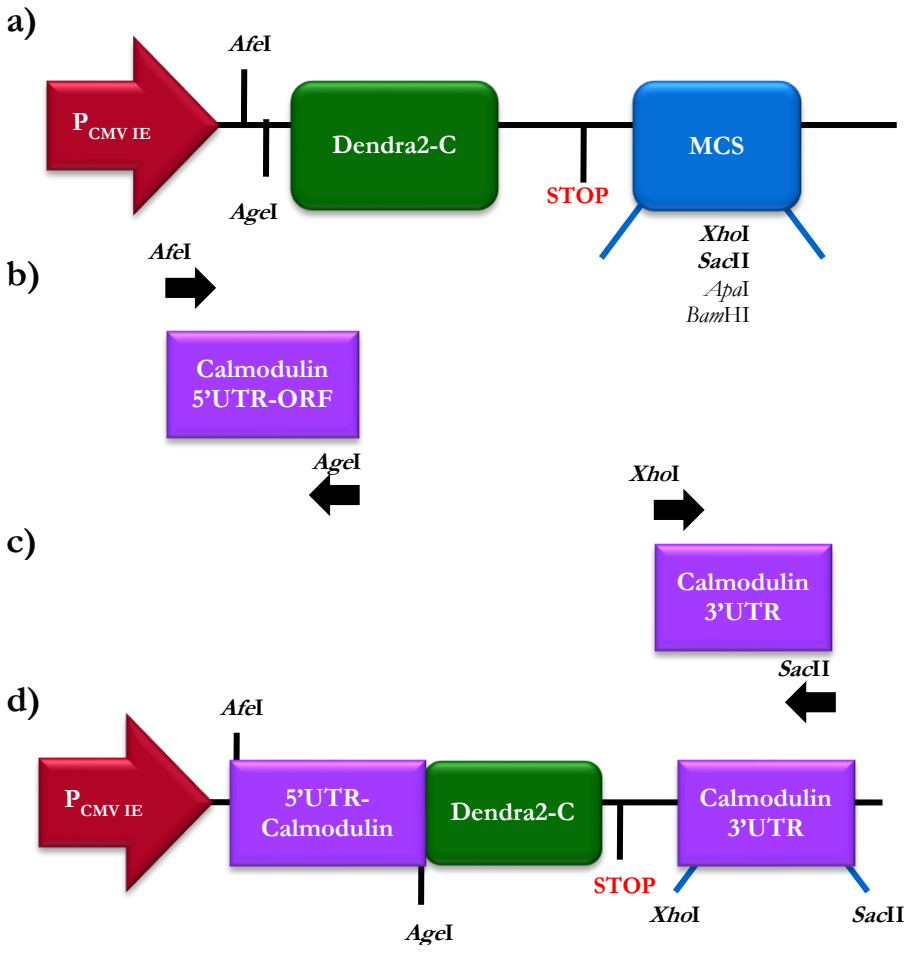

Fig.29 – Cloning strategy for Calmodulin-Dendra translational report | **a)** The STOP EL Mut Dendra2-C vector contains the PCMV IE promoter, the Dendra2-C protein, a multiple cloning site (MCS) and the stop codon of Dendra2-C protein. **b)** Specific 5'UTR-ORF primers were designed to introduce the recognition sites of the endonuclease *Afe*I and *Age*I in the amplification products. **c)** Specific 3'UTR primers were designed to introduce the recognition sites of the endonuclease *Xho*I and *Sac*II in the amplification products; **d)** Final construct with Dendra containing 5'UTR-Calmodulin-3'UTR transcript.

As seen in figure 29 the 5'UTR-ORF of Calmodulin will be inserted before Dendra2 protein with the endonucleases *Afe*I (5') and *Age*I (3') allowing for the expression of a fusion protein that will be regulated similarly to endogenous Calmodulin due to the presence of the 5'UTR. The 3'UTR will be inserted into the *Xho*I and *Sac*II recognition sites in the same Dendra containing vector.

These fragments were amplified using proof reading DNA polymerase to avoid the occurrence of any mutation with a 55ºC primer annealing temperature (Fig. 30). As seen in figure 30 lane 1, a single band was observed corresponding to the expected 5'UTR-ORF of Calmodulin amplified product (623 bp) and in lane 2 a very intense band corresponding to the 3'UTR of Calmodulin is also observed (3378 bp), suggesting that the PCR reactions are specific.

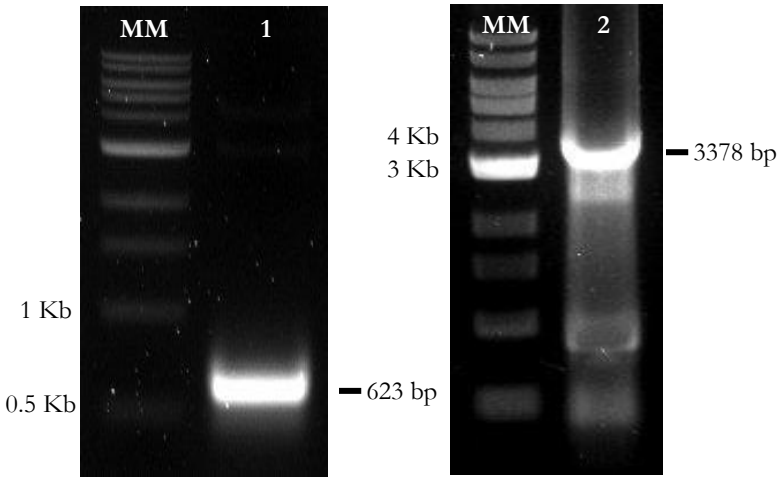

Fig.30 – Calmodulin PCR cloning fragments: 5'UTR-ORF and 3'UTR| A 1 Kb ladder was run in the MM lane of the 0.8% agarose gel.

Lane 1: 5'UTR and ORF of Calmodulin amplified products using 55°C primer annealing temperature (expected size: 896 bp);

Lane 2: 3'UTR of Calmodulin amplified products using 55°C primer annealing temperature (expected size: 3378 bp).

Following amplification, the 5'UTR-ORF fragment of Calmodulin was purified and digested with *Afe*I and *Age*I endonucleases and the 3'UTR fragment was digested with *Xho*I and *Sac*II. The frame shifted Dendra vector was also linearized with *Afe*I and *Age*I restriction enzymes(Fig. 31) and the digested plasmid was run on a 0.8% agarose gel to confirm the size (expected size: 4.7 Kb) and obtain a purified, linear plasmid.

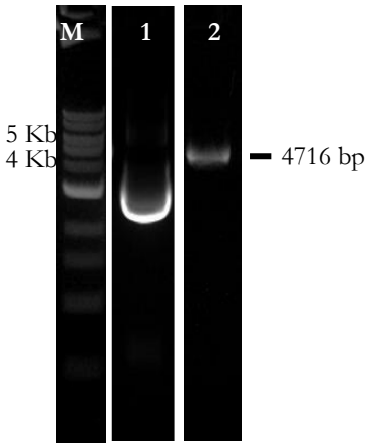

Fig. 31 – Dendra vector linearized for 5' cloning. | A 1 Kb ladder was run in the MM lane of the 0.8% agarose gel.
Lane 1: Uncut pSTOP EL Mut Dendra2-C vector (supercoiled);
Lane 2: pSTOP EL Mut Dendra2-C vector digested with *Afe*I and *Age*I (expected size 4716 bp);

The 5'UTR-ORF restriction fragments were ligated and transformed in *E. coli* DH5α competent cells. Colonies transformed with the construct were capable of growing in medium supplemented with Kanamycin (50 µg/mL). A colony PCR was then conducted to select positive clones with the primers designated in figure 32, for each of the respective clones. For the 5'UTR-Calmodulin-Dendra construct, a 623 bp amplified product was expected for a positive clone. Several 5'UTR-ORF Calmodulin-Dendra positive clones were observed (Fig. 33).

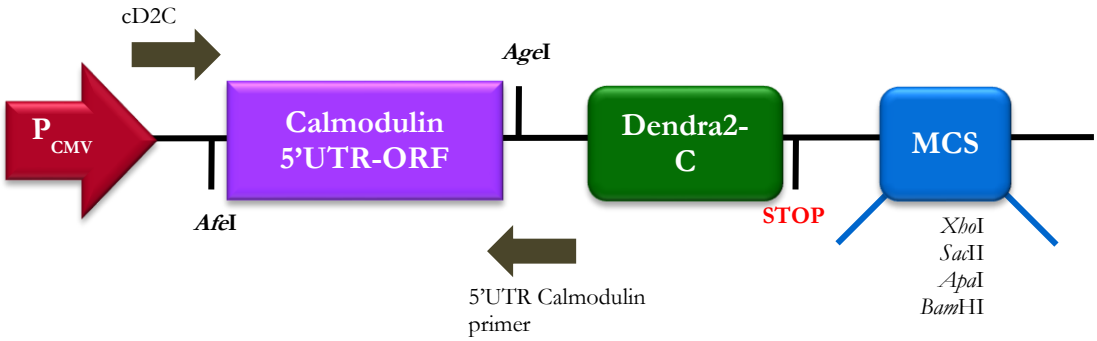

Fig. 32 – PCR colony screening for 5'UTR-Calmodulin-Dendra |For p5'UTR+ORF Calmodulin-STOP EL Mut Dendra2-C vectors screening, the cD2C forward and the 5'UTR Calmodulin reverse primers were used.

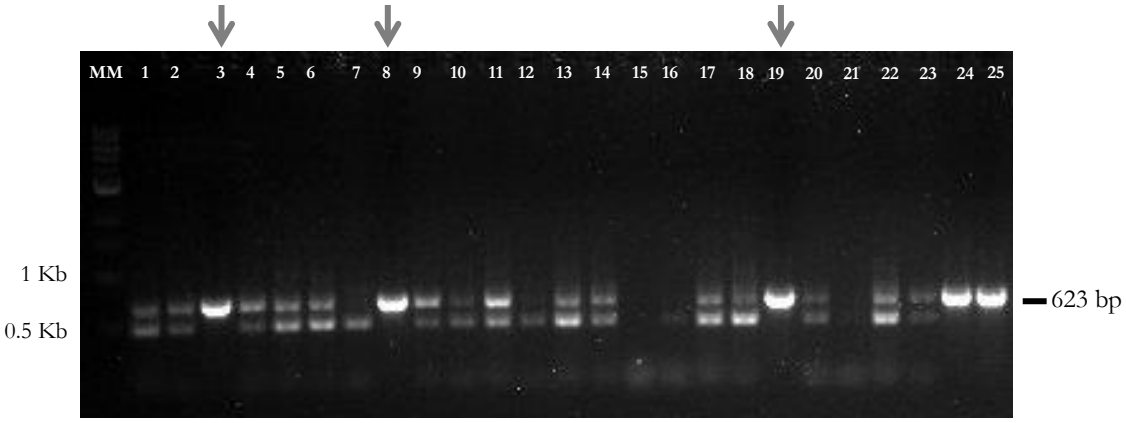

Fig.33 – 5'UTR-Calmodulin-Dendra positive clones obtained by colony PCR. Expected size for positive clones: 623 bp fragment. | A 1 Kb ladder was run in the MM lane of each 0.8% agarose gel; Arrows indicate the clones selected to isolate.

Plasmids from clones 3, 8 and 19 containing 5'UTR-Calmodulin-Dendra (Fig.33, lanes 3, 8 and 19) were isolated and digested with the same endonucleases used in the cloning to confirm the presence of the insert and that the plasmid was not altered during digestion and ligation.

As seen in figure 34, all the constructs digested shown the expected insert size (623 bp) and plasmid (4.7 Kb). The plasmid from clone 3 (Fig.34, lane 2) was isolated and sent for sequencing, and was found to be properly orientated, in frame with Dendra2 protein, and without mutations.

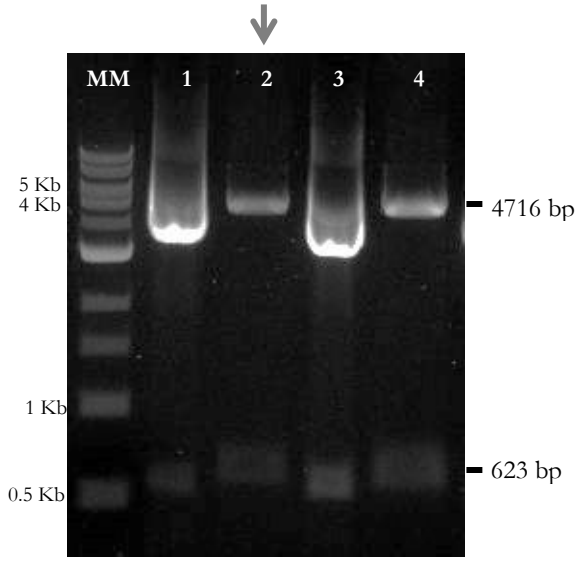

Fig. 34 – Confirmation of 5'UTR-Calmodulin-Dendra fusion construct.
Plasmid was digested with *Afe*I and *Age*I endonucleases to confirm the insert size. | A 1 Kb ladder was run in the MM lane of each 0.8% agarose gel;
Lane 1 and 3: Uncut p5'UTR+ORF Calmodulin-STOP Mut EL Dendra2-C vector (supercoiled)
Lane 2 and 4: Digested p5'UTR+ORF Calmodulin-STOP Mut EL Dendra2-C vector (expected size for positive clone: 623 bp + 4716 bp); Arrows indicate the clones selected to sequencing.

Once the 5'UTR-Calmodulin-Dendra construct was done, we digested it with *Xho*I and *Sac*II endonucleases and the digested plasmid was run on an agarose gel (Fig. 35). The expected band was visible (5339 bp) and the reaction was purified to obtain the linearized plasmid.

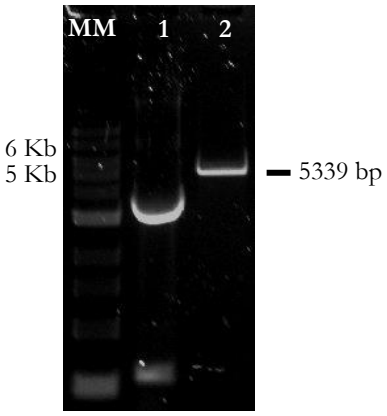

Fig. 35 – Linearized 5'UTR-Calmodulin-Dendra vector | A 1 Kb ladder was run in the MM lane of the 0.8% agarose gel.
Lane 1: Uncut p5'UTR+ORF Calmodulin- STOP EL Mut Dendra2-C vector (supercoiled);
Lane 2: Digested p5'UTR+ORF Calmodulin- STOP EL Mut Dendra2-C vector with *Xho*I and *Sac*II (expected size 5339 bp).

The Calmodulin 3'UTR restriction fragment was ligated into the linearized 5'UTR-Calmodulin-Dendra vector and transformed in *E. coli* DH5α competent cells. Colonies transformed with the construct were capable of growing in medium supplemented with Kanamycin (50 µg/mL). A colony PCR was then conducted to select positive clones with the primers designated in figure 36, for each of the respective clones. A 3378 bp amplified product was expected for positive clones, and only one positive clone was observed (Fig. 37). This clone (#5) contained the 5'UTR+ORF+3'UTR of Calmodulin with Dendra (Fig.37, lane 5), and was isolated and digested again with the same endonucleases to confirm the presence of the insert and that the plasmid did not contain any changes during digestion and ligation.

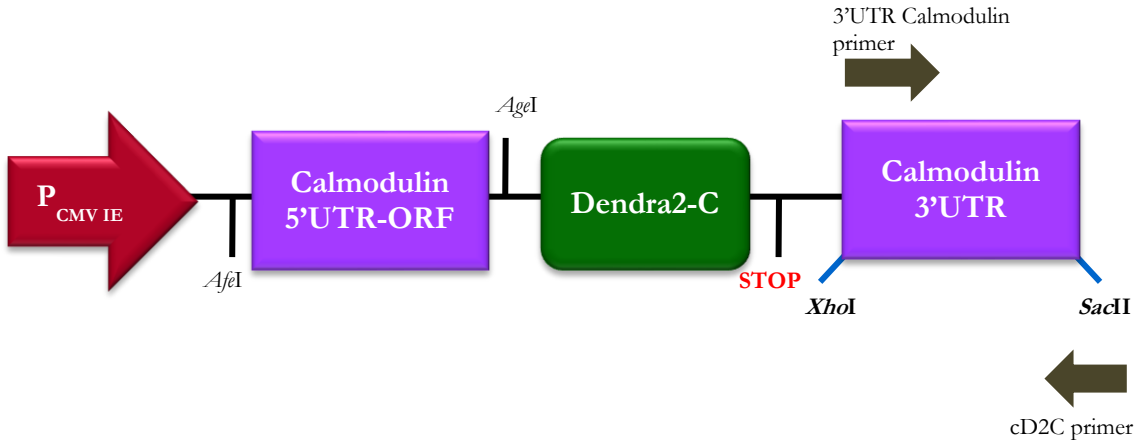

Fig. 36 – Colony PCR screening for 5'UTR-Calmodulin-Dendra2-3'UTR construct | For 5'UTR+ORF Calmodulin-Dendra2-C-3'UTR screening, the 3'UTR Calmodulin forward and the cD2C reverse primers were chosen.

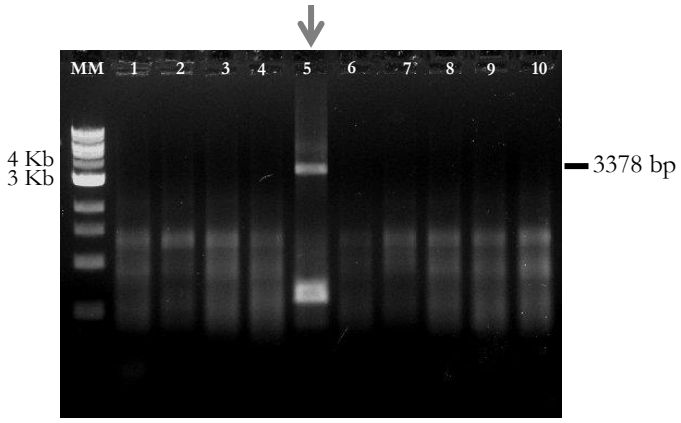

Fig.37 – Complete Calmodulin-Dendra fusion construct identified by colony PCR: 5'UTR-Calmodulin-Dendra-3'UTR |Calmodulin positive clones obtained by colony PCR (expected size for positive clone: 3378 bp); A 1 Kb ladder was run in the MM lane of each 0.8% agarose gel; Arrow indicate the clone selected to isolate.

As seen in figure 38, the digested construct contained the expected insert size (3378 bp) and plasmid (5.3 Kb). The plasmid from clone 5 (Fig.38, lane 2) was sent for sequencing, and found to be properly orientated and without mutations.

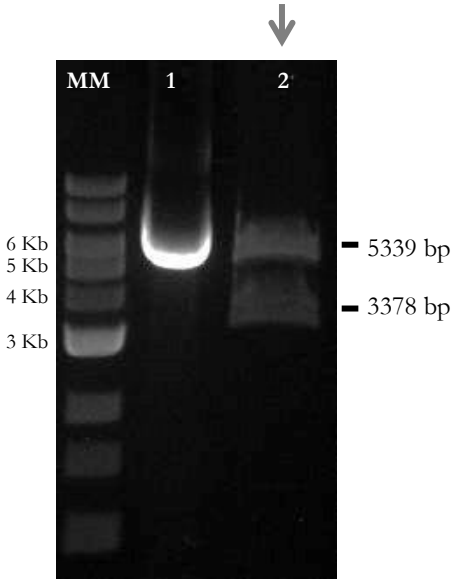

Fig. 38 – Confirmation of the complete Calmodulin-Dendra fusion construct |5'UTR+ORF - STOP Mut EL Dendra2-C-3'UTR Calmodulin plasmids digestion with *Xho*I and *Sac*II endonucleases to confirm its presence; A 1 Kb ladder was run in the MM lane of each 0.8% agarose gel;
Lane 1: Uncut 5'UTR+ORF Calmodulin STOP Mut EL Dendra2-C -3'UTR Calmodulin vector (supercoiled)
Lane 2: Digested 5'UTR+ORF Calmodulin-STOP Mut EL Dendra2-C-3'UTR Calmodulin (expected size for positive clone: 5339 bp + 3378 bp); Arrow indicate the clone selected to sequencing.

These constructs will be introduced into CA1 pyramidal neurons in hippocampal organotypic slices by biolistics and tested for their ability to be dendritically localized and photoconverted. Additionally, once this construct also contain 5'UTR-ORF Calmodulin it may give us information about the regulation and diffusion of this protein after synaptic activity.

3.4. Cloning of Arc cDNA into pDendra2-C

To obtain a construct with the Arc UTRs and open reading frame fused with Dendra2 we designed a strategy where we first cloned the 5'UTR-ORF into the restriction sites *Nhe*I (both 5' and 3') of the frame shifted Dendra vector previously described (pSTOP EL Mut Dendra2-C vector) (Fig. 39), followed by the cloning of the 3'UTR into the *Xho*I (both 5' and 3') restriction sites. The primers were designed to introduce the recognition sequences of *Nhe*I (both 5' and 3') in the PCR product of the 5'UTR-ORF, while the recognition sequences of *Xho*I (both 5' and 3') were introduced into the 3'UTR product. The primers for the Arc 5'UTR-ORF product also accounted for the correct frame when cloned into the Dendra2 construct such that the fusion protein is properly generated.

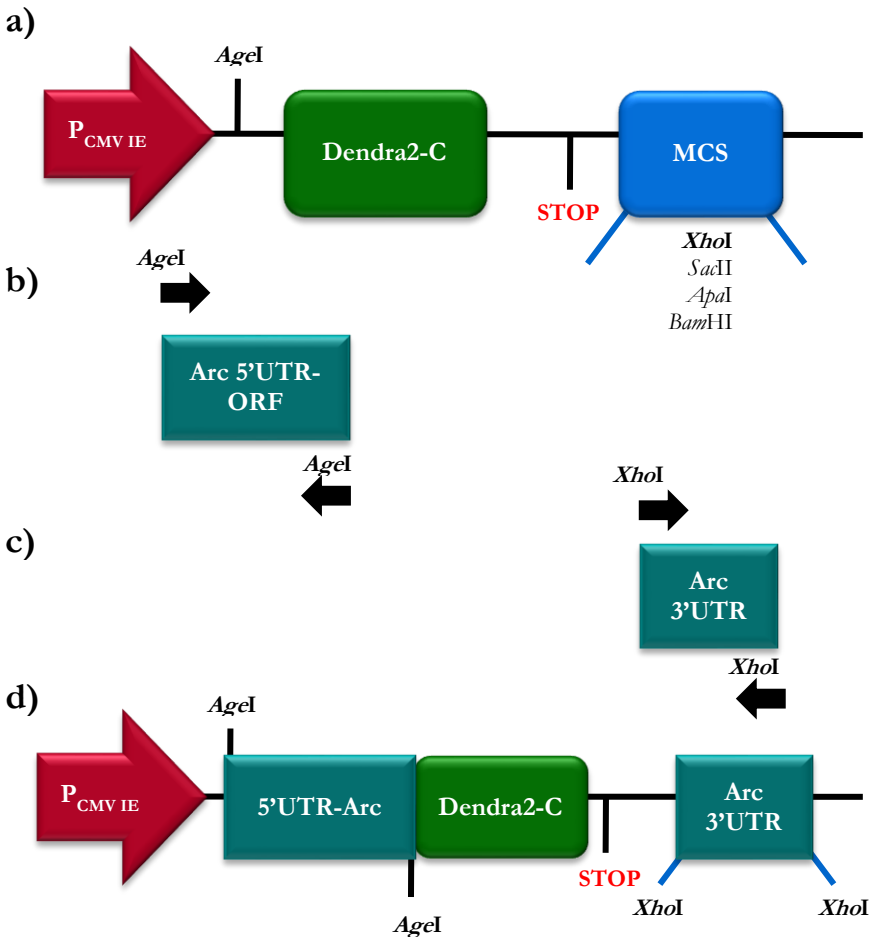

Fig.39 – Cloning strategy for Arc-Dendra translational report | **a)** The STOP EL Mut Dendra2-C vector contains the PCMV IE promoter, the Dendra2-C protein, a multiple cloning site (MCS) and the stop codon of Dendra2-C protein. **b)** Specific 5'UTR-ORF primers were designed to introduce the recognition sites of the endonuclease *Age*I in the amplification products. **c)** Specific 3'UTR primers were designed to introduce the recognition sites of the endonuclease *Xho*I in the amplification products; **d)** Final construct with Dendra containing 5'UTR-Arc-3'UTR transcript.

As seen in figure 39 the 5'UTR-ORF of Arc will be inserted before Dendra2 protein with the endonucleases *Nhe*I (both 5' and 3') allowing for the expression of a fusion protein that will be regulated similarly to endogenous Arc due to the presence of the 5'UTR. The 3'UTR will be inserted into the *Xho*I recognition sites in the same Dendra containing vector.

The 5'UTR-Arc and 3'UTR Arc were amplified using proof reading DNA polymerase to avoid the occurrence of any mutation with a 68°C and 61°C primer annealing temperature, respectively (Fig. 40). As seen in figure 40 lane 1, a single band was observed corresponding to the expected 5'UTR-ORF of Arc amplified product (1378 bp) and in lane 2 a single band corresponding to the 3'UTR of Arc is also observed (1664 bp), suggesting that the PCR reactions are specific.

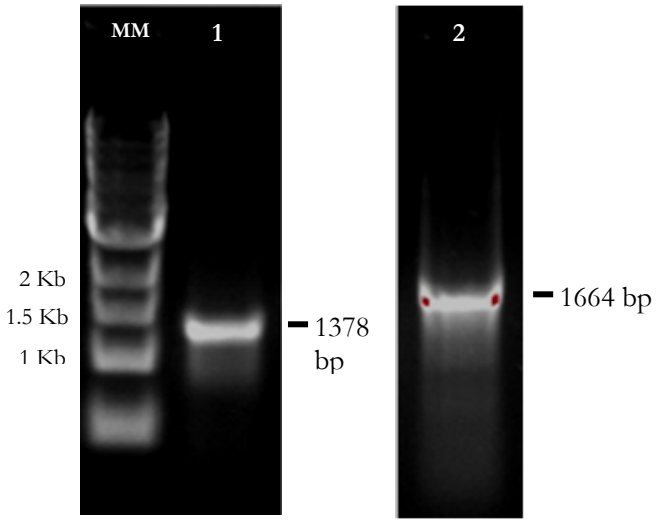

Fig. 40– Arc PCR cloning fragments: 5'UTR-ORF and 3'UTR| A 1 Kb ladder was run in the MM lane of the 0.8% agarose gel.

Lane 1: 5'UTR and ORF of Arc amplified products using 68°C primer annealing temperature (expected size: 896 bp);

Lane 2: 3'UTR of Arc amplified products using 61°C primer annealinfg temperature (expected size: 3378 bp).

Following amplification, the 5'UTR-ORF fragment of Arc was purified and digested with with *Nhe*I endonuclease and the 3'UTR was digested with *Xho*I. The frame shifted Dendra vector was also linearized with *Nhe*I (Fig. 41) and the digested plasmid was run on a 0.8% agarose gel to confirm the size (expected size: 4.7 Kb) and obtain a purified, linear plasmid.

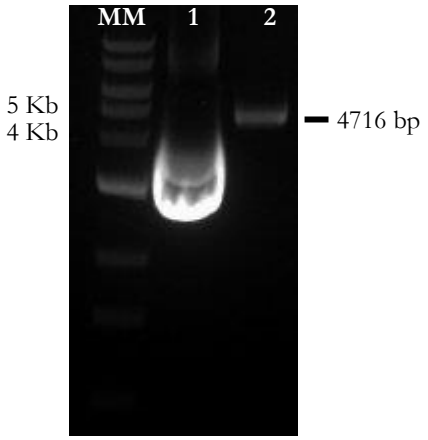

Fig.41 – Dendra vector linearized for 5' cloning. | A 1 Kb ladder was run in the MM lane of the 0.8% agarose gel.
Lane 1: Uncut pSTOP EL Mut Dendra2-C vector (supercoiled);
Lane 2: pSTOP EL Mut Dendra2-C vector digested with *Nhe*I (expected size 4716 bp);

The 5'UTR-ORF restriction fragments were ligated and transformed in *E. coli* DH5α competent cells. Colonies transformed with the construct were capable of growing in medium supplemented with Kanamycin (50 µg/mL). A colony PCR was then conducted to select positive clones with the primers designated in figure 42, for each of the respective clones. For the 5'UTR-Arc-Dendra construct, a 1378 bp amplified product was expected for a positive clone. Several 5'UTR-ORF Calmodulin-Dendra positive clones were observed (Fig. 43).

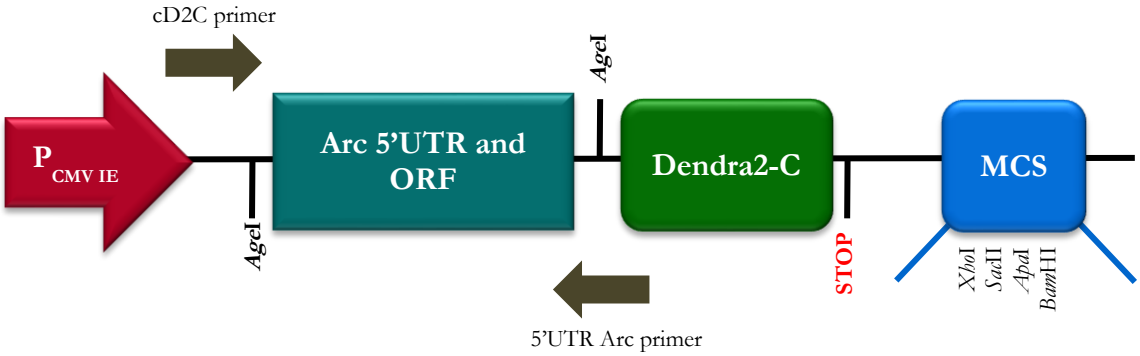

Fig. 42 – PCR colony screening for 5'UTR-Arc-Dendra | For p5'UTR+ORF Arc-STOP EL Mut Dendra2-C vectors screening, the cD2C forward and 5'UTRArc reverse primers were chosen.

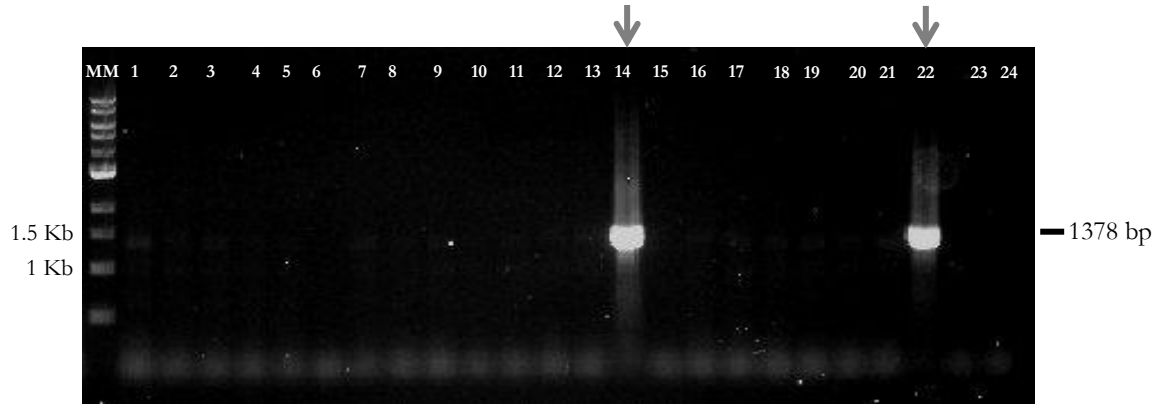

Fig.43 – 5'UTR-Arc-Dendra positive clones obtained by colony PCR. Expected size for positive clones: 1378 bp fragment. | A 1 Kb ladder was run in the MM lane of each 0.8% agarose gel; Arrows indicate the clones selected to isolate.

Plasmids from clones 14 and 22 containing 5'UTR-Arc-Dendra (Fig.43, lanes 14 and 22) were isolated and digested with the same endonucleases used in the cloning to confirm the presence of the insert and that the plasmid was not altered during digestion and ligation.

As seen in figure 44, all the constructs digested shown the expected insert size (1378 bp) and plasmid (4.7 Kb). The plasmid from clone 22 (Fig.44, lane 4) was isolated and sent for sequencing, and was found to be properly orientated, in frame with Dendra2 protein, and without mutations.

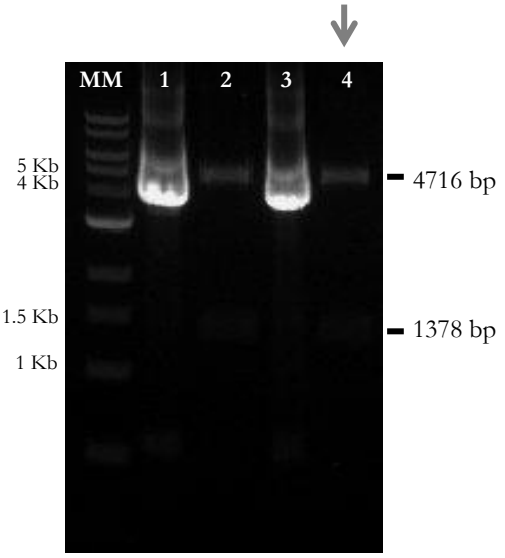

Fig. 44 – Confirmation of 5'UTR-Arc-Dendra fusion construct.
Plasmid was digested with *Nhe*I endonucleases to confirm the insert size. | A 1 Kb ladder was run in the MM lane of each 0.8% agarose gel;
Lane 1 and 3: Uncut 5'UTR+ORF Arc-STOP EL Mut Dendra2-C (supercoiled)
Lane 2 and 4: Digested 5'UTR+ORF Arc-STOP EL Mut Dendra2-C (expected size for positive clone: 1378 bp + 4716 bp); Arrow indicate the clone selected to sequencing.

Once the 5'UTR-Arc-Dendra construct was done, we digested it with *Xho*I endonucleases and the digested plasmid was run on an agarose gel (Fig. 45). The expected band was visible (6094 bp) and the reaction was purified to obtain the linearized plasmid.

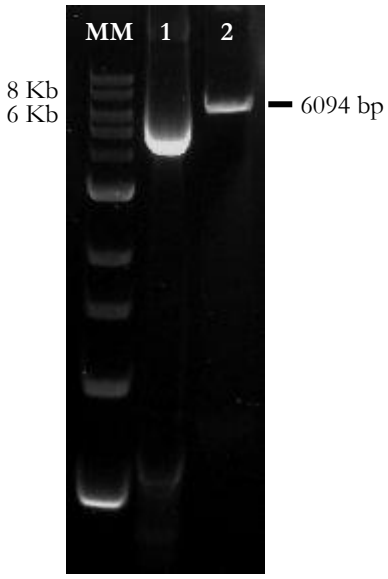

Fig.45 – Linearized 5'UTR-Arc-Dendra vector | A 1 Kb ladder was run in the MM lane of the 0.8% agarose gel.
Lane 1: Uncut 5'UTR+ORF Arc-STOP EL Mut Dendra2-C Vector (supercoiled);
Lane 2: 5'UTR+ORF Arc-STOP EL Mut Dendra2-C Vector digested with *Xho*I (expected size 6094 bp);

The Arc 3'UTR restriction fragment was ligated into the linearized 5'UTR-Arc-Dendra vector and transformed in *E. coli* DH5α competent cells. Colonies transformed with the construct were capable of growing in medium supplemented with Kanamycin (50 µg/mL). A colony PCR was then conducted to select positive clones with the primers designated in figure 46, for each of the respective clones. A 1664 bp amplified product was expected for positive clones, and several positive clones were observed (Fig. 47). Plasmids from clones 8 and 24 containing 5'UTR+ORF+3'UTR of Arc with Dendra (Fig.47, lane 8 and 24) were isolated and digested with the same endonucleases used in the cloning to confirm the presence of the insert and that the plasmid was not altered during digestion and ligation.

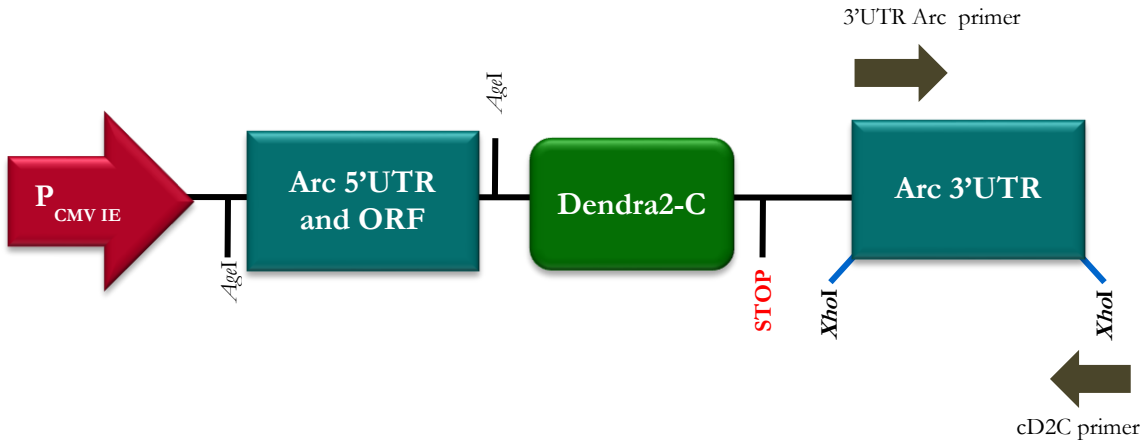

Fig. 46 – Colony PCR screening for 5'UTR-Arc-Dendra2-3'UTR construct | For 5'UTR+ORF Arc-Dendra2-C-3'UTR Arc screening, the 3'UTR Arc forward and the cD2C reverse primers were chosen.

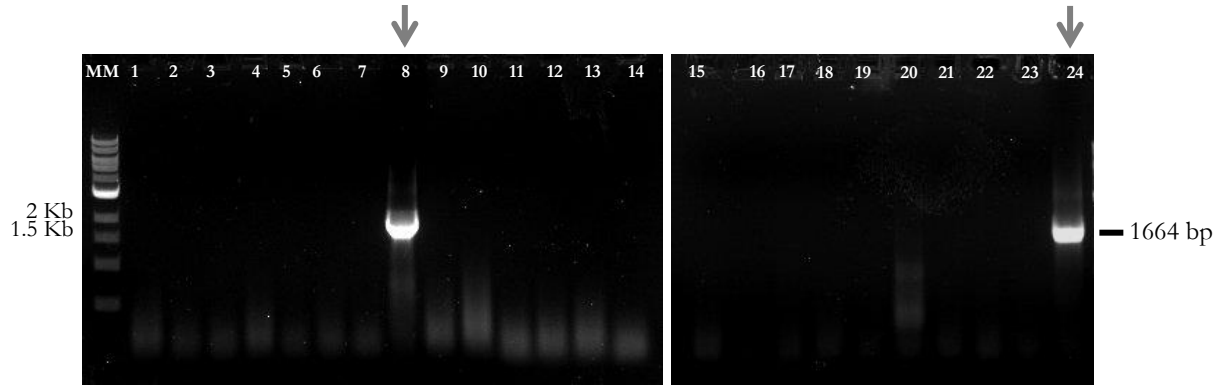

Fig.47 – Complete Arc-Dendra fusion construct identified by colony PCR: 5'UTR-Arc-Dendra-3'UTR | Arc positive clones obtained by colony PCR (expected size for positive clone: 1664 bp) | A 1 Kb ladder was run in the MM lane of each 0.8% agarose gel; Arrows indicate the clones selected to isolate.

As seen in figure 48, the digested construct contained the expected insert size (1664 bp) and plasmid (6.1 Kb). The plasmid from clone 24 (Fig.48, lane 4) was sent for sequencing, and found to be properly orientated and without mutations.

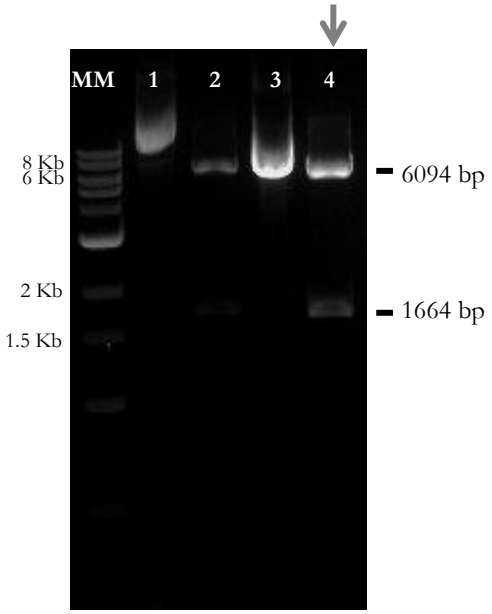

Fig. 48 – Confirmation of the complete Arc-Dendra fusion construct | 5'UTR+ORF -STOP Mut EL Dendra2-C-3'UTR Arc plasmids digestion with *Xho*I endonucleases to confirm its presence; A 1 Kb ladder was run in the MM lane of each 0.8% agarose gel;
Lane 1 and 3: Uncut 5'UTR+ORF Arc-STOP EL Mut Dendra2-C-3'UTR Arc Vactor (supercoiled)
Lane 2 and 4: Digested 5'UTR+ORF Arc-STOP EL Mut Dendra2-C-3'UTR Arc Vector (expected size for positive clone: 1664 bp + 6094 bp); Arrow indicate the clone selected to sequencing.

These constructs will be introduced into CA1 pyramidal neurons in hippocampal organotypic slices by biolistics and tested for their ability to be dendritically localized and photoconverted. Additionally, once this construct also contain 5'UTR-ORF Arc it may give us information about the regulation and diffusion of this protein after synaptic activity.

3.5. Cloning of GluA1 cDNA into pDendra2-C

To obtain a construct with the GluA1 UTRs and open reading frame fused with Dendra2 we designed a strategy where we first cloned the 5'UTR-ORF into the restriction sites *Afe*I (both 5' and 3') of the frame shifted Dendra vector previously described (pSTOP EL Mut Dendra2-C vector) (Fig. 49), followed by the cloning of the 3'UTR into the *Xho*I (5') *Sac*II (3') restriction sites. The primers were designed to introduce the recognition sequences of *Afe*I (both 5' and 3') in the PCR product of the 5'UTR-ORF, while the recognition sequences of *Xho*I (5') and *Sac*II (3') were introduced into the 3'UTR product. The primers for the GluA1 5'UTR-ORF product also accounted for the correct frame when cloned into the Dendra2 construct such that the fusion protein is properly generated.

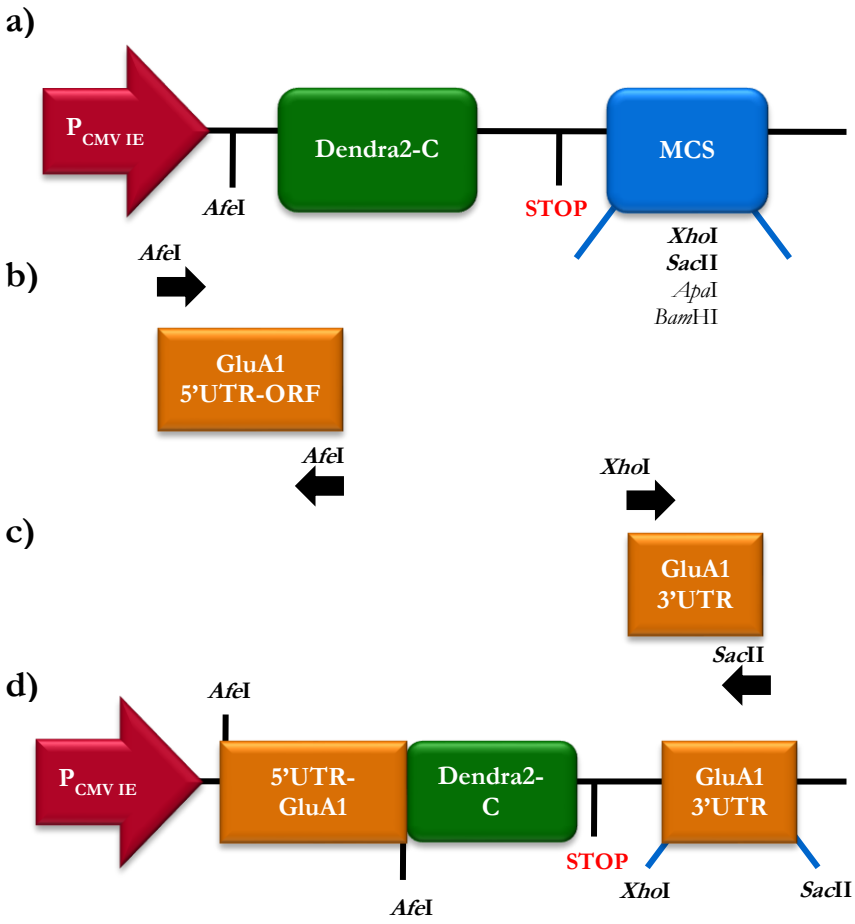

Fig.49 – Cloning strategy for GluA1-Dendra translational report | **a)** The STOP EL Mut Dendra2-C vector contains the PCMV IE promoter, the Dendra2-C protein, a multiple cloning site (MCS) and the stop codon of Dendra2-C protein. **b)** Specific 5'UTR-ORF primers were designed to introduce the recognition sites of the endonuclease *Afe*I in the amplification products. **c)** Specific 3'UTR primers were designed to introduce the recognition sites of the endonuclease *Xho*I and *Sac*II in the amplification products; **d)** Final construct with Dendra containing 5'UTR-GluA1-3'UTR transcript.

As seen in figure 49 the 5'UTR-ORF of GluA1will be inserted before Dendra2 protein with the endonucleases *Afe*I (both 5' and 3') allowing for the expression of a fusion protein that will be regulated similarly to endogenous GluA1 due to the presence of the 5'UTR. The 3'UTR will be inserted into the *Xho*I and *Sac*II recognition sites in the same Dendra containing vector.

To test for primer specificity, 5'UTR and ORF of GluA1 was amplified by PCR using eight different primer annealing temperatures (70^{o}C, 68.8^{o}C, 66.6^{o}C, 62.6^{o}C, 57.8^{o}C, 53.9^{o}C, 51.3^{o}C and 50^{o}C), as seen in figure 50a. The same was done to test primer specificity for 3'UTR GluA1 amplification (Fig. 50b).

As seen in the figure 50a, a single band was observed corresponding to the expected 2802 bp of 5'UTR and ORF GluA1 in lanes 5 - 7 and in figure 50b a single band was also observed corresponding the expected 2600 bp 3'UTR GluA1 in lanes 5 – 8, suggesting that the PCR reactions are specific. The primer annealing temperature of 57.8^{o}C was chosen for the both PCR reactions, in order to avoid cloning of any non-specific fragments. Amplification of both fragments was then performed with *Pfu* polymerase to avoid the introduction of mutations in the DNA.

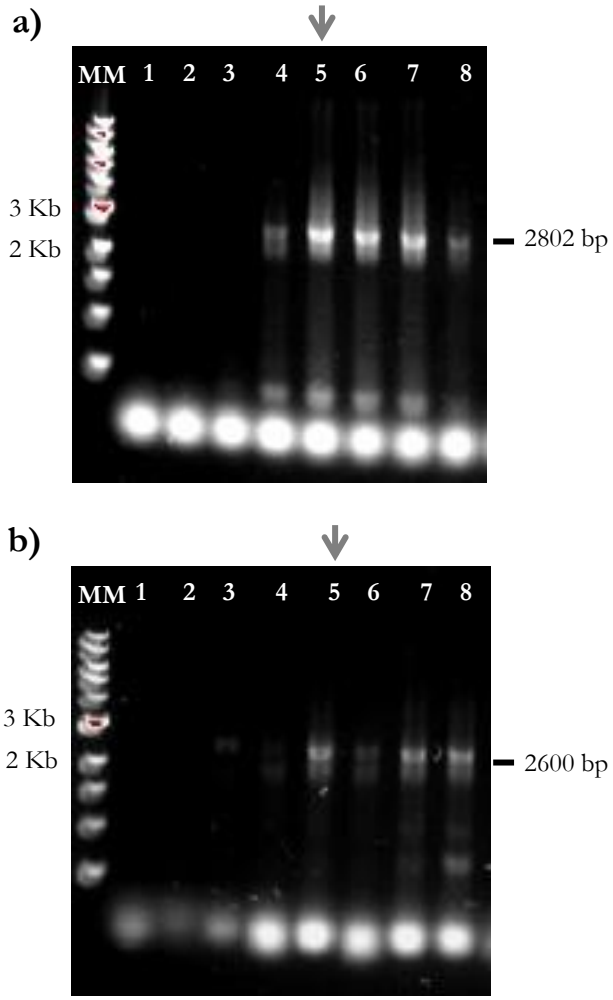

Fig. 50 – GluA1 PCR cloning fragments: 5'UTR-ORF and 3'UTR| A 1 Kb ladder was run in the MM lane of the 0.8% agarose gel.
. Lane 1 – 8: 5'UTR and ORF of GluA1 amplified products using different primer annealing temperatures (70°C, 68.8°C, 66.6°C, 62.6°C, 57.8°C, 53.9°C, 51.3°C and 50°C, respectively) (expected size: 2802 bp). **b)** A 1 Kb ladder was run in the MM lane of the 0.8% agarose gel. Lane 1 – 8: 3'UTR of GluA1 amplified products using different primer annealing temperatures (70°C, 68.8°C, 66.6°C, 62.6°C, 57.8°C, 53.9°C, 51.3°C and 50°C, respectively) (expected size: 2600 bp).

Following amplification, the 5'UTR-ORF fragment of GluA1 was purified and digested with *Afe*I endonucleases and the 3'UTR fragment was digested with *Xho*I and *Sac*II. The frame shifted Dendra vector was also linearized with *Afe*I restriction enzymes(Fig. 51) and the digested plasmid was run on a 0.8% agarose gel to confirm the size (expected size: 4.7 Kb) and obtain a purified, linear plasmid.

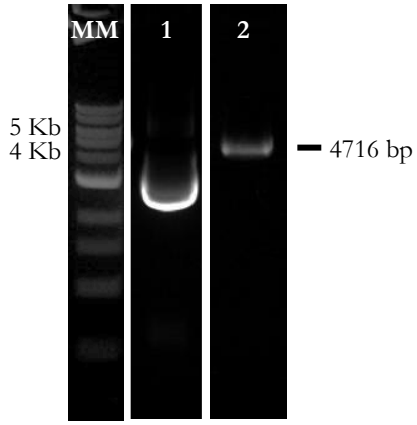

Fig. 51 – Dendra vector linearized for 5' cloning. | A 1 Kb ladder was run in the MM lane of the 0.8% agarose gel.
Lane 1: Uncut pSTOP EL Mut Dendra2-C vector (supercoiled);
Lane 2: STOP EL Mut Dendra2-C vector digested with *Afe*I (expected size 4716 bp);

The 5'UTR-ORF restriction fragments were ligated and transformed in *E. coli* DH5α competent cells. Colonies transformed with the construct were capable of growing in medium supplemented with Kanamycin (50 µg/mL). A colony PCR was then conducted to select positive clones with the primers designated in figure 52, for each of the respective clones. A 2802 bp amplified product was expected for positive clones, and only one positive clone was observed (Fig. 53). This clone (#10) contained the 5'UTR+ORF of GluA1 with Dendra (Fig. 53, lane 10) and was isolated and digested again with the same endonucleases to confirm the presence of the insert and that the plasmid did not contain any changes during digestion and ligation.

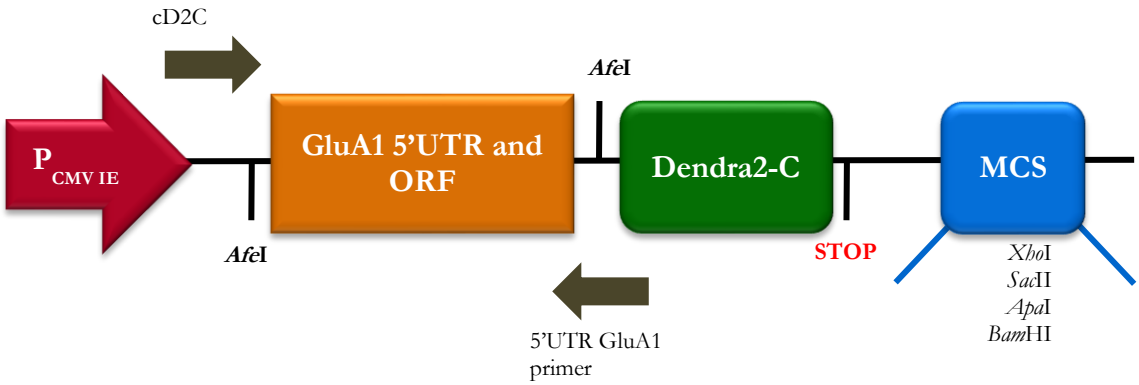

Fig. 52 – PCR colony screening for 5'UTR-GluA1-Dendra | For 5'UTR+ORF GluA1-STOP EL Mut Dendra2-C vector screening, the cD2C forward and the 5' GluA1 reverse primers were chosen.

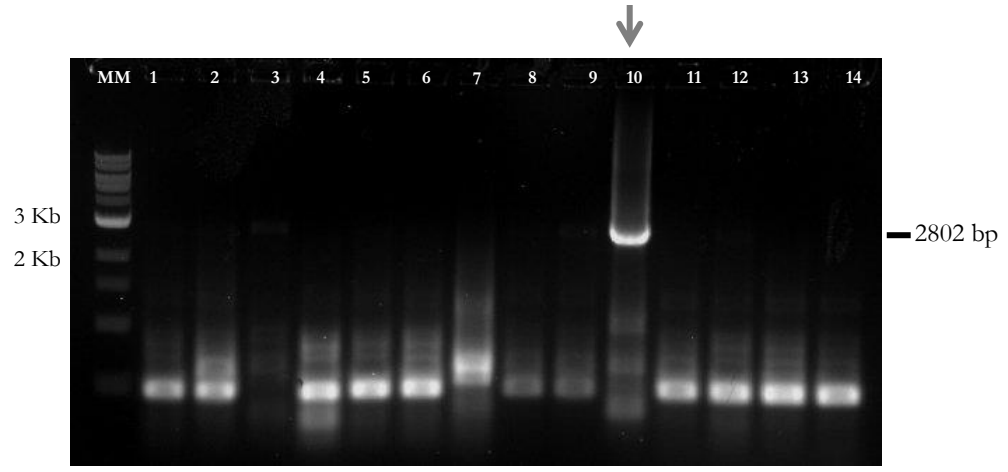

Fig.53 – 5'UTR-GluA1-Dendra positive clones obtained by colony PCR. Expected size for positive clones: 2802 bp fragment. | A 1 Kb ladder was run in the MM lane of each 0.8% agarose gel; Arrows indicate the clones selected to isolate.

As seen in figure 54, the construct digested contained the expected insert size (2802 bp) and plasmid (4.7 Kb). Plasmid from clone 10 (Fig.54, lane 2) was sent for sequencing, and found to be properly orientated and without mutations.

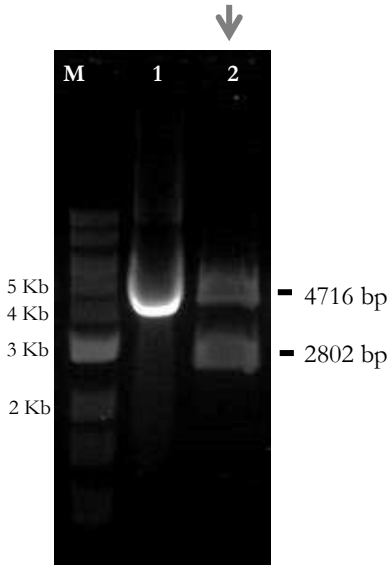

Fig. 54 – Confirmation of 5'UTR-GluA1-Dendra fusion construct. Plasmid was digested with *Afe*I endonucleases to confirm the insert size. | A 1 Kb ladder was run in the MM lane of each 0.8% agarose gel;
Lane 1: Uncut 5'UTR+ORF GluA1 STOP Mut EL Dendra2-C vector (supercoiled)
Lane 2: Digested 5'UTR+ORF GluA1 STOP Mut EL Dendra2-C vector (expected size for positive clone: 2802 bp + 4716 bp); Arrow indicate the clone selected to sequencing.

Once the 5'UTR-Calmodulin-Dendra construct was done, we digested it with *Xho*I and *Sac*II endonucleases and the digested plasmid was run on an agarose gel (Fig. 55). The expected band was visible (7.5 Kb) and the reaction was purified to obtain the linearized plasmid.

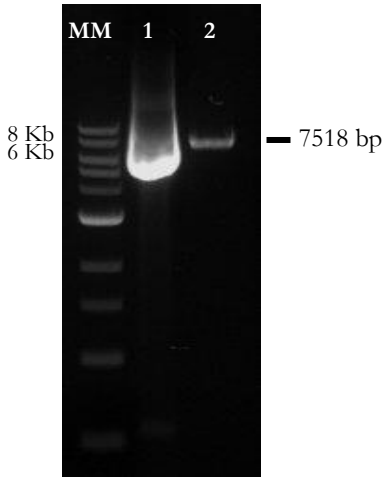

Fig. 55 – Linearized 5'UTR-GluA1-Dendra vector | A 1 Kb ladder was run in the MM lane of the 0.8% agarose gel.
Lane 1: Uncut 5'UTR+ORF GluA1-STOP EL Mut Dendra2-C vector (supercoiled);
Lane 2: 5'UTR+ORF GluA1-STOP EL Mut Dendra2-C vector with *Xho*I and *Sac*II (expected size 5339 bp);

The GluA1 3'UTR restriction fragments were ligated and transformed in *E. coli* DH5α competent cells. Colonies transformed with the construct were capable of growing in medium supplemented with Kanamycin (50 µg/mL). A colony PCR was then conducted to select positive clones with the primers designated in figure 56, for each of the respective clones. A 2600 bp amplified product was expected for positive clones, and only one positive clone was observed (Fig. 57). This clone (#10) contained the 5'UTR+ORF+3'UTR of GluA1 with Dendra (Fig. 57, lane 4) and was isolated and digested again with the same endonucleases to confirm the presence of the insert and that the plasmid did not contain any changes during digestion and ligation.

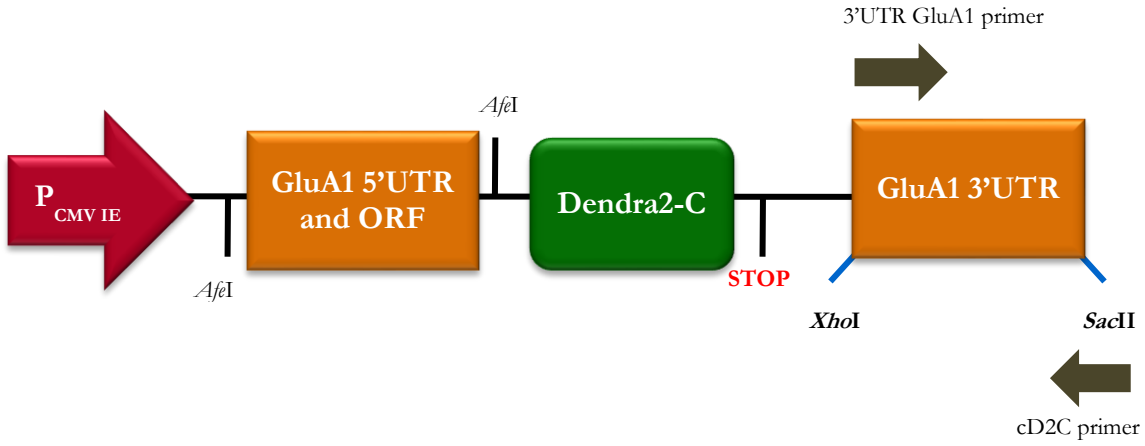

Fig. 56 – Colony PCR screening for 5'UTR-GluA1-Dendra2-3'UTR construct | For 5'UTR+ORF GluA1-Dendra2-C-3'UTR GluA1 screening, the 3'UTR GluA1 forward and the cD2C reverse primers were chosen.

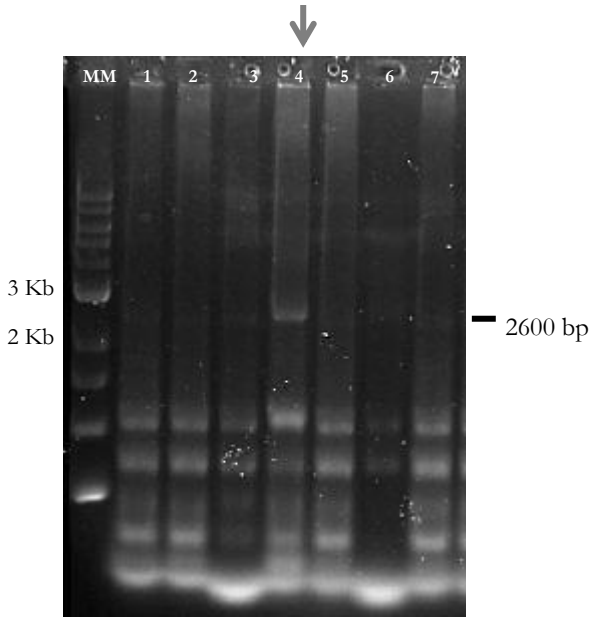

Fig.57 – Complete GluA1-Dendra fusion construct identified by colony PCR: 5'UTR-Calmodulin-Dendra-3'UTR | GluA1 positive clones obtained by colony PCR (expected size for positive clone: 2600 bp); A 1 Kb ladder was run in the MM lane of each 0.8% agarose gel; Arrows indicate the clones selected to isolate.

As seen in figure 58, the digested construct contained the expected insert size (2600 bp) and plasmid (7.5 Kb). The plasmid from clone 4 (Fig.58, lane 2) was sent for sequencing, and found to be properly orientated and without mutations.

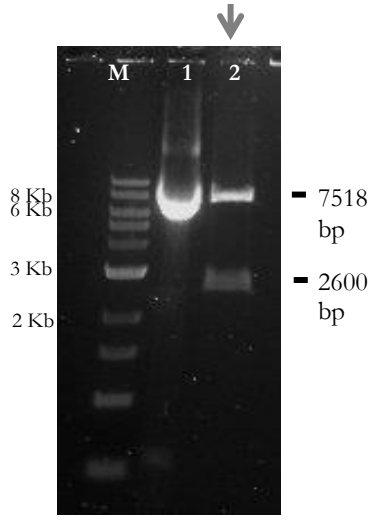

Fig. 58 – Confirmation of the complete GluA1-Dendra fusion construct |5'UTR+ORF GluA1-STOP EL Mut Dendra2-C-3'UTR GluA1 plasmid digestion with *Xho*I and *Sac*II endonuclease to confirm its presence; A 1 Kb ladder was run in the MM lane of each 0.8% agarose gel;
Lane 1: Uncut 5'UTR+ORF GluA1-STOP EL Mut Dendra2-C-3'UTR GluA1 vector (supercoiled)
Lane 2: Digested 5'UTR+ORF 5'UTR+ORF GluA1-STOP EL Mut Dendra2-C-3'UTR GluA1 (expected size for positive clone: 2802 bp + 7518 bp); Arrow indicate the clone selected to sequencing.

This construct was later transfected by biolistics into hippocampal organotypic slices. Following transfection, we were unable to confirm the expression of this GluA1-Dendra fluorescent fusion protein, as no green fluorescence was detectable. This finding suggests that the fusion of Dendra to GluA1 may disrupt the endogenous folding of the protein, and compromise its stability. Further testing will need to be carried

out to determine whether the location of the fusion (for example, on the amino versus carboxy terminal) will alters protein function differentially. Indeed, other fusions have been successfully carried out as C-terminal fusions [106, 222]. Protein linkers can also contribute to the proper folding of the fusion protein and these options will be explored.

Additionally, the low yield of biolistic transfection may also contribute to the lack of construct visibility. Thus, taking these items into consideration, further testing will be required to identify and potentially correct this construct.

3.6. Model system

We are interested in understanding how activity can lead to long lasting and specific functional and structural changes in neurons, which may be important for learning, and how such changes affect connectivity within neural circuits. To answer these questions, we are utilizing organotypic hippocampal slice cultures, since they have physiologically relevant connectivity and neuronal branching patterns that are important for our studies. Additionally, synaptic plasticity at these synapses is relatively well defined, and will allow us to test various forms of activity with known functional outputs. Acute slices are commonly used to study long lasting potentiation and depression, however, it is not easy to introduction genetic sensors – this needs to be done through *in vivo* survival surgeries several days prior to generating slices. Hippocampal slice cultures, on the other hand, in which hippocampal slices from P7-P10 mice are cultured *in vitro*, undergo a stabilization period, after which time gene delivery can be performed using biolistics. Another benefit of slice cultures is that protein synthesis levels have adequate opportunity to equilibrate, unlike the case for acute slices, which are undergoing repair of cut axons and dendrites. This is an important point to consider when studying protein synthesis kinetics.

Dissociated primary hippocampal cultures also have certain advantages, and we will utilize this system in order to validate some aspects of our study. Dissociated cultures are relatively easy to manipulate in terms of: introduction of constructs- such as translational sensors, imaging, and patch-clamp electrophysiology. Additionally, dissociated cultures are amenable to biochemical studies which will be important in order to verify the biological functioning of our tagged proteins.

3.6.1. Organotypic hippocampal culture

In general, slices of central nervous system (CNS) tissue prepared from young rodents can be maintained in culture for many weeks to months with some simple basic requirements: a stable substratum, culture medium, sufficient oxygenation and incubation at a temperature of about 36°C. Under these conditions, nerve cells continue to differentiate and to develop a tissue organization that closely resembles that observed *in situ*.

Hippocampal slices are prepared from 2–23-day-old neonates and are maintained in culture at the interface between air and a culture medium. This method yields thin slices which remain 1–4 cell layers thick and are characterized by a well preserved organotypic organization allowing studies related to circuit connectivity (Fig. 59a).

Pyramidal neurons in culture (Fig.59c) are similar in organization and complexity of their dendritic processes to those observed *in vivo* at comparable developmental stages. Excitatory and inhibitory synaptic

potentials can easily be analyzed using extra- or intracellular recording techniques and after a few days in culture, long-term potentiation of synaptic responses can be reliably induced [245].

Figure 59 shows a bright field image of a hippocampal slice, in which it is possible to see the distinct layer of hippocampal pyramidal neurons that constitute the tri-synaptic pathway (Fig. 59a). The hippocampal slice has been biolistically transfected resulting in sparse fluorescence of different cell types including a pyramidal cell, which allows for the clear visualization of neuronal structures (Fig. 59b). The red box highlights a region of the pyramidal neuron that it is visible at higher magnification in the panel on the right in Figure 59c.

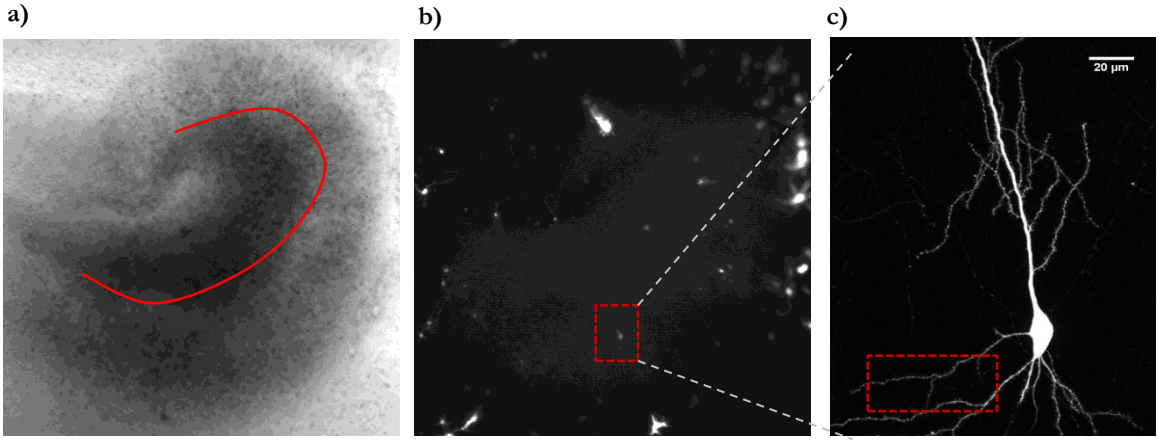

Fig. 59 – Organotypic hippocampal slice culture we biolistically transfected with Dendra. | **a)** Organoytic hippocampal slice culture, bright field image; The red line indicates the location of the pyramidal cell body layer that constitutes the classic tri-synaptic pathway. **b)** A biolistically transfected hippocampal slice culture with fluorescent cells; The red box indicates a pyramidal neuron imaged during experiments; **c)** Fluorescent pyramidal neuron used for experiments at higher magnification; The red box delimits secondary and tertiary dendrites within the stratum radiatum which are imaged during experiments.

3.6.2. Dissociated hippocampal neuronal culture

Dissociated hippocampal neuronal cultures present several advantages for testing the photoconvertible translational reporters. Due to the fact that the cells grow in a monolayer, the penetration of UV-light is more efficient than the case for slice cultures, facilitating experiments to determine photoconversion kinetics. This model will be useful for the validation of our constructs through biochemical analyses of protein folding.

Moreover, dissociated primary cultures afford an ideal environment within which to examine the individual factors that might trigger or regulate alterations in synaptic morphology [247]. Segal and Manor demonstrated tissue culture conditions in which it is possible to monitor dendrites and dendritic spines for several weeks [248] allowing the potential use of this system for studies of plasticity-related and morphological changes in neurons. In this model, one week old cultures already contain "headless" spines, constituting 50% of the spine population, which increases with time in culture. By three weeks in culture, spines observed are similar

to those seen *in vivo* [247].

In figure 60 we show the development of dissociated hippocampal cultures done in our lab.

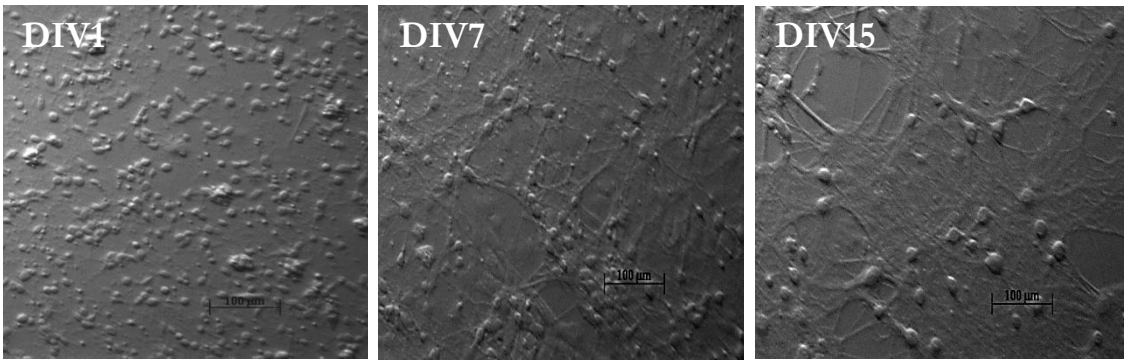

Fig.60 – Dissociated hippocampal neurons maintained in our lab for two weeks or more. | Development of processes in dissociated hippocampal neurons in monolayer culture; At DIV1 the neurons have very few processes being mainly round; At DIV 7 it is already possible to see some connections between neurons and they still look healthy; At DIV15 the neurons have lot of connections; Scale: 100 µm .

3.7. Photoconversion of Dendra and Calmodulin-Dendra

As shown by Chudakov and colleagues, excitation of Dendra2 with short wavelengths, of around 405 nm, leads to a very efficient conversion of Dendra2 into the red fluorescent state, similarly to other Kaede-like proteins [249]. Moreover, green fluorescence of Dendra2 decreases significantly upon its photoconversion to the red fluorescent form allowing tracking of migration of nonactivated or newly produced green fluorescent Dendra2 into the region of activation (similarly to photobleaching techniques). However, it is important, for such tracking to work, that a significant portion of the protein be photoswitched from green to red fluorescence, to allow monitoring of redistribution of the green form[249].

Given these characteristics of Dendra2, we decided to use it to generate tagged reporters of local protein synthesis upon long lasting synaptic plasticity. Therefore, the initial form of Dendra2 that will be generated will be green, and when exposed to UV light-(405 nm) or blue-(488 nm) light it will be converted to an irreversible red form. In the beginning of the experiment, the majority of basal Dendra2 reporter fusion protein is expected to be green, and after photoconversion, a dramatic increase in red fluorescence is expected, with a concomitant decrease in green fluorescence.

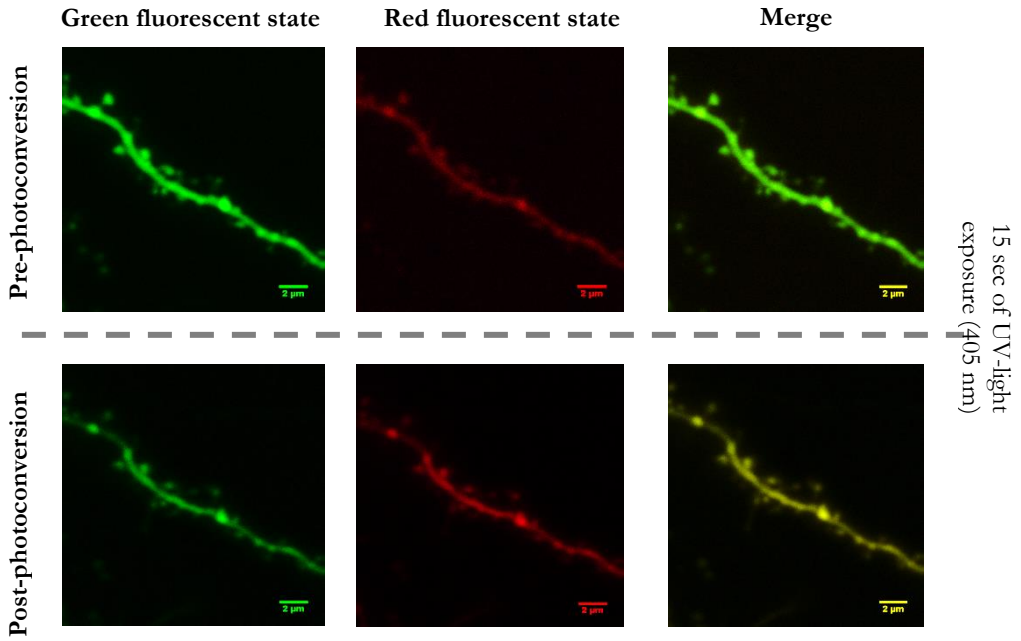

Fig. 61 – Dendra2 photoconversion process leads to an increase in red signal and a decrease in green signal. | In the beginning of the protocol the fluorescent green state is more intense than the red fluorescent state (Pre-photoconversion). After 15 sec of UV-light (405 nm) the red form of Dendra2 appears more intense and the green form decreases its intensity, once it is converted to red form (Post-photoconversion). As it is seen in the last column the red fluorescent state gets brighter and the green pale which results in a more yellowish merge image (Merge); Scale bar: 2 µm.

As seen in figure 61, Dendra2 is mainly produced in the green form and after 15 sec of UV-light (405 nm) it

is converted to a red form, leading to a decrease in the green fluorescence state. It is possible to visualize that after photoconversion, the ratio between the green and red forms has completely changed from the original relationship, resulting in a decrease in green and increase in red fluorescence. This results in a yellow color in the merged picture (Fig.61, right column). The selection of UV-light instead of the non-harmful blue-light was based on the highest efficiency of conversion obtained by the UV-light.

We first tested the photoconversion protocol in 2 pyramidal neuron dendrites that were transfected with STOP Dendra2-C vector (subsequently referred to as Dendra) and then in 2 dendrites transfected with 5'UTR-ORF-Calmodulin-Dendra-3'UTR (subsequently referred to as Calmodulin-Dendra), the results of which were analyzed and can be seen in Figure 62. In the experiment, the pictures of each fluorescent channel were aligned and a region of interest was selected (ROI) for intensity fluorescence measurements: spine region (red box) and dendritic shaft (blue box) (Fig. 62). We decided to use only the intensity fluorescence data related to the dendritic shaft as it is known that the machinery necessary for protein synthesis is present on dendrites adjacent to dendritic spines and not within the spine heads [158-160]. In the future, spine head analysis of fluorescence will also be carried out.

In previous experiments we saw that a small amount of the blue-light used to visualize the green fluorescence is able to photoconvert the green form to the red one. Therefore, we limited this exposure, and keep in mind this small effect.

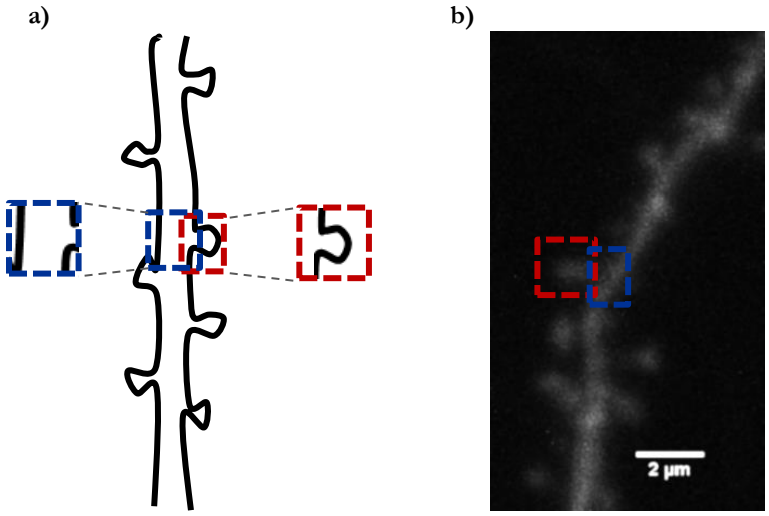

Fig. 62 – Analysis of fluorescence intensity| **a)** Scheme explaining how we selected the regions to do the analysis of fluorescence intensity; **b)** Example of one of the cells analyzed using these method; Red box: spine selected for analysis; Blue box: dendrite adjacent to the selected spine also selected for analysis.

After fluorescence intensity analysis we normalized the data to the first image before photoconversion and calculated the ratio of green fluorescence (Fig. 63a) and red fluorescence (Fig. 63b). As expected, before photoconversion the ratio of normalized intensity of both forms of Dendra2 and Calmodulin-Dendra2 stay

stable (-20 to -1 min). After photoconversion (min 1), the green fluorescence decreased (Fig. 63a) while the red increases in the ratio of normalized intensity (Fig. 63b), as expected.

The ratio of normalized intensity of green and red fluorescent forms was then followed for 30 min to visualize the basal changes in its fluorescence such as basal translation and basal degradation of these proteins.

a)

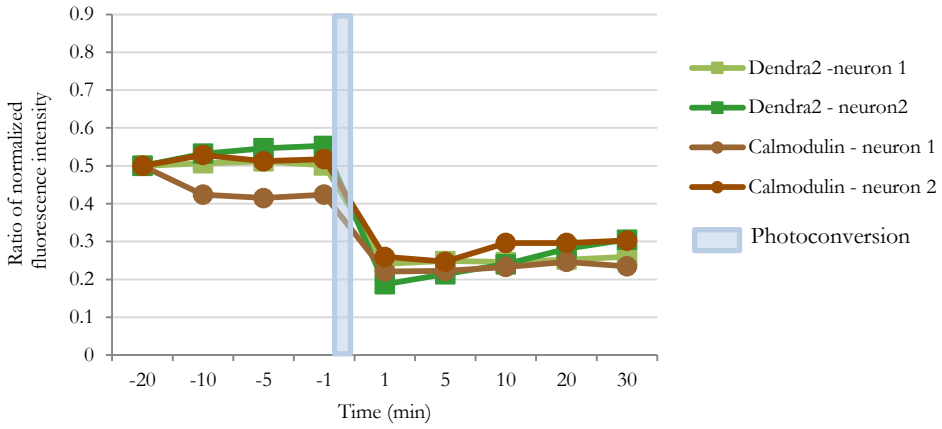

b)

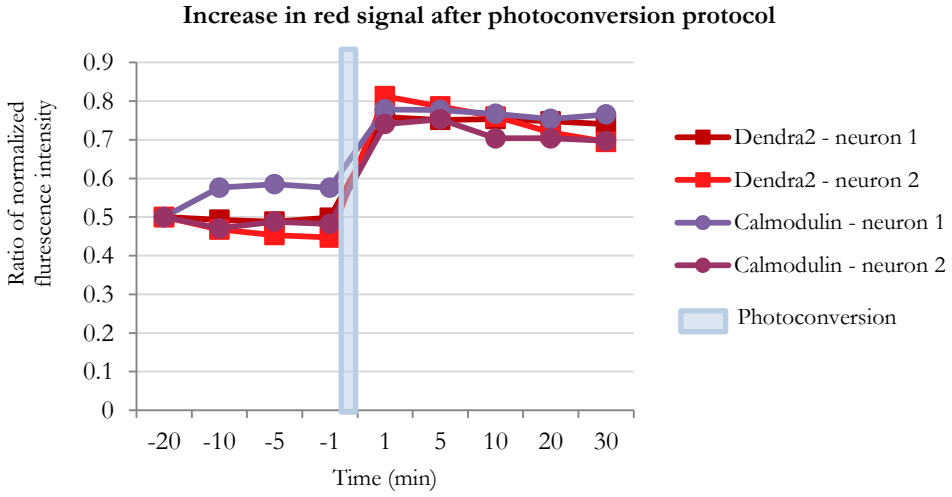

Fig. 63 – Kinetics of photoconversion phenomenon| Changes in fluorescence state of Dendra2 and Calmodulin after photoconversion **a)** Ratio of change in green fluorescent state; **b)** Ratio of change in red fluorescent state; Squares represent the controls; Circles represent change in Calmodulin construct; Blue box indicates time of photoconversion.

The comparison between the kinetics of Dendra and Calmodulin-Dendra fusion protein shows that the photoconversion efficiency is quite similar for these two constructs. Basal translation and protein degradation do not appear to be significantly different in either case. The main difference observed is that the fusion protein Calmodulin-Dendra appears to be less bright than Dendra alone (likely due to the size and

efficiency of transcribing a larger construct by the neuron), but this does not seem to interfere with the photoconversion process.

3.8. Global stimulation of translation via mGluR mediated LTD

Activation of group 1 metabotropic glutamate receptors (mGluRs) induces long-lasting changes in neuronal and synaptic function that rely on new protein synthesis but are independent of transcription [149] suggesting that mGluRs can directly regulate mRNA translation in neurons [137].

One consequence of mGluR activation, either with the selective agonist DHPG or with synaptic stimulation (PP-LFS), is long-term depression [250].

Recent findings in the lab identify long lasting structural changes in spines, such as shrinkage and elimination, following mGluR LTD induced by DHPG. It is well established that this form of plasticity requires the induction of protein synthesis. Therefore, we choose to use DHPG to stimulate LTD globally, with the expectation that robust protein translation will also be induced. This provides a good system in which to test the functionality of the translation reporters which we are developing.

In the following experiments, we first photoconverted positive neurons expressing either Dendra alone (controls) or Calmodulin-Dendra from the green fluorescent state to red state with 15 sec of UV-light exposure (Fig. 64). As expected, before photoconversion the ratio of normalized intensity of both forms stays stable (-20 to -1 min).

As seen in figure 64, after photoconversion (1 min), the green fluorescence of all cells decreases as expected; both ratios of normalized intensities decrease significantly after UV-light exposure (Dendra alone or with Calmodulin-Dendra). Similarly to the finding for the green fluorescence, after photoconversion (min 1), the red fluorescence of the cells increases; both the ratios of normalized intensities increase significantly after UV-light photoconversion in control Dendra and Calmodulin-Dendra examples (Fig. 64)

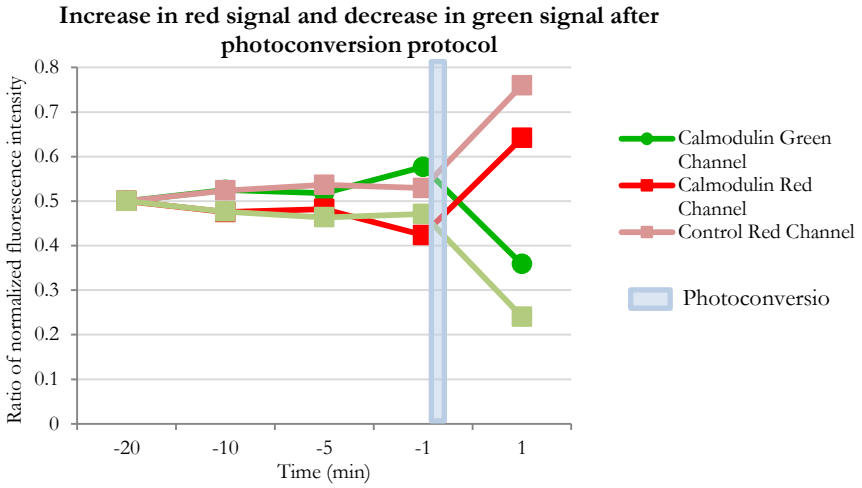

Fig. 64 – Changes in fluorescence state before photoconversion | Ratio of change in green and red fluorescent state; Squares represent the controls; Circle represent change in Calmodulin baseline; Blue box indicates time of photoconversion.

After photoconversion, LTD was induced by incubating the cell with DHPG for 5 min (time = minute 2, indicated by the yellow bar in the graph) to activate global synaptic depression as well as protein translation. Fluorescence intensity was monitored for 30 min (Fig. 65) to visualize any change in the ratio of normalized fluorescence that may arise due to protein translation or degradation. As newly made proteins will be expected to be synthesized as a green form and the pre-existent proteins will remain red, we can analyze whether we are able to detect any increase in dendritic protein synthesis by an increase in green signal after DHPG application.

Following stimulation with DHPG (at min 2), different kinetics of increased green fluorescence can be observed when comparing stimulated and non-stimulated controls. As seen in figure 65 the increase in the green signal of the stimulated cells compared to non-stimulated cells occurs very rapidly: 5 min after photoconversion the DHPG stimulated cell increases in green fluorescence, while the control increases at a slower rate of 10 min after photoconversion. In the red channel the same kinetics can be seen (Fig. 65); there is an abrupt decease in red normalized fluorescence of the stimulated cells, while the non-stimulated ones show a decrease 10 min after photoconversion. These results may represent an increase in dendritic protein synthesis after DHPG stimulation, shown by an increase in green ratio and a decrease in red fluorescence.

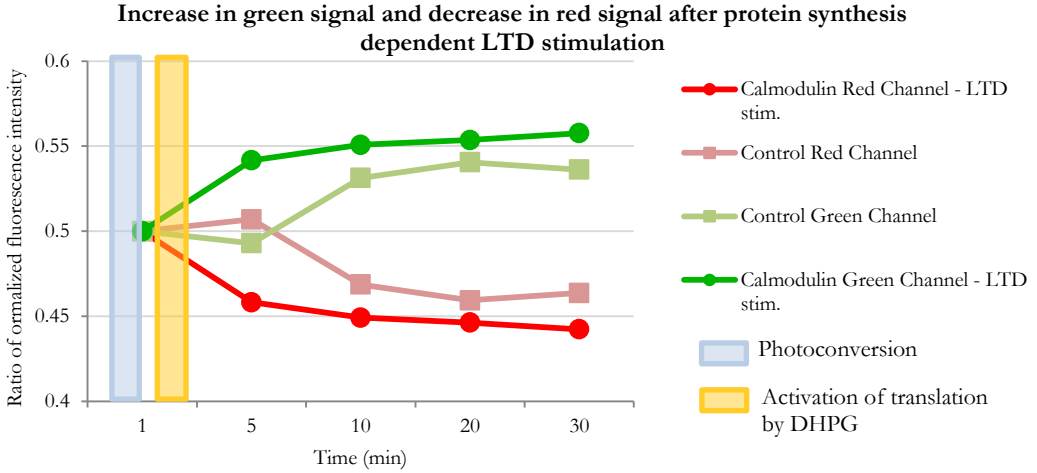

Fig. 65 – Translational reporter after LTD stimulation with DHPG | **a)** Ratio of change in green fluorescent state; **b)** Ratio of change in red fluorescent state; Circle represent change in Calmodulin-Dendra2 construct after protein synthesis dependent LTD stimulation; Squares represent the control; Blue bar represents time of photoconversion after baseline imaging; Yellow bar represents LTD stimulation using DHPG after photoconversion.

3.8. Uncaging Synapse specific stimulation of translation by glutamate uncaging LTP

Govindarajan and Israely showed that uncaging MNI-glutamate with a stimulus train (30 pulses of 4 ms each at 0.5 Hz) in the presence of forskolin leads to L-LTP dependent on protein synthesis [156]. Thus, to see local protein synthesis after synaptic activity, uncaging LTP is the best way to induce localized plasticity that requires protein synthesis and that can be followed in a defined spatial region. Using this protocol we stimulate a unique spine and follow the change in protein translation near this site after photoconversion.

The experiment initially requires the convertion of the green signal to red one by exposing the cells to 15 sec of UV-light. As seen in Figure 66, there is no difference in baseline fluorescence between the cell that will undergo uncaging LTP and the non-stimulated controls. Before photoconversion, both green and red forms stay stable. Photoconversion induces the expected change in fluorescence as seen previously, wherein the green signal is diminished and the red signal increases.

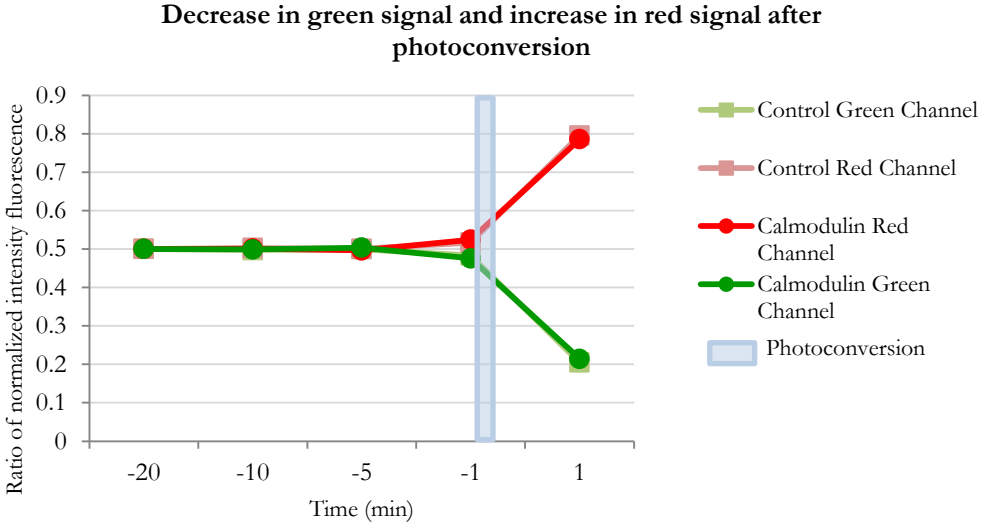

Fig. 66 – Changes in fluorescence state after photoconversion | Ratio of change in red and green fluorescent state; Squares represent the internal controls; Circle represent Calmodulin baseline; Blue box indicates time of photoconversion.

After photoconversion the uncaging LTP protocol was carried out as described in section 2.7.2. and as shown in figure 67. One spine is stimulated to undergo LTP with glutamate uncaging in the presence of the cAMP analog Forskolin. Neighboring spines are analyzed for changes in volume as internal controls. Spine volume analysis was carried out to verify that LTP was indeed induced. The diameter of each spine is calculated for each time point, and is measured and used to calculate the volume of the spine (assuming that

the structure is spherical.)

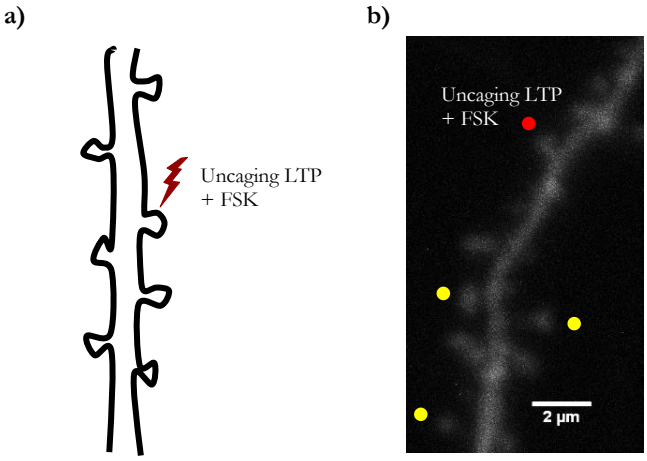

Fig. 67 – Protein synthesis dependent LTP by uncaging at single dendritic spines. | **a)** Scheme explaining how we did the uncaging protocol; **b)** Example of stimulated spine; Red circle marks the spine stimulated; Lightning bolt symbols the uncaging LTP protocol; Yellow circle marks the spine used as internal control for volume spine analysis.

After inducing uncaging LTP (at time = 1.5 min, dashed red line) an increase in the volume of the stimulated spine can be seen, while the control spine does not appear to demonstrate stimulation specific volume changes (Fig. 68). The fluctuations in spine volumes observed could be due to the lack of TTX in the experiment, which allowed spontaneous activity to occur in the slice while Forskolin was present. This could result in multiple spines being activated and could lead to competition between the inputs. Indeed, it appears that in this example, the growth and shrinkage of the spines analyzed are negatively correlated. Further experiments will need to be done to ascertain the source of this fluctuation.

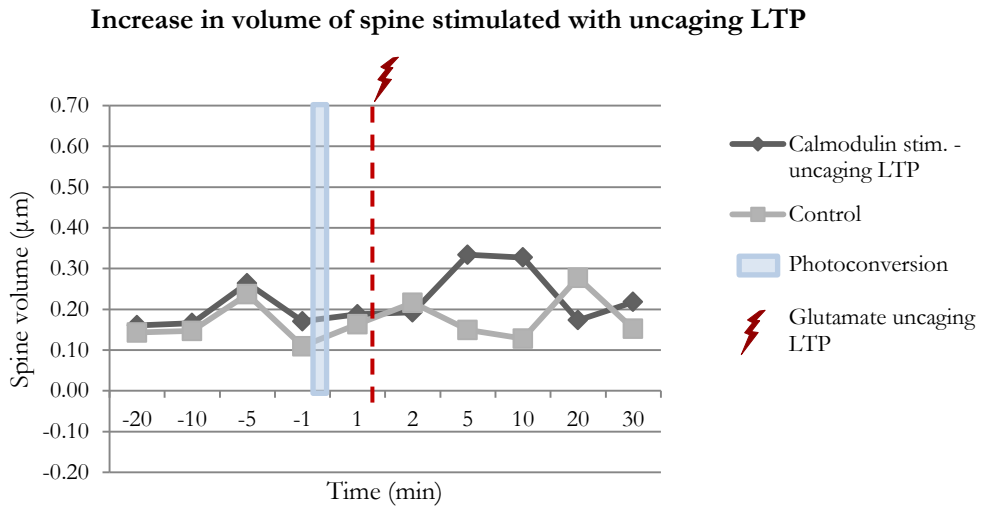

Fig. 68 – Spine volume changes during photoconversion and uncaging LTP | Change in volume of spine stimulated with uncaging LTP protocol (circle) and neighbors spine that was not stimulated (square); At time 0 photoconversion occur and between time 1 and 2 induction uncaging LTP; Square represent the controls; Circles represent spine stimulated with uncaging LTP; Blue box indicates time of photoconversion protocol; Dashed red line represents induction of uncaging LTP.

After induction of the uncaging LTP protocol (at 1.5 min), the cell was imaged for 30 min (Fig. 69) to visualize any change in fluorescence that may arise from induction of protein translation. The expectation is that newly made proteins will be synthesized with a green fluorescent tag, thus leading to an increase in the green signal, while the red fluorescence is maintained. Indeed, the green ratio of normalized fluorescence signal increases in intensity, while the red signal slightly decreases (Fig. 69).

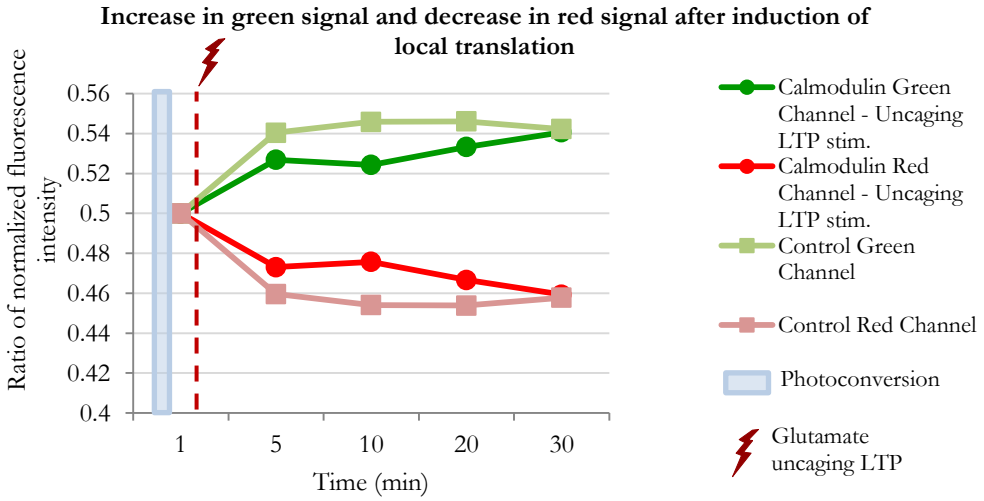

Fig. 69 – Translational reporter after uncaging LTP in specific spine | Ratio of change in red and green fluorescent state; Square represent the internal controls; Circle represent spine stimulated with uncaging LTP; Blue box indicates time of photoconversion protocol; Dashed red line represent time of uncaging LTP protocol.

Chapter 4. Conclusions

4. Conclusions

In this study we aim to understand where proteins thought to be involved in synaptic plasticity are produced after synaptic activation and where they influence plasticity. The availability of these proteins is thought to limit the structural changes behind synaptic plasticity. Thus, in this work we focus mainly on the study of local protein translation after synaptic activity.

In this study, we designed translational reporters that allow us to understand the kinetics of Dendra2 photoconversion; a fluorophore with unique features that will be our main tool for studying local protein translation and protein diffusion. Dendra2 is synthesized as a green fluorescent form and after exposure to UV- or blue-light it is converted to a red mature form, resulting in a time-stamp between pre-existent and newly made proteins. We demonstrate that Dendra2 is efficiently photoconverted by 15 sec of exposure to UV-light; that 30 sec of exposure leads to bleaching of the fluorescent signal, mainly in the green channel. Moreover, UV-light is harmful to the cells and thus the least possible exposure time is best for the complete viability of cells. The selection of UV-light instead of the non-noxious blue-light was based on the highest efficiency of conversion by the UV-light. Simultaneously we saw that the blue-light used to visualized the green fluorescence is able to photoconvert the green form to the red one; a constraint to take into account when photoconversion is being done.

We were also able to design and construct several fusion protein constructs with the Dendra2 fluorophore, using native proteins of different classes of proteins present in the PSD region, thought to be important for synaptic plasticity and thus locally translated. Native proteins were fused to the N-terminus of the Dendra2 ORF and the *untranslated regions* of each specific protein were cloned on either side of the fluorophore. The UTRs were added to the construct to target the mRNAs to the dendrites and regulate them similarly to the native proteins. To begin with, we first tested the completed Calmodulin-Dendra construct as a proof of principle, and compared it to Dendra alone. We verified that the photoconversion phenomenon occurs, as expected, and conducted pilot analyses of protein synthesis dependent LTP (with glutamate uncaging) and LTD (with DHPG application) in cells expressing the Calmodulin-Dendra construct. We observe an increase in green fluorescence and a decrease in red fluorescence following the induction of protein synthesis dependent synaptic plasticity and find that the reporter seems to be functioning. Further studies to assess the functionality of this fusion protein, as well as the others successfully cloned thus far, will be needed next. Completed constructs include: GluA1, Arc, and CaMKIIα. In sum, we now have several translational reporters which remain to be tested for proteins thought to be important for synaptic plasticity, and which may be locally produced,

Using 5'UTR-Calmodulin-Dendra-3'UTR construct, we were able to photoconvert the green fluorescent form to a red form to the same extent as the Dendra2 control. Afterwards, we induced global protein

synthesis using mGluR agonist (DHPG) and saw an increase in the ratio of green signal, with kinetics different from the one seen in the control experiments, which may reflect an increase in local protein synthesis. We also used spine specific uncaging LTP to test local translation, however further studies are required.

Thus far, we have been able to construct and visualize a fluorescent photoconvertible protein fusion that will allow us to study local protein synthesis after synaptic stimulation and follow the newly made proteins along dendrites and spines. The movement of these proteins may provide clues as to how a limited pool of available proteins can lead to competition for plasticity and how synapses may cooperate after production of dendritic proteins.

In the future we will continue to optimize the protocols for protein synthesis dependent plasticity in order to visualize local translation. We will test all the constructs that we have developed, with the hypothesis that different native proteins will have different kinetics of translation and trafficking after synaptic activation. It will be important, for such tracking to be successful, to optimize the quantity of the protein to be photoswitched from green to red fluorescence, in order to allow monitoring of the green form redistribution.

Overall, understanding how local protein availability affects synapses and synaptic plasticity, as well as how an imbalance of this system could affect neuronal function, may have a significant impact on our understanding of mental retardation disorders in which protein translation is misregulated, such as Fragile X syndrome.

Chapter 5. References

5. References

1. Ramon y Cajal, S., *Histology of the nervous system of man and vertebrates*. 1995: Oxford University Press, New York.
2. Bliss, T.V.P. and G.L. Collingridge, *A synaptic model of memory: long-term potentiation in the hippocampus.* Nature, 1993. **361**(6407): p. 31-39.
3. Bailey, C.H. and E.R. Kandel, *Structural changes accompanying memory storage.* Annual review of physiology, 1993. **55**(1): p. 397-426.
4. Hebb, D., *0.(1949) The organization of behavior: A neuropsychological theory.* New York.
5. Corkin, S., *What's new with the amnesic patient HM?* Nature Reviews Neuroscience, 2002. **3**(2): p. 153-160.
6. Scoville, W.B. and B. Milner, *Loss of recent memory after bilateral hippocampal lesions.* Journal of Neurology, Neurosurgery & Psychiatry, 1957. **20**(1): p. 11-21.
7. Squire, L.R. and S. Zola-Morgan, *The medial temporal lobe memory system.* Science, 1991. **253**(5026): p. 1380-1386.
8. Squire, L.R. and S.M. Zola, *Structure and function of declarative and nondeclarative memory systems.* Proceedings of the National Academy of Sciences, 1996. **93**(24): p. 13515.
9. Morris, R., *Developments of a water-maze procedure for studying spatial learning in the rat.* Journal of neuroscience methods, 1984. **11**(1): p. 47-60.
10. Squire, L.R., C.E.L. Stark, and R.E. Clark, *The medial temporal lobe*.* Annu. Rev. Neurosci., 2004. **27**: p. 279-306.
11. Amaral, D. and M. Witter, *The three-dimensional organization of the hippocampal formation: a review of anatomical data.* Neuroscience, 1989. **31**(3): p. 571.
12. Eichenbaum, H., *A cortical-hippocampal system for declarative memory.* Nature Reviews Neuroscience, 2000. **1**(1): p. 41-50.
13. Witter, M., et al., *Functional organization of the extrinsic and intrinsic circuitry of the parahippocampal region.* Progress in neurobiology, 1989. **33**(3): p. 161.
14. Brun, V.H., et al., *Place cells and place recognition maintained by direct entorhinal-hippocampal circuitry.* Science, 2002. **296**(5576): p. 2243-2246.
15. Nakazawa, K., et al., *Requirement for hippocampal CA3 NMDA receptors in associative memory recall.* Science, 2002. **297**(5579): p. 211-218.
16. Nakashiba, T., et al., *Transgenic inhibition of synaptic transmission reveals role of CA3 output in hippocampal learning.* Science's STKE, 2008. **319**(5867): p. 1260.
17. McHugh, T.J., et al., *Dentate gyrus NMDA receptors mediate rapid pattern separation in the hippocampal network.* Science, 2007. **317**(5834): p. 94-99.
18. Yasuda, M., et al., *Multiple Forms of Activity-Dependent Competition Refine Hippocampal Circuits InáVivo.* Neuron, 2011. **70**(6): p. 1128-1142.
19. Spruston, N., *Pyramidal neurons: dendritic structure and synaptic integration.* Nature Reviews Neuroscience, 2008. **9**(3): p. 206-221.
20. Megias, M., et al., *Total number and distribution of inhibitory and excitatory synapses on hippocampal CA1 pyramidal cells.* Neuroscience, 2001. **102**(3): p. 527-540.
21. Gao, W.J. and Z.H. Zheng, *Target-specific differences in somatodendritic morphology of layer V pyramidal neurons in rat motor cortex.* The Journal of comparative neurology, 2004. **476**(2): p. 174-185.
22. Kasper, E.M., et al., *Pyramidal neurons in layer 5 of the rat visual cortex. I. Correlation among cell morphology, intrinsic electrophysiological properties, and axon targets.* The Journal of comparative neurology, 1994. **339**(4): p. 459-474.
23. Petreanu, L., et al., *The subcellular organization of neocortical excitatory connections.* Nature, 2009. **457**(7233): p. 1142-1145.
24. Sajikumar, S. and M. Korte, *Different compartments of apical CA1 dendrites have different plasticity thresholds for expressing synaptic tagging and capture.* Learning & Memory, 2011. **18**(5): p. 327-331.
25. Witter, M.P., *Organization of the entorhinal-hippocampal system: a review of current anatomical data.* Hippocampus, 1993. **3**: p. 33.
26. London, M. and M. Häusser, *Dendritic computation.* Annu. Rev. Neurosci., 2005. **28**: p. 503-532.
27. Schiller, J., et al., *Calcium action potentials restricted to distal apical dendrites of rat neocortical pyramidal neurons.* The Journal of Physiology, 1997. **505**(3): p. 605-616.
28. Golding, N.L. and N. Spruston, *Dendritic sodium spikes are variable triggers of axonal action potentials in hippocampal CA1 pyramidal neurons.* Neuron, 1998. **21**(5): p. 1189-1200.
29. Schiller, J., et al., *NMDA spikes in basal dendrites of cortical pyramidal neurons.* Nature, 2000. **404**(6775): p. 285-288.
30. Branco, T., B.A. Clark, and M. Hausser, *Dendritic discrimination of temporal input sequences in cortical neurons.* Science's STKE, 2010. **329**(5999): p. 1671.
31. Larkum, M.E., J.J. Zhu, and B. Sakmann, *A new cellular mechanism for coupling inputs arriving at different cortical layers.* Nature, 1999. **398**(6725): p. 338-341.
32. Alvarez, V.A. and B.L. Sabatini, *Anatomical and physiological plasticity of dendritic spines.* Annu. Rev. Neurosci., 2007. **30**: p. 79-97.
33. Fu, M. and Y. Zuo, *Experience-dependent structural plasticity in the cortex.* Trends in Neurosciences, 2011. **34**(4): p. 177-187.
34. Holtmaat, A. and K. Svoboda, *Experience-dependent structural synaptic plasticity in the mammalian brain.* Nature Reviews Neuroscience, 2009. **10**(9): p. 647-658.
35. Holtmaat, A., et al., *Experience-dependent and cell-type-specific spine growth in the neocortex.* Nature, 2006. **441**(7096): p. 979-983.
36. Ballesteros-Yáñez, I., et al., *Density and morphology of dendritic spines in mouse neocortex.* Neuroscience, 2006. **138**(2): p. 403-409.

37. Harris, K.M. and J.K. Stevens, *Dendritic spines of CA 1 pyramidal cells in the rat hippocampus: serial electron microscopy with reference to their biophysical characteristics.* The Journal of neuroscience, 1989. **9**(8): p. 2982-2997.
38. Bourne, J.N. and K.M. Harris, *Balancing structure and function at hippocampal dendritic spines.* Annual review of neuroscience, 2008. **31**: p. 47.
39. Shepherd, G.M., *The dendritic spine: a multifunctional integrative unit.* Journal of neurophysiology, 1996. **75**(6): p. 2197-2210.
40. Svoboda, K., D.W. Tank, and W. Denk, *Direct measurement of coupling between dendritic spines and shafts.* Science, 1996. **272**(5262): p. 716-719.
41. Elson, G.N. and J. DeFelipe, *Spine distribution in cortical pyramidal cells: a common organizational principle across species.* Progress in brain research, 2002. **136**: p. 109-133.
42. Yankova, M., S.A. Hart, and C.S. Woolley, *Estrogen increases synaptic connectivity between single presynaptic inputs and multiple postsynaptic CA1 pyramidal cells: a serial electron-microscopic study.* Proceedings of the National Academy of Sciences, 2001. **98**(6): p. 3525.
43. Sorra, K. and K.M. Harris, *Occurrence and three-dimensional structure of multiple synapses between individual radiatum axons and their target pyramidal cells in hippocampal area CA1.* The Journal of neuroscience, 1993. **13**(9): p. 3736-3748.
44. Woolley, C.S., H.J. Wenzel, and P.A. Schwartzkroin, *Estradiol increases the frequency of multiple synapse boutons in the hippocampal CA1 region of the adult female rat.* The Journal of comparative neurology, 1996. **373**(1): p. 108-117.
45. Hering, H. and M. Sheng, *Dendritic spines: structure, dynamics and regulation.* Nature Reviews Neuroscience, 2001. **2**(12): p. 880-888.
46. Majewska, A.K., J.R. Newton, and M. Sur, *Remodeling of synaptic structure in sensory cortical areas in vivo.* The Journal of neuroscience, 2006. **26**(11): p. 3021-3029.
47. Zuo, Y., et al., *Development of long-term dendritic spine stability in diverse regions of cerebral cortex.* Neuron, 2005. **46**(2): p. 181-189.
48. Grutzendler, J., N. Kasthuri, and W.B. Gan, *Long-term dendritic spine stability in the adult cortex.* Nature, 2002. **420**(6917): p. 812-816.
49. Majewska, A. and M. Sur, *Motility of dendritic spines in visual cortex in vivo: changes during the critical period and effects of visual deprivation.* Proceedings of the National Academy of Sciences of the United States of America, 2003. **100**(26): p. 16024.
50. Zuo, Y., et al., *Long-term sensory deprivation prevents dendritic spine loss in primary somatosensory cortex.* Nature, 2005. **436**(7048): p. 261-265.
51. Harris, K.M., F.E. Jensen, and B. Tsao, *Three-dimensional structure of dendritic spines and synapses in rat hippocampus (CA1) at postnatal day 15 and adult ages: implications for the maturation of synaptic physiology and long-term potentiation.* J Neurosci, 1992. **12**(7): p. 2685-705.
52. Kasai, H., et al., *Structure-stability-function relationships of dendritic spines.* Trends in Neurosciences, 2003. **26**(7): p. 360-368.
53. Parnass, Z., A. Tashiro, and R. Yuste, *Analysis of spine morphological plasticity in developing hippocampal pyramidal neurons.* Hippocampus, 2000. **10**(5): p. 561-568.
54. Trachtenberg, J.T., et al., *Long-term in vivo imaging of experience-dependent synaptic plasticity in adult cortex.* Nature, 2002. **420**(6917): p. 788-794.
55. Maletic-Savatic, M., R. Malinow, and K. Svoboda, *Rapid dendritic morphogenesis in CA1 hippocampal dendrites induced by synaptic activity.* Science, 1999. **283**(5409): p. 1923-1927.
56. Engert, F. and T. Bonhoeffer, *Dendritic spine changes associated with hippocampal long-term synaptic plasticity.* Nature, 1999. **399**(6731): p. 66-70.
57. Matsuzaki, M., et al., *Dendritic spine geometry is critical for AMPA receptor expression in hippocampal CA1 pyramidal neurons.* Nature neuroscience, 2001. **4**(11): p. 1086-1092.
58. Ganeshina, O., et al., *Synapses with a segmented, completely partitioned postsynaptic density express more AMPA receptors than other axospinous synaptic junctions.* Neuroscience, 2004. **125**(3): p. 615-623.
59. Ganeshina, O., et al., *Differences in the expression of AMPA and NMDA receptors between axospinous perforated and nonperforated synapses are related to the configuration and size of postsynaptic densities.* The Journal of comparative neurology, 2004. **468**(1): p. 86-95.
60. Ashby, M.C., et al., *Lateral diffusion drives constitutive exchange of AMPA receptors at dendritic spines and is regulated by spine morphology.* The Journal of neuroscience, 2006. **26**(26): p. 7046-7055.
61. Nimchinsky, E.A., et al., *The number of glutamate receptors opened by synaptic stimulation in single hippocampal spines.* Science's STKE, 2004. **24**(8): p. 2054.
62. Okabe, S., *Molecular anatomy of the postsynaptic density.* Molecular and Cellular Neuroscience, 2007. **34**(4): p. 503-518.
63. Spacek, J. and K.M. Harris, *Three-dimensional organization of smooth endoplasmic reticulum in hippocampal CA1 dendrites and dendritic spines of the immature and mature rat.* The Journal of neuroscience, 1997. **17**(1): p. 190-203.
64. Ostroff, L.E., et al., *Polyribosomes redistribute from dendritic shafts into spines with enlarged synapses during LTP in developing rat hippocampal slices.* Neuron, 2002. **35**(3): p. 535-545.
65. Kang, H. and E.M. Schuman, *A requirement for local protein synthesis in neurotrophin-induced hippocampal synaptic plasticity.* Science, 1996. **273**(5280): p. 1402-1406.
66. Kelleher, R.J., et al., *Translational control by MAPK signaling in long-term synaptic plasticity and memory.* Cell, 2004. **116**(3): p. 467-479.
67. Cracco, J.B., et al., *Protein synthesis-dependent LTP in isolated dendrites of CA1 pyramidal cells.* Hippocampus, 2005. **15**(5): p. 551-556.
68. Bourne, J. and K.M. Harris, *Do thin spines learn to be mushroom spines that remember?* Current opinion in neurobiology, 2007. **17**(3): p. 381-386.

69. Koch, C. and A. Zador, *The function of dendritic spines: devices subserving biochemical rather than electrical compartmentalization.* J Neurosci, 1993. **13**(2): p. 413-422.
70. Swindale, N., *Dendritic spines only connect.* Trends in Neurosciences, 1981. **4**: p. 240-241.
71. Stepanyants, A., P.R. Hof, and D.B. Chklovskii, *Geometry and structural plasticity of synaptic connectivity.* Neuron, 2002. **34**(2): p. 275-288.
72. Nimchinsky, E.A., B.L. Sabatini, and K. Svoboda, *Structure and function of dendritic spines.* Annual review of physiology, 2002. **64**(1): p. 313-353.
73. Tsay, D. and R. Yuste, *On the electrical function of dendritic spines.* Trends in Neurosciences, 2004. **27**(2): p. 77-83.
74. Korkotian, E. and M. Segal, *Regulation of dendritic spine motility in cultured hippocampal neurons.* The Journal of neuroscience, 2001. **21**(16): p. 6115-6124.
75. Citri, A. and R.C. Malenka, *Synaptic plasticity: multiple forms, functions, and mechanisms.* Neuropsychopharmacology, 2007. **33**(1): p. 18-41.
76. Hughes, J.R., *Post-tetanic potentiation.* Physiological reviews, 1958. **38**(1): p. 91-113.
77. Gerrow, K. and A. Triller, *Synaptic stability and plasticity in a floating world.* Current opinion in neurobiology, 2010. **20**(5): p. 631-639.
78. Shi, S.H., et al., *Rapid spine delivery and redistribution of AMPA receptors after synaptic NMDA receptor activation.* Science, 1999. **284**(5421): p. 1811-1816.
79. Zhu, J.J., et al., *Ras and Rap control AMPA receptor trafficking during synaptic plasticity.* Cell, 2002. **110**(4): p. 443-455.
80. Carew, T.J., H.M. Pinsker, and E.R. Kandel, *Long-term habituation of a defensive withdrawal reflex in Aplysia.* Science, 1972. **175**(4020): p. 451-454.
81. Pinsker, H.M., et al., *Long-term sensitization of a defensive withdrawal reflex in Aplysia.* Science, 1973. **182**(4116): p. 1039-1042.
82. Bliss, T.V.P. and T. Lømo, *Long-lasting potentiation of synaptic transmission in the dentate area of the anaesthetized rabbit following stimulation of the perforant path.* The Journal of Physiology, 1973. **232**(2): p. 331-356.
83. Malenka, R.C., *Synaptic plasticity in the hippocampus: LTP and LTD.* Cell, 1994. **78**(4): p. 535-538.
84. Frey, U. and R. Morris, *Weak before strong: dissociating synaptic tagging and plasticity-factor accounts of late-LTP.* Neuropharmacology, 1998. **37**(4-5): p. 545-552.
85. Lüscher, C. and R.C. Malenka, *NMDA receptor-dependent long-term potentiation and long-term depression (LTP/LTD).* Cold Spring Harbor Perspectives in Biology, 2012. **4**(6).
86. Morris, R.G.M., S. Davis, and S.P. Butcher, *Hippocampal synaptic plasticity and NMDA receptors: a role in information storage?* Philosophical Transactions of the Royal Society of London. Series B: Biological Sciences, 1990. **329**(1253): p. 187-204.
87. Malenka, R.C. and M.F. Bear, *LTP and LTD: an embarrassment of riches.* Neuron, 2004. **44**(1): p. 5-21.
88. Augustine, G.J., F. Santamaria, and K. Tanaka, *Local calcium signaling in neurons.* Neuron, 2003. **40**(2): p. 331-346.
89. Johnston, D. and R. Narayanan, *Active dendrites: colorful wings of the mysterious butterflies.* Trends in Neurosciences, 2008. **31**(6): p. 309-316.
90. Chklovskii, D.B., B. Mel, and K. Svoboda, *Cortical rewiring and information storage.* Nature, 2004. **431**(7010): p. 782-788.
91. Malenka, R.C. and R.A. Nicoll, *Long-term potentiation--a decade of progress?* Science, 1999. **285**(5435): p. 1870-1874.
92. Malenka, R.C., et al., *Postsynaptic calcium is sufficient for potentiation of hippocampal synaptic transmission.* Science, 1988. **242**(4875): p. 81-84.
93. Lynch, G., et al., *Intracellular injections of EGTA block induction of hippocampal long-term potentiation.* Nature, 1983. **305**(5936): p. 719-721.
94. Silva, A., et al. *a Calcium/Calmodulin Kinase II Mutant Mice: Deficient Long-term Potentiation and Impaired Spatial Learning.* 1992. Cold Spring Harbor Laboratory Press.
95. Lisman, J., H. Schulman, and H. Cline, *The molecular basis of CaMKII function in synaptic and behavioural memory.* Nature Reviews Neuroscience, 2002. **3**(3): p. 175-190.
96. Mayford, M., S.A. Siegelbaum, and E.R. Kandel, *Synapses and memory storage.* Cold Spring Harbor Perspectives in Biology, 2012. **4**(6).
97. Collingridge, G., S. Kehl, and H. McLennan, *The antagonism of amino acid-induced excitations of rat hippocampal CA1 neurones in vitro.* The Journal of Physiology, 1983. **334**(1): p. 19-31.
98. Blake, J., M. Brown, and G. Collingridge, *CNQX blocks acidic amino acid induced depolarizations and synaptic components mediated by non-NMDA receptors in rat hippocampal slices.* Neuroscience letters, 1988. **89**(2): p. 182-186.
99. Malinow, R., H. Schulman, and R.W. Tsien, *Inhibition of postsynaptic PKC or CaMKII blocks induction but not expression of LTP.* Science (New York, NY), 1989. **245**(4920): p. 862.
100. Malenka, R.C., et al., *An essential role for postsynaptic calmodulin and protein kinase activity in long-term potentiation.* Nature, 1989. **340**(6234): p. 554-557.
101. Malinow, R., D.V. Madison, and R.W. Tsien, *Persistent protein kinase activity underlying long-term potentiation.* 1988.
102. O'Dell, T.J., E.R. Kandel, and S.G. Grant, *Long-term potentiation in the hippocampus is blocked by tyrosine kinase inhibitors.* Nature, 1991. **353**(6344): p. 558-560.
103. Fukunaga, K., et al., *Long-term potentiation is associated with an increased activity of Ca2+/calmodulin-dependent protein kinase II.* Journal of Biological Chemistry, 1993. **268**(11): p. 7863-7867.
104. Lang, C., et al., *Transient expansion of synaptically connected dendritic spines upon induction of hippocampal long-term potentiation.* Proceedings of the National Academy of Sciences of the United States of America, 2004. **101**(47): p. 16665.
105. Matsuzaki, M., et al., *Structural basis of long-term potentiation in single dendritic spines.* Nature, 2004. **429**(6993): p. 761-766.
106. Kopec, C.D., et al., *Glutamate receptor exocytosis and spine enlargement during chemically induced long-term potentiation.* The Journal of

neuroscience, 2006. **26**(7): p. 2000-2009.
107. Park, M., et al., *Plasticity-induced growth of dendritic spines by exocytic trafficking from recycling endosomes.* Neuron, 2006. **52**(5): p. 817-830.
108. De Roo, M., P. Klauser, and D. Muller, *LTP promotes a selective long-term stabilization and clustering of dendritic spines.* PLoS biology, 2008. **6**(9): p. e219.
109. Carroll, R.C., et al., *Dynamin-dependent endocytosis of ionotropic glutamate receptors.* Proceedings of the National Academy of Sciences, 1999. **96**(24): p. 14112-14117.
110. Nicoll, R.A., S. Tomita, and D.S. Bredt, *Auxiliary subunits assist AMPA-type glutamate receptors.* Science, 2006. **311**(5765): p. 1253-1256.
111. Kim, J., et al., *Regulation of dendritic excitability by activity-dependent trafficking of the A-type K+ channel subunit Kv4. 2 in hippocampal neurons.* Neuron, 2007. **54**(6): p. 933-947.
112. Dudek, S.M. and M.F. Bear, *Homosynaptic long-term depression in area CA1 of hippocampus and effects of N-methyl-D-aspartate receptor blockade.* Proceedings of the National Academy of Sciences, 1992. **89**(10): p. 4363.
113. Zhou, Q., K.J. Homma, and M. Poo, *Shrinkage of dendritic spines associated with long-term depression of hippocampal synapses.* Neuron, 2004. **44**(5): p. 749-757.
114. Nägerl, U.V., et al., *Bidirectional activity-dependent morphological plasticity in hippocampal neurons.* Neuron, 2004. **44**(5): p. 759-767.
115. Chen, Y., et al., *The role of actin in the regulation of dendritic spine morphology and bidirectional synaptic plasticity.* Neuroreport, 2004. **15**(5): p. 829.
116. Trommald, M., G. Hulleberg, and P. Andersen, *Long-term potentiation is associated with new excitatory spine synapses on rat dentate granule cells.* Learning & Memory, 1996. **3**(2-3): p. 218-228.
117. Popov, V., et al., *Remodelling of synaptic morphology but unchanged synaptic density during late phase long-term potentiation (LTP): a serial section electron micrograph study in the dentate gyrus in the anaesthetised rat.* Neuroscience, 2004. **128**(2): p. 251-262.
118. Stewart, M., et al., *Chemically induced long-term potentiation increases the number of perforated and complex postsynaptic densities but does not alter dendritic spine volume in CA1 of adult mouse hippocampal slices.* European Journal of Neuroscience, 2005. **21**(12): p. 3368-3378.
119. Bourne, J.N., et al., *Polyribosomes are increased in spines of CA1 dendrites 2 h after the induction of LTP in mature rat hippocampal slices.* Hippocampus, 2007. **17**(1): p. 1-4.
120. Kandel, E.R., *The molecular biology of memory storage: a dialogue between genes and synapses.* Science's STKE, 2001. **294**(5544): p. 1030.
121. Frey, U., Y.-Y. Huang, and E. Kandel, *Effects of cAMP simulate a late stage of LTP in hippocampal CA1 neurons.* Science; Science, 1993.
122. Abel, T., et al., *Genetic demonstration of a role for PKA in the late phase of LTP and in hippocampus-based long-term memory.* Cell, 1997. **88**(5): p. 615-626.
123. Thiels, E., et al., *Transient and persistent increases in protein phosphatase activity during long-term depression in the adult hippocampus< i> in vivo</i>.* Neuroscience, 1998. **86**(4): p. 1023-1029.
124. Sutton, M.A. and E.M. Schuman, *Local translational control in dendrites and its role in long-term synaptic plasticity.* Journal of neurobiology, 2005. **64**(1): p. 116-131.
125. Otani, S., et al., *Maintenance of long-term potentiation in rat dentate gyrus requires protein synthesis but not messenger RNA synthesis immediately post-tetanization.* Neuroscience, 1989. **28**(3): p. 519-526.
126. Montarolo, P., E. Kandel, and S. Schacher, *Long-term heterosynaptic inhibition in Aplysia.* 1988.
127. Nguyen, P.V., T. Abel, and E.R. Kandel, *Requirement of a critical period of transcription for induction of a late phase of LTP.* Science, 1994. **265**(5175): p. 1104-1107.
128. Kelleher III, R.J. and M.F. Bear, *The autistic neuron: troubled translation?* Cell, 2008. **135**(3): p. 401-406.
129. Flexner, J.B., L.B. Flexner, and E. Stellar, *Memory in mice as affected by intracerebral puromycin.* Science, 1963. **141**(3575): p. 57-59.
130. Kandel, E.R., *The molecular biology of memory storage: a dialogue between genes and synapses.* Science, 2001. **294**(5544): p. 1030-1038.
131. Waddell, S. and W.G. Quinn, *Flies, genes, and learning.* Annual review of neuroscience, 2001. **24**(1): p. 1283-1309.
132. Weiler, I.J. and W.T. Greenough, *Metabotropic glutamate receptors trigger postsynaptic protein synthesis.* Proceedings of the National Academy of Sciences, 1993. **90**(15): p. 7168.
133. Job, C. and J. Eberwine, *Identification of sites for exponential translation in living dendrites.* Proceedings of the National Academy of Sciences, 2001. **98**(23): p. 13037.
134. Cohen, A.S. and W.C. Abraham, *Facilitation of long-term potentiation by prior activation of metabotropic glutamate receptors.* Journal of neurophysiology, 1996. **76**(2): p. 953-962.
135. Raymond, C.R., et al., *Metabotropic glutamate receptors trigger homosynaptic protein synthesis to prolong long-term potentiation.* The Journal of neuroscience, 2000. **20**(3): p. 969-976.
136. Oliet, S.H.R., R.C. Malenka, and R.A. Nicoll, *Two distinct forms of long-term depression coexist in CA1 hippocampal pyramidal cells.* Neuron, 1997. **18**(6): p. 969-982.
137. Gallagher, S.M., et al., *Extracellular signal-regulated protein kinase activation is required for metabotropic glutamate receptor-dependent long-term depression in hippocampal area CA1.* The Journal of neuroscience, 2004. **24**(20): p. 4859-4864.
138. Hou, L. and E. Klann, *Activation of the phosphoinositide 3-kinase-Akt-mammalian target of rapamycin signaling pathway is required for metabotropic glutamate receptor-dependent long-term depression.* The Journal of neuroscience, 2004. **24**(28): p. 6352-6361.
139. Tang, S.J., et al., *A rapamycin-sensitive signaling pathway contributes to long-term synaptic plasticity in the hippocampus.* Science's STKE, 2002. **99**(1): p. 467.
140. English, J.D. and J.D. Sweatt, *A requirement for the mitogen-activated protein kinase cascade in hippocampal long term potentiation.*

Journal of Biological Chemistry, 1997. **272**(31): p. 19103-19106.
141. Sweatt, J.D., *Mitogen-activated protein kinases in synaptic plasticity and memory.* Current opinion in neurobiology, 2004. **14**(3): p. 311-317.
142. Martin, K.C. and A. Ephrussi, *mRNA localization: gene expression in the spatial dimension.* Cell, 2009. **136**(4): p. 719-730.
143. Sutton, M.A. and E.M. Schuman, *Dendritic protein synthesis, synaptic plasticity, and memory.* Cell, 2006. **127**(1): p. 49-58.
144. Richter, J.D. and E. Klann, *Making synaptic plasticity and memory last: mechanisms of translational regulation.* Genes & development, 2009. **23**(1): p. 1-11.
145. Torre, E.R. and O. Steward, *Protein synthesis within dendrites: glycosylation of newly synthesized proteins in dendrites of hippocampal neurons in culture.* The Journal of neuroscience, 1996. **16**(19): p. 5967-5978.
146. Crino, P.B. and J. Eberwine, *Molecular characterization of the dendritic growth cone: regulated mRNA transport and local protein synthesis.* Neuron, 1996. **17**(6): p. 1173-1187.
147. Aakalu, G., et al., *Dynamic visualization of local protein synthesis in hippocampal neurons.* Neuron, 2001. **30**(2): p. 489-502.
148. Martin, K.C., et al., *Synapse-specific, long-term facilitation of Aplysia sensory to motor synapses: a function for local protein synthesis in memory storage.* Cell, 1997. **91**(7): p. 927-938.
149. Huber, K.M., M.S. Kayser, and M.F. Bear, *Role for rapid dendritic protein synthesis in hippocampal mGluR-dependent long-term depression.* Science, 2000. **288**(5469): p. 1254-1256.
150. Bradshaw, K., N. Emptage, and T. Bliss, *A role for dendritic protein synthesis in hippocampal late LTP.* European Journal of Neuroscience, 2003. **18**(11): p. 3150-3152.
151. Smith, W.B., et al., *Dopaminergic stimulation of local protein synthesis enhances surface expression of GluR1 and synaptic transmission in hippocampal neurons.* Neuron, 2005. **45**(5): p. 765-779.
152. Sutton, M.A., et al., *Regulation of dendritic protein synthesis by miniature synaptic events.* Science's STKE, 2004. **304**(5679): p. 1979.
153. Mayford, M., et al., *The 3'-untranslated region of CaMKIIa is a cis-acting signal for the localization and translation of mRNA in dendrites.* Proceedings of the National Academy of Sciences, 1996. **93**(23): p. 13250.
154. Ouyang, Y., et al., *Tetanic stimulation leads to increased accumulation of Ca2+/calmodulin-dependent protein kinase II via dendritic protein synthesis in hippocampal neurons.* The Journal of neuroscience, 1999. **19**(18): p. 7823-7833.
155. Scheetz, A., A.C. Nairn, and M. Constantine-Paton, *NMDA receptor-mediated control of protein synthesis at developing synapses.* Nature neuroscience, 2000. **3**(3): p. 211-216.
156. Govindarajan, A., et al., *The dendritic branch is the preferred integrative unit for protein synthesis-dependent LTP.* Neuron, 2011. **69**(1): p. 132-146.
157. Govindarajan, A., R.J. Kelleher, and S. Tonegawa, *A clustered plasticity model of long-term memory engrams.* Nature Reviews Neuroscience, 2006. **7**(7): p. 575-583.
158. Hanus, C. and M.D. Ehlers, *Secretory outposts for the local processing of membrane cargo in neuronal dendrites.* Traffic, 2008. **9**(9): p. 1437-1445.
159. Gardiol, A., C. Racca, and A. Triller, *Dendritic and postsynaptic protein synthetic machinery.* The Journal of neuroscience, 1999. **19**(1): p. 168-179.
160. Horton, A.C. and M.D. Ehlers, *Dual modes of endoplasmic reticulum-to-Golgi transport in dendrites revealed by live-cell imaging.* The Journal of neuroscience, 2003. **23**(15): p. 6188-6199.
161. Steward, O. and W.B. Levy, *Preferential localization of polyribosomes under the base of dendritic spines in granule cells of the dentate gyrus.* The Journal of neuroscience, 1982. **2**(3): p. 284-291.
162. Mori, Y., et al., *Two cis-acting elements in the 3'untranslated region of alpha-CaMKII regulate its dendritic targeting.* Nature neuroscience, 2000. **3**: p. 1079-1084.
163. Steward, O. and E.M. Schuman, *Protein synthesis at synaptic sites on dendrites.* Annual review of neuroscience, 2001. **24**: p. 299-325.
164. Garner, C.C., R.P. Tucker, and A. Matus, *Selective localization of messenger RNA for cytoskeletal protein MAP2 in dendrites.* Nature, 1988. **336**(6200): p. 674-677.
165. Davis, H.P. and L.R. Squire, *Protein synthesis and memory: a review.* Psychological Bulletin; Psychological Bulletin, 1984. **96**(3): p. 518.
166. Miller, S., et al., *Disruption of dendritic translation of CaMKIIa impairs stabilization of synaptic plasticity and memory consolidation.* Neuron, 2002. **36**(3): p. 507-519.
167. Feig, S. and P. Lipton, *Pairing the cholinergic agonist carbachol with patterned Schaffer collateral stimulation initiates protein synthesis in hippocampal CA1 pyramidal cell dendrites via a muscarinic, NMDA-dependent mechanism.* The Journal of neuroscience, 1993. **13**(3): p. 1010-1021.
168. Cajigas, I.J., et al., *The Local Transcriptome in the Synaptic Neuropil Revealed by Deep Sequencing and High-Resolution Imaging.* Neuron, 2012. **74**(3): p. 453-466.
169. Burgin, K.E., et al., *In situ hybridization histochemistry of Ca2+/calmodulin-dependent protein kinase in developing rat brain.* The Journal of neuroscience, 1990. **10**(6): p. 1788-1798.
170. Böckers, T.M., et al., *Differential expression and dendritic transcript localization of Shank family members: identification of a dendritic targeting element in the 3' untranslated region of Shank1 mRNA.* Molecular and Cellular Neuroscience, 2004. **26**(1): p. 182-190.
171. Tiruchinapalli, D.M., et al., *Activity-dependent trafficking and dynamic localization of zipcode binding protein 1 and β-actin mRNA in dendrites and spines of hippocampal neurons.* The Journal of neuroscience, 2003. **23**(8): p. 3251-3261.
172. Herb, A., et al., *Prominent dendritic localization in forebrain neurons of a novel mRNA and its product, dendrin.* Molecular and Cellular Neuroscience, 1997. **8**(5): p. 367-374.
173. Muddashetty, R.S., et al., *Dysregulated metabotropic glutamate receptor-dependent translation of AMPA receptor and postsynaptic density-95*

mRNAs at synapses in a mouse model of fragile X syndrome. The Journal of neuroscience, 2007. **27**(20): p. 5338-5348.
174. Tucker, R., C. Garner, and A. Matus, *In situ localization of microtubule-associated protein mRNA in the developing and adult rat brain.* Neuron, 1989. **2**(3): p. 1245.
175. Johnston, D., et al., *Active dendrites, potassium channels and synaptic plasticity.* Philosophical Transactions of the Royal Society of London. Series B: Biological Sciences, 2003. **358**(1432): p. 667-674.
176. Tiedge, H., F.E. Bloom, and D. Richter, *RNA, whither goest thou?* Science, 1999. **283**(5399): p. 186-187.
177. Steward, O., et al., *Synaptic Activation Causes the mRNA for the IEG< i> Arc</i> to Localize Selectively near Activated Postsynaptic Sites on Dendrites.* Neuron, 1998. **21**(4): p. 741-751.
178. Holbro, N., Å. Grunditz, and T.G. Oertner, *Differential distribution of endoplasmic reticulum controls metabotropic signaling and plasticity at hippocampal synapses.* Proceedings of the National Academy of Sciences, 2009. **106**(35): p. 15055-15060.
179. Li, Z., et al., *The importance of dendritic mitochondria in the morphogenesis and plasticity of spines and synapses.* Cell, 2004. **119**(6): p. 873-887.
180. Kennedy, M.B., M.K. Bennett, and N.E. Erondu, *Biochemical and immunochemical evidence that the" major postsynaptic density protein" is a subunit of a calmodulin-dependent protein kinase.* Proceedings of the National Academy of Sciences, 1983. **80**(23): p. 7357.
181. Lisman, J., R. Yasuda, and S. Raghavachari, *Mechanisms of CaMKII action in long-term potentiation.* Nature Reviews Neuroscience, 2012. **13**(3): p. 169-182.
182. Bayer, K.U., et al., *Transition from reversible to persistent binding of CaMKII to postsynaptic sites and NR2B.* The Journal of neuroscience, 2006. **26**(4): p. 1164-1174.
183. Lemieux, M., et al., *Translocation of CaMKII to dendritic microtubules supports the plasticity of local synapses.* The Journal of Cell Biology, 2012. **198**(6): p. 1055-1073.
184. Toni, N., et al., *LTP promotes formation of multiple spine synapses between a single axon terminal and a dendrite.* Nature, 1999. **402**(6760): p. 421-425.
185. Jourdain, P., K. Fukunaga, and D. Muller, *Calcium/calmodulin-dependent protein kinase II contributes to activity-dependent filopodia growth and spine formation.* The Journal of neuroscience, 2003. **23**(33): p. 10645-10649.
186. Lohmann, C. and T. Bonhoeffer, *A role for local calcium signaling in rapid synaptic partner selection by dendritic filopodia.* Neuron, 2008. **59**(2): p. 253.
187. Miller, S.G. and M.B. Kennedy, *Regulation of brain Type II Ca2+ calmodulin-dependent protein kinase by autophosphorylation: A Ca< sup> 2+</sup>-triggered molecular switch.* Cell, 1986. **44**(6): p. 861-870.
188. Lisman, J.E., *A mechanism for memory storage insensitive to molecular turnover: a bistable autophosphorylating kinase.* Proceedings of the National Academy of Sciences, 1985. **82**(9): p. 3055-3057.
189. Lledo, P.-M., et al., *Calcium/calmodulin-dependent kinase II and long-term potentiation enhance synaptic transmission by the same mechanism.* Proceedings of the National Academy of Sciences, 1995. **92**(24): p. 11175-11179.
190. Pi, H.J., et al., *CaMKII control of spine size and synaptic strength: role of phosphorylation states and nonenzymatic action.* Proceedings of the National Academy of Sciences, 2010. **107**(32): p. 14437-14442.
191. Giese, K.P., et al., *Autophosphorylation at Thr286 of the a calcium-calmodulin kinase II in LTP and learning.* Science, 1998. **279**(5352): p. 870-873.
192. Lucchesi, W., K. Mizuno, and K.P. Giese, *Novel insights into CaMKII function and regulation during memory formation.* Brain research bulletin, 2011. **85**(1): p. 2-8.
193. Lee, Y.-S. and A.J. Silva, *The molecular and cellular biology of enhanced cognition.* Nature Reviews Neuroscience, 2009. **10**(2): p. 126-140.
194. Walaas, S.I., et al., *Cell-specific localization of the α-subunit of calcium/calmodulin-dependent protein kinase II in Purkinje cells in rodent cerebellum.* Molecular Brain Research, 1988. **4**(3): p. 233-242.
195. Rook, M.S., M. Lu, and K.S. Kosik, *CaMKIIα 3' untranslated region-directed mRNA translocation in living neurons: visualization by GFP linkage.* The Journal of neuroscience, 2000. **20**(17): p. 6385-6393.
196. Bagni, C., et al., *Chemical stimulation of synaptosomes modulates alpha-Ca2+/calmodulin-dependent protein kinase II mRNA association to polysomes.* The Journal of neuroscience: the official journal of the Society for Neuroscience, 2000. **20**(10): p. RC76.
197. Bian, F., et al., *Differential mRNA transport and the regulation of protein synthesis: selective sensitivity of Purkinje cell dendritic mRNAs to translational inhibition.* Molecular and Cellular Neuroscience, 1996. **7**(2): p. 116-133.
198. Giovannini, M.G., et al., *Mitogen-activated protein kinase regulates early phosphorylation and delayed expression of Ca2+/calmodulin-dependent protein kinase II in long-term potentiation.* The Journal of neuroscience, 2001. **21**(18): p. 7053-7062.
199. Stevens, F.C., *Calmodulin: an introduction.* Canadian journal of biochemistry and cell biology, 1983. **61**(8): p. 906-910.
200. Chin, D. and A.R. Means, *Calmodulin: a prototypical calcium sensor.* Trends in cell biology, 2000. **10**(8): p. 322-328.
201. Sabatini, B.L., T.G. Oertner, and K. Svoboda, *The Life Cycle of Ca< sup> 2+</sup> Ions in Dendritic Spines.* Neuron, 2002. **33**(3): p. 439-452.
202. Neher, E. and G. Augustine, *Calcium gradients and buffers in bovine chromaffin cells.* The Journal of Physiology, 1992. **450**(1): p. 273-301.
203. Feng, B., S. Raghavachari, and J. Lisman, *Quantitative estimates of the cytoplasmic, PSD, and NMDAR-bound pools of CaMKII in dendritic spines.* Brain research, 2011. **1419**: p. 46-52.
204. Wallace, C.S., et al., *Differential intracellular sorting of immediate early gene mRNAs depends on signals in the mRNA sequence.* The Journal of neuroscience, 1998. **18**(1): p. 26-35.
205. McIntyre, C.K., et al., *Memory-influencing intra-basolateral amygdala drug infusions modulate expression of Arc protein in the hippocampus.* Proceedings of the National Academy of Sciences of the United States of America, 2005. **102**(30): p. 10718-10723.

206. Guzowski, J.F., et al., *Environment-specific expression of the immediate-early gene Arc in hippocampal neuronal ensembles.* Nature neuroscience, 1999. **2**(12): p. 1120-1124.
207. Ramírez-Amaya, V., et al., *Spatial exploration-induced Arc mRNA and protein expression: evidence for selective, network-specific reactivation.* The Journal of neuroscience, 2005. **25**(7): p. 1761-1768.
208. Ploski, J.E., et al., *The activity-regulated cytoskeletal-associated protein (Arc/Arg3. 1) is required for memory consolidation of pavlovian fear conditioning in the lateral amygdala.* The Journal of neuroscience, 2008. **28**(47): p. 12383-12395.
209. Chowdhury, S., et al., *Arc/Arg3. 1 interacts with the endocytic machinery to regulate AMPA receptor trafficking.* Neuron, 2006. **52**(3): p. 445-459.
210. Moga, D., et al., *Activity-regulated cytoskeletal-associated protein is localized to recently activated excitatory synapses.* Neuroscience, 2004. **125**(1): p. 7-11.
211. Waung, M.W., et al., *Rapid translation of Arc/Arg3. 1 selectively mediates mGluR-dependent LTD through persistent increases in AMPAR endocytosis rate.* Neuron, 2008. **59**(1): p. 84-97.
212. Smith-Hicks, C., et al., *SRF binding to SRE 6.9 in the Arc promoter is essential for LTD in cultured Purkinje cells.* Nature neuroscience, 2010. **13**(9): p. 1082-1089.
213. Shepherd, J.D., et al., *Arc/Arg3. 1 mediates homeostatic synaptic scaling of AMPA receptors.* Neuron, 2006. **52**(3): p. 475-484.
214. Honoré, T., J. Lauridsen, and P. Krogsgaard-Larsen, *The binding of [3H] AMPA, a structural analogue of glutamic acid, to rat brain membranes.* Journal of neurochemistry, 1982. **38**(1): p. 173-178.
215. Leonard, A.S., et al., *SAP97 is associated with the α-amino-3-hydroxy-5-methylisoxazole-4-propionic acid receptor GluR1 subunit.* Journal of Biological Chemistry, 1998. **273**(31): p. 19518-19524.
216. Boehm, J., et al., *Synaptic incorporation of AMPA receptors during LTP is controlled by a PKC phosphorylation site on GluR1.* Neuron, 2006. **51**(2): p. 213-225.
217. Hayashi, Y., et al., *Driving AMPA receptors into synapses by LTP and CaMKII: requirement for GluR1 and PDZ domain interaction.* Science Signaling, 2000. **287**(5461): p. 2262.
218. Lee, H.-K., et al., *Regulation of distinct AMPA receptor phosphorylation sites during bidirectional synaptic plasticity.* Nature, 2000. **405**(6789): p. 955-959.
219. Lledo, P.-M., et al., *Postsynaptic membrane fusion and long-term potentiation.* Science, 1998. **279**(5349): p. 399-403.
220. Shi, S.-H., et al., *Subunit-specific rules governing AMPA receptor trafficking to synapses in hippocampal pyramidal neurons.* Cell, 2001. **105**(3): p. 331-343.
221. Park, M., et al., *Recycling endosomes supply AMPA receptors for LTP.* Science Signaling, 2004. **305**(5692): p. 1972.
222. Kopec, C.D., et al., *GluR1 links structural and functional plasticity at excitatory synapses.* The Journal of neuroscience, 2007. **27**(50): p. 13706-13718.
223. Frey, U. and R.G.M. Morris, *Synaptic tagging and long-term potentiation.* Nature, 1997. **385**(6616): p. 533-536.
224. Sajikumar, S. and J.U. Frey, *Late-associativity, synaptic tagging, and the role of dopamine during LTP and LTD.* Neurobiology of learning and memory, 2004. **82**(1): p. 12-25.
225. Fonseca, R., et al., *Competing for memory: hippocampal LTP under regimes of reduced protein synthesis.* Neuron, 2004. **44**(6): p. 1011-1020.
226. Gasparini, S. and J.C. Magee, *State-dependent dendritic computation in hippocampal CA1 pyramidal neurons.* The Journal of neuroscience, 2006. **26**(7): p. 2088-2100.
227. Tsien, R.Y., *The green fluorescent protein.* Annual review of biochemistry, 1998. **67**(1): p. 509-544.
228. Chudakov, D.M., S. Lukyanov, and K.A. Lukyanov, *Fluorescent proteins as a toolkit for< i> in vivo</i> imaging.* Trends in biotechnology, 2005. **23**(12): p. 605-613.
229. Lippincott-Schwartz, J., N. Altan-Bonnet, and G.H. Patterson, *Photobleaching and photoactivation: following protein dynamics in living cells.* Nature Cell Biology, 2003: p. S7-14.
230. Yokoe, H. and T. Meyer, *Spatial dynamics of GFP-tagged proteins investigated by local fluorescence enhancement.* Nature biotechnology, 1996. **14**(10): p. 1252-1256.
231. Marchant, J.S., et al., *Multiphoton-evoked color change of DsRed as an optical highlighter for cellular and subcellular labeling.* Nature biotechnology, 2001. **19**(7): p. 645-649.
232. Ando, R., et al., *An optical marker based on the UV-induced green-to-red photoconversion of a fluorescent protein.* Proceedings of the National Academy of Sciences, 2002. **99**(20): p. 12651-12656.
233. Lukyanov, K.A., et al., *Photoactivatable fluorescent proteins.* Nature Reviews Molecular Cell Biology, 2005. **6**(11): p. 885-890.
234. Wiedenmann, J., et al., *EosFP, a fluorescent marker protein with UV-inducible green-to-red fluorescence conversion.* Proceedings of the National Academy of Sciences of the United States of America, 2004. **101**(45): p. 15905-15910.
235. Tsutsui, H., et al., *Semi-rational engineering of a coral fluorescent protein into an efficient highlighter.* EMBO reports, 2005. **6**(3): p. 233-238.
236. Gurskaya, N.G., et al., *Engineering of a monomeric green-to-red photoactivatable fluorescent protein induced by blue light.* Nature biotechnology, 2006. **24**(4): p. 461-465.
237. Mizuno, H., et al., *Photo-induced peptide cleavage in the green-to-red conversion of a fluorescent protein.* Molecular cell, 2003. **12**(4): p. 1051-1058.
238. Zhang, L., et al., *Method for real-time monitoring of protein degradation at the single cell level.* Biotechniques, 2007. **42**(4): p. 446.
239. Chudakov, D.M., S. Lukyanov, and K.A. Lukyanov, *Tracking intracellular protein movements using photoswitchable fluorescent proteins PS-CFP2 and Dendra2.* Nature protocols, 2007. **2**(8): p. 2024-2032.
240. Chudakov, D.M., et al., *Photoswitchable cyan fluorescent protein for protein tracking.* Nature biotechnology, 2004. **22**(11): p. 1435-1439.

241. Post, J.N., et al., *One-and two-photon photoactivation of a paGFP-fusion protein in live< i> Drosophila</i> embryos.* FEBS letters, 2005. **579**(2): p. 325-330.
242. Mezei, L., et al., *PCR technology: Current innovations.* 1994.
243. Suggs, S., et al. *Developmental biology using purified genes*. in *ICN-UCLA Symposium on Molecular and Cellular Biology Vol.* 1981.
244. Saiki, R.K., et al., *Primer-directed enzymatic amplification of DNA with a thermostable DNA polymerase.* Science, 1988. **239**(4839): p. 487-491.
245. Stoppini, L., P.-A. Buchs, and D. Muller, *A simple method for organotypic cultures of nervous tissue.* Journal of neuroscience methods, 1991. **37**(2): p. 173-182.
246. Moore, M.J., *From birth to death: the complex lives of eukaryotic mRNAs.* Science Signaling, 2005. **309**(5740): p. 1514.
247. Papa, M., et al., *Morphological analysis of dendritic spine development in primary cultures of hippocampal neurons.* The Journal of neuroscience, 1995. **15**(1): p. 1-11.
248. Segal, M. and D. Manor, *Confocal microscopic imaging of [Ca2+] i in cultured rat hippocampal neurons following exposure to N-methyl-D-aspartate.* The Journal of Physiology, 1992. **448**(1): p. 655-676.
249. Chudakov, D.M., S. Lukyanov, and K.A. Lukyanov, *Using photoactivatable fluorescent protein Dendra2 to track protein movement.* Biotechniques, 2007. **42**(5): p. 553.
250. Palmer, M., et al., *The group I mGlu receptor agonist DHPG induces a novel form of LTD in the CA1 region of the hippocampus.* Neuropharmacology, 1997. **36**(11): p. 1517-1532.

Chapter 6. Appendix

6. Appendix

I. pDrive Cloning Vector

The pDrive Cloning Vector is supplied in a linear form, ready-to-use for direct ligation of PCR products. This vector allows ampicillin and kanamycin selection, as well as blue/white colony screening. The vector contains several unique restriction endonuclease recognition sites around the cloning site, allowing easy restriction analysis of recombinant plasmids (Fig. 1). The vector also contains a T7 and SP6 promoter on either side of the cloning site, allowing in vitro transcription of cloned PCR products as well as sequence analysis using standard sequencing primers. In addition, the pDrive Cloning Vector has a phage f1 origin to allow preparation of single-stranded DNA.

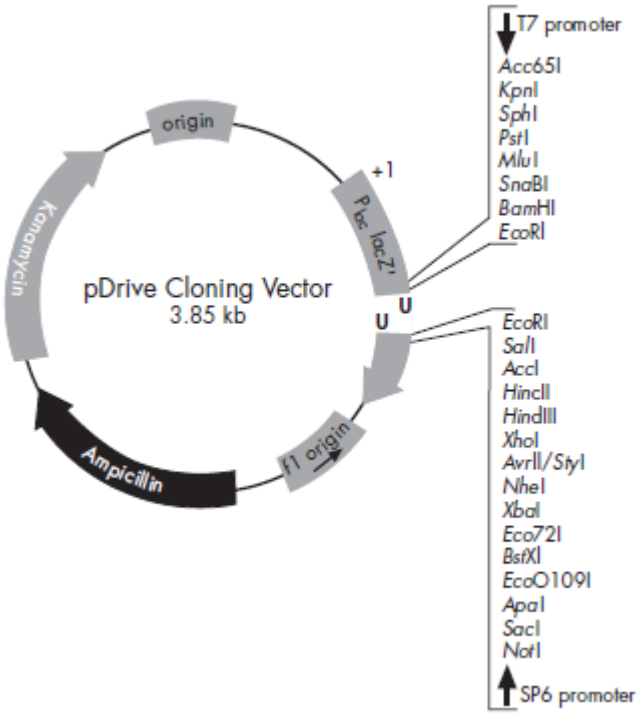

Fig. 1 – pDrive Clonng Vector Map | Representation of the linearized pDrive Cloning Vector with U overhangs. The unique restriction endonuclease recognition sites on either side of the cloning site are listed.

II. pDendra2-C Vector

pDendra2-C is a mammalian expression vector from Evrogen encoding green-red fluorescent protein Dendra2 (Fig.1). The vector allows generation of fusions to the Dendra2 C-terminus and expression of Dendra2 fusions or Dendra2 alone in eukaryotic (mammalian) cells.

Dendra2 codon usage is optimized for high expression in mammalian cells (humanized) [Haas et al. 1996]. To increase mRNA translation efficiency, Kozak consensus translation initiation site is generated upstream of the Dendra2 sequence [Kozak 1987]. Multiple cloning site (MCS) is located between

Dendra2 coding sequence and SV40 polyadenylation signal (SV40 polyA). The vector backbone contains immediate early promoter of cytomegalovirus (PCMV IE) for protein expression, SV40 origin for replication in mammalian cells expressing SV40 T-antigen, pUC origin of replication for propagation in *E. coli* and f1 origin for single-stranded DNA production. SV40 polyadenylation signals (SV40 poly A) direct proper processing of the 3'-end of the reporter mRNA.

SV40 early promoter (PSV40) provides neomycin resistance gene (Neo^r) expression to select stably transfected eukaryotic cells using G418. Bacterial promoter (P) provides kanamycin resistance gene expression (Kan^r) in *E. coli*. Kan^r/Neo^r gene is linked with herpes simplex virus (HSV) thymidine kinase (TK) polyadenylation signals.

Suitable host strains for propagation in *E. coli* include DH5alpha, HB101, XL1-Blue, and other general purpose strains. Plasmid incompatibility group is pMB1/ColE1. The vector confers resistance to kanamycin (30 μg/ml) to *E. coli* hosts. Copy number in *E. coli* is about 500.

pDendra2-C vector can be transfected into mammalian cells by any known transfection method. If required, stable transformants can be selected using G418 [Gorman 1985].

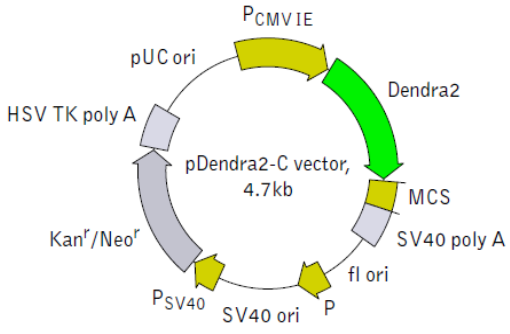

Fig. 2 – pDendra2-C Vector Map | Representation of the pDendra2-C Vector. The restriction endonuclease recognition sites on Multiple Cloning Site (MCS) positioned at 3' side of Dendra2 protein. Majority of these restriction endonuclease sites are unique, except the ones tagged with *. Sites tagged with # are blocked by dam methylation.

pDendra2-C vector MCS

Dendra2 → ... TCC.GGC.GAC.AGC.GGC.GTG.TAC.AAG.ACT.CGA.GCT.CAA.GCT.TCG.AAT.TCT.GCA.GTC.GAC.GGT.ACC.GCG.GGC.CCG.GGA.TCC.ACC.GGA.TCT.AGA.TAA.CTG.ATC.A ...

Xho I (Sac I) | Hind III (EcoR I) | Pst I (Sal I) | Kpn I (Sac II) | Apa I | BamH I (Sma I/Xma I*) | STOPs (Xba I#) | Bcl I#*

* — not unique sites.

\# — sites are blocked by *dam* methylation. If you wish to digest the vector with these enzymes, you will need to transform the vector into a *dam*⁻ host and make fresh DNA.